The Astrophysical Journal Supplement Series, 212:13 (35pp), 2014 May doi:10.1088/0067-0049/212/1/13

CHASING THE IDENTIFICATION OF *ASCA* GALACTIC OBJECTS (ChIcAGO): AN X-RAY SURVEY OF UNIDENTIFIED SOURCES IN THE GALACTIC PLANE. I. SOURCE SAMPLE AND INITIAL RESULTS

Gemma E. Anderson[1,16], B. M. Gaensler[1], David L. Kaplan[2], Patrick O. Slane[3], Michael P. Muno[4,17], Bettina Posselt[5], Jaesub Hong[3], Stephen S. Murray[6], Danny T. H. Steeghs[7], Crystal L. Brogan[8], Jeremy J. Drake[3], Sean A. Farrell[1], Robert A. Benjamin[9], Deepto Chakrabarty[10], Janet E. Drew[11], John P. Finley[12], Jonathan E. Grindlay[3], T. Joseph W. Lazio[13], Julia C. Lee[3], Jon C. Mauerhan[14], and Marten H. van Kerkwijk[15]
[1] Sydney Institute for Astronomy, School of Physics, The University of Sydney, NSW 2006, Australia; gemma.anderson@astro.ox.ac.uk
[2] Department of Physics, University of Wisconsin, Milwaukee, WI 53201, USA
[3] Harvard-Smithsonian Center for Astrophysics, Cambridge, MA 02138, USA
[4] Space Radiation Laboratory, California Institute of Technology, Pasadena, CA 91125, USA
[5] Department of Astronomy and Astrophysics, Pennsylvania State University, PA 16802, USA
[6] Department of Physics and Astronomy, John Hopkins University, Baltimore, MD 21218, USA
[7] Department of Physics, University of Warwick, Coventry CV4 7AL, UK
[8] National Radio Astronomy Observatory, Charlottesville, VA 22903, USA
[9] Department of Physics, University of Wisconsin, Whitewater, WI 53190, USA
[10] MIT Kavli Institute for Astrophysics and Space Research and Department of Physics, Massachusetts Institute of Technology, Cambridge, MA 02139, USA
[11] Centre for Astrophysics Research, STRI, University of Hertfordshire, Hatfield AL10 9AB, UK
[12] Department of Physics, Purdue University, West Lafayette, IN 47907, USA
[13] Jet Propulsion Laboratory, California Institute of Technology, Pasadena, CA 91109, USA
[14] Spitzer Science Center, California Institute of Technology, Pasadena, CA 91125, USA
[15] Department of Astronomy and Astrophysics, University of Toronto, Toronto, ON M5S 3H4, Canada
Received 2013 July 2; accepted 2014 February 28; published 2014 April 28

ABSTRACT

We present the Chasing the Identification of *ASCA* Galactic Objects (ChIcAGO) survey, which is designed to identify the unknown X-ray sources discovered during the *ASCA* Galactic Plane Survey (AGPS). Little is known about most of the AGPS sources, especially those that emit primarily in hard X-rays (2–10 keV) within the $F_x \sim 10^{-13}$ to 10^{-11} erg cm^{-2} s^{-1} X-ray flux range. In ChIcAGO, the subarcsecond localization capabilities of *Chandra* have been combined with a detailed multiwavelength follow-up program, with the ultimate goal of classifying the >100 unidentified sources in the AGPS. Overall to date, 93 unidentified AGPS sources have been observed with *Chandra* as part of the ChIcAGO survey. A total of 253 X-ray point sources have been detected in these *Chandra* observations within 3′ of the original *ASCA* positions. We have identified infrared and optical counterparts to the majority of these sources, using both new observations and catalogs from existing Galactic plane surveys. X-ray and infrared population statistics for the X-ray point sources detected in the *Chandra* observations reveal that the primary populations of Galactic plane X-ray sources that emit in the $F_x \sim 10^{-13}$ to 10^{-11} erg cm^{-2} s^{-1} flux range are active stellar coronae, massive stars with strong stellar winds that are possibly in colliding wind binaries, X-ray binaries, and magnetars. There is also another primary population that is still unidentified but, on the basis of its X-ray and infrared properties, likely comprises partly Galactic sources and partly active galactic nuclei.

Key words: surveys – X-rays: binaries – X-rays: galaxies – X-rays: general – X-rays: stars

Online-only material: color figures, machine-readable tables

1. INTRODUCTION

From 1996–1999, the *Advanced Satellite for Cosmology and Astrophysics* (*ASCA*) performed the *ASCA* Galactic Plane Survey (AGPS), which was designed to study 40 deg^2 of the X-ray sky over the Galactic coordinates $|l| \lesssim 45°$ and $|b| \lesssim 0.^{\circ}4$ in the 0.7–10 keV energy range (Sugizaki et al. 2001). This survey resulted in a catalog of 163 discrete X-ray sources with X-ray fluxes between $F_x \sim 10^{-13}$ and 10^{-11} erg cm^{-2} s^{-1}, many of which are much harder and more absorbed than any other X-ray source previously detected in the Galactic plane. While the AGPS yielded the first ever log N–log S distribution of hard (2–10 keV) Galactic plane X-ray sources, *ASCA*'s limited spatial resolution (3′) and large positional uncertainty (1′) left >100 AGPS sources unidentified. Even in the era of *Chandra* and the *XMM-Newton* telescope, a substantial fraction of the AGPS source catalog and therefore a large fraction of the Galactic plane X-ray population still remain unidentified.

For the last few years, new and archival multiwavelength data have been used to improve the general understanding of the Galactic X-ray sources detected in the AGPS. Recent work has demonstrated that unidentified *ASCA* sources represent a whole range of unusual objects. For example, Gelfand & Gaensler (2007) used new and archival *Chandra* and *XMM* observations to identify the AGPS source AX J155052–5418 (also known as 1E 1547.0–5408) as a magnetar sitting at the center of a faint and small, previously unidentified, radio supernova remnant (SNR) called G327.24–0.13. Investigations of archival *XMM* data allowed Kaplan et al. (2007) to identify the AGPS source AX J183528–0737 as a likely symbiotic X-ray binary (SyXB) comprising a late-type giant or supergiant and a neutron star (NS) with a 112 s pulse period. Gaensler et al. (2008) identified the AGPS source AX J172105–3726 as the X-ray emission associated with the radio SNR G350.1–0.3. The *XMM* X-ray

[16] Current address: Department of Physics, Astrophysics, University of Oxford, Denys Wilkinson Building, Oxford, OX1 3RH, UK.
[17] Current address: Lincoln Laboratory, Massachusetts Institute of Technology, Lexington, MA 02420-9108, USA.

spectrum, combined with the presence of nonthermal, polarized, radio emission, showed G350.1–0.3 to be a very young and luminous SNR. A central compact object (CCO) was also resolved in these X-ray observations and identified as a NS. *XMM* (Funk et al. 2007) and *Chandra* (Lemiere et al. 2009) observations have demonstrated that the AGPS source AX J164042–4632 is an X-ray pulsar wind nebula (PWN) located at the center of the radio SNR G338.3–0.0. *Chandra* results, discussed in Anderson et al. (2011), have revealed that two AGPS sources, AX J163252–4746 and AX J184738–0156, are massive stars in colliding wind binaries (CWBs). New *Chandra*, *XMM*, and Australia Telescope Compact Array (ATCA) observations have also been used to identify the AGPS source AX J162246–4946 as the radio and X-ray emitting magnetar, PSR J1622–4950, and have exposed the likely X-ray transient nature of this source (Anderson et al. 2012). These identifications over the last 8 yr have therefore demonstrated that many of the unidentified AGPS sources are unusual and rare Galactic plane X-ray objects.

The most comprehensive X-ray survey to date, in terms of area coverage, was performed by the *ROSAT* X-ray satellite (for example, see Voges et al. 1999), which mapped the soft X-ray source population (0.1–2.4 keV) down to a flux sensitivity of a few 10^{-13} erg cm^{-2} s^{-1}. Projects that focused on the *ROSAT* data covering the Galactic plane (e.g., the ROSAT Galactic Plane Survey; Motch et al. 1997, 1998) demonstrated that stars and active galactic nuclei (AGNs) dominate the soft X-ray sky. However, performing a similar Galactic plane survey to include those sources with energies up to 10 keV, sensitive to the $F_x \sim 10^{-13}$ to $\sim 10^{-11}$ erg cm^{-2} s^{-1} flux range, would be impractical to achieve with the current X-ray telescopes *Chandra* and *XMM* because of their limited fields of view. Astronomers have therefore had to rely upon characterizing the distribution of the harder X-ray source populations within much smaller regions of the Galactic plane (e.g., Hands et al. 2004; Ebisawa et al. 2005; Grindlay et al. 2005). For example, Motch et al. (2010) used the XGPS (Hands et al. 2004) to determine the contributions of active stellar coronae (ASCs) and accreting X-ray source populations in the Galactic plane for $F_x \lesssim 10^{-12}$ erg cm^{-2} s^{-1}. The Chandra Multiwavelength Plane survey (ChaMPlane; Grindlay et al. 2005) has now surveyed 7 deg^2 of the Galactic plane and bulge with *Chandra* (van den Berg et al. 2012), identifying the contributions of magnetic cataclysmic variables (CVs) to the Galactic ridge X-ray emission (Hong 2012).

The key to obtaining a complete understanding of the Galactic plane X-ray source populations, from 0.3 to 10 keV, that make up the $F_x \sim 10^{-13}$ to 10^{-11} erg cm^{-2} s^{-1} X-ray flux range is to identify the unidentified AGPS sources, as *ASCA* covered a much larger area of the Galactic plane ($\sim$40 deg^2) than other X-ray surveys (for example, the XGPS and ChaMPlane; Hands et al. 2004; Motch et al. 2010; Grindlay et al. 2005; van den Berg et al. 2012). In order to identify the AGPS sources, the Chasing the Identification of *ASCA* Galactic Objects (ChIcAGO) survey was conceived. In this survey the subarcsecond capabilities of *Chandra* are used to localize the unidentified AGPS sources listed by Sugizaki et al. (2001). Once the positions of these sources have been determined, an extensive multiwavelength program is activated, which is aimed at determining the identities of the sources and the nature of their X-ray emission.

In this paper, we present the results of *Chandra* observations of 93 unidentified AGPS sources, along with the multiwavelength follow-up that has allowed the identification of optical, infrared, and radio counterparts. Section 2 explains the *Chandra* observing strategy employed to localize the unidentified AGPS sources. To begin the identification process, we automated the *Chandra* data analysis and preliminary multiwavelength follow-up, which involves comparisons with existing optical, near-infrared (NIR), and IR surveys. X-ray spectral modeling using "quantile analysis" (Hong et al. 2004) and Cash (1979) statistics and further multiwavelength observations in the optical, IR, and radio bands required to ultimately classify each source are also described. Section 3 details the results of each AGPS position observed with *Chandra*. These results include details on the individual X-ray sources detected, the parameters of their likely X-ray spectral shapes, and the names and magnitudes of their infrared, optical, and radio counterparts. The possibility of short-term variability or periodicity is also explored. In Section 4, we discuss the AGPS sources that have been identified through a visual inspection of radio Galactic plane surveys. The X-ray fluxes and NIR and IR magnitudes of the remaining unidentified sources, reported in Section 3, are then used to conduct X-ray and infrared population statistics. Resulting flux and color–color diagrams allow the identification of likely Galactic plane X-ray populations with infrared counterparts. This analysis is followed by a discussion of particularly interesting individual sources that have been identified as a result of this work. The final part of this section includes a tabulated summary of all 163 AGPS sources along with their confirmed identifications (obtained from the literature and the present paper) or their tentative identifications, which are based on our ChIcAGO survey statistical results. In Section 5 we summarize the results from this paper, with a particular focus on our statistical findings.

2. METHOD

2.1. Chandra Observations

The main goal of the ChIcAGO survey is to localize the positions of the unidentified AGPS sources, so that multiwavelength follow-up can be used to identify them. It is therefore necessary to design an experiment that will allow each source to be localized precisely enough to identify counterparts in the crowded Galactic plane. *Chandra* can provide subarcsecond localization as it has an intrinsic astrometric precision accuracy of 0.″6 at 90% confidence within 2′ of the aimpoint (Weisskopf et al. 2003).

For all but the brightest targets, *Chandra*'s Advanced CCD Imaging Spectrometer (ACIS; Garmire et al. 2003) was used as it provides simultaneous positional, temporal, and spectroscopic information. The ACIS-S configuration was chosen as it fully encompasses the AGPS positional uncertainties of up to 3′ (Sugizaki et al. 2001). (The aimpoint of the ACIS-I configuration is near a chip gap.) The High Resolution Camera (HRC; Murray et al. 2000) in the I focal plane array was used to observe those sources with a predicted ACIS count rate >0.2 counts s^{-1} to avoid positional, spectral, and temporal degradation associated with pileup (Davis 2001).

At *Chandra*'s high angular resolution, only a small number of X-ray counts are required to localize each source sufficiently to overcome confusion from IR field stars in the Galactic plane. We first considered the number density of such stars in the K_s band at low Galactic latitudes. Figure 24 of Kaplan et al. (2004) shows that 0.2 stars arcsec^{-2} are expected with a magnitude $K_s \lesssim 19$. For there to be a <25% chance of random alignment of the *Chandra* source with an infrared field star of this magnitude, a total astrometric error <0.″7 is required. Using 2MASS as

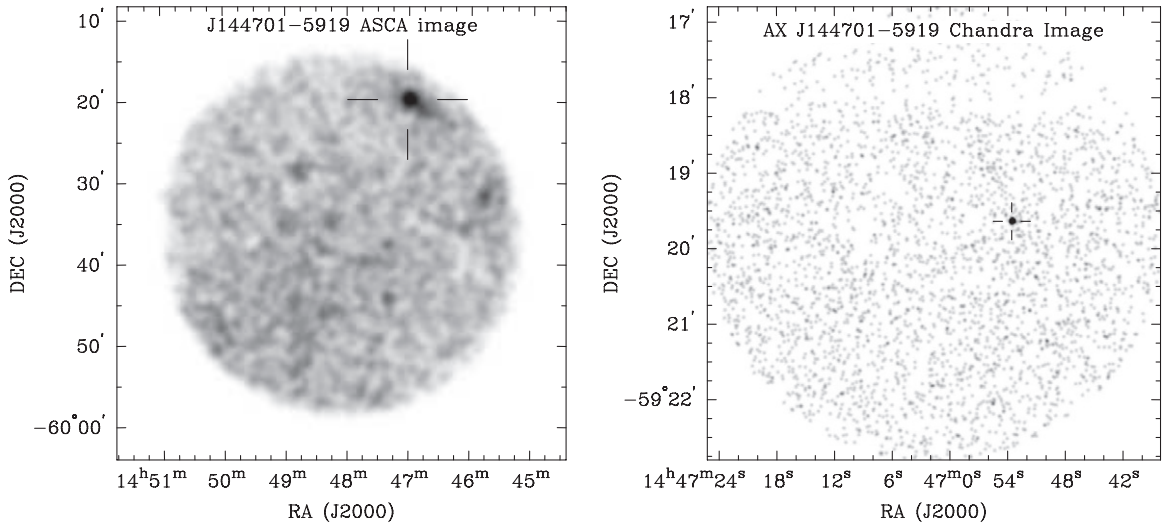

Figure 1. X-ray images of AX J144701–5919 as output by ChIcAGO MAP. Left: the *ASCA* GIS detection of the AGPS source AX J144701–5919. The circular field of view has a 50′ diameter, and the position of this AGPS source, as listed by Sugizaki et al. (2001), is indicated by the black crosshair. Right: the 3′ radius field of view of the *Chandra* observation of AX J144701–5919, which is centered on the position of this AGPS source listed by Sugizaki et al. (2001). The one ChIcAGO source detected in this field is indicated by a black crosshair and is likely the *Chandra* counterpart to AX J144701–5919.

a guide, given its extremely high positional precision (0.″1 1σ error) and *Chandra*'s 90% absolute astrometry error of 0.″6, a centroiding error of <0.″4 with 95% accuracy is required for *Chandra*. The *Chandra* Interactive Analysis of Observations (CIAO)[18] software tool `wavdetect` (Freeman et al. 2002) was chosen to detect the point sources in our fields. Equation (5) of Hong et al. (2005) provides the 95% confidence position error circle of a point source detected with `wavdetect` for a given number of source counts at a given off-axis angle. At the maximum off-axis angle expected for an *ASCA* source localization (<3′), ∼100 X-ray counts are required to ensure that a source's centroiding error is below 0.″4.

Using the count rates and power-law spectral fits calculated by Sugizaki et al. (2001) for each AGPS source and the *Chandra* Proposal Planning Toolkit (PIMMS),[19] the exposure time required to detect ∼100 counts with *Chandra* for each source was estimated. For those AGPS sources that were too faint for Sugizaki et al. (2001) to calculate spectral fit parameters, an absorbed power-law model with a photon index $\Gamma = 2$ and an absorption $N_{\rm H} = 10^{22}$ cm^{-2} was used; these values are representative of a nonthermal X-ray source and typical Galactic plane absorption.

In order to select the AGPS source candidates to be observed with *Chandra*, each source was investigated individually. First, those AGPS sources that have already been conclusively identified, either by Sugizaki et al. (2001) or by other groups in the literature, were removed from the *Chandra* target list. On the basis of this criterion, a total of 43 AGPS sources were identified and therefore rejected for *Chandra* follow-up (these sources are described in Appendix A). The *ASCA* images of each of the remaining unidentified AGPS sources were then studied to determine if any sources appeared to be too extended for *Chandra* to successfully localize in a short amount of time. These sources were also rejected for *Chandra* follow-up. The remaining unidentified AGPS sources were then prioritized for *Chandra* follow-up on the basis of their absorbed X-ray flux or count rate that was listed by Sugizaki et al. (2001).

A total of 93 AGPS sources have been observed with *Chandra* as part of the ChIcAGO survey, of which 84 were imaged with ACIS-S and 9 were imaged with HRC-I. The ChIcAGO *Chandra* observations took place over a 3.5 yr period, from 2007 January to 2010 July. The *Chandra* exposure times ranged from ∼1 to 10 ks. All the details of these *Chandra* observations are listed in Table 1. The initial automated analysis of these *Chandra* observations was conducted using the ChIcAGO Multi-wavelength Analysis Pipeline, described in Section 2.2. We then performed a more detailed X-ray analysis and counterpart study for those 74 sources with >20 X-ray counts, as such sources are approximately within the original AGPS sources X-ray flux range (see Sections 3.2 and 3.3).

2.2. ChIcAGO Multi-wavelength Analysis Pipeline (MAP)

It is crucial to the efficiency of the project to automate the analysis of the *Chandra* observations, such as the detection and extraction of sources, as well as the search for multiwavelength counterparts. We therefore created the ChIcAGO Multi-wavelength Analysis Pipeline (MAP) for this task. ChIcAGO MAP takes the ACIS-S or HRC-I *Chandra* observation of an AGPS source field and detects and analyzes all point sources within 3′, equivalent to the largest likely position error, for the original AGPS source positions supplied by Sugizaki et al. (2001). From hereon we refer to all point sources detected in the *Chandra* observations of the AGPS fields as "ChIcAGO sources." The X-ray analysis component of this pipeline uses the `CIAO` software, version 4.3, with CALDB, version 4.5.5, and follows standard reduction recipes given in the online `CIAO` 4.3 science threads.[20]

ChIcAGO MAP carries out the following steps, all of which are explained in more detail below. These steps apply to both ACIS-S and HRC-I data sets unless otherwise stated.

1. An image of the original *ASCA* detection of the AGPS source is created (for example, see the left image of Figure 1).
2. The `CIAO` tool `chandra_repro` is run to reprocess the *Chandra* data.

[18] http://cxc.harvard.edu/ciao/index.html
[19] http://cxc.harvard.edu/toolkit/pimms.jsp
[20] http://cxc.harvard.edu/ciao4.3/threads/index.html

Table 1
ChIcAGO MAP X-Ray Results, Including the Position, Position Errors, Net Counts, and Quantile Analysis Values for Each ChIcAGO Source

Chandra Obs[a]	ChIcAGO[b]	`wavdetect` Position		Offset[c]	Positional Errors[d]		Net Counts[e]			Energy Quantiles[f]		CSC[g]	2XMMi-DR3[h]
(ID, Date, Inst, Exp)	Source ID ChI	R.A. (J2000)	Decl. (J2000)	from *ASCA* (′)	wav (″)	Total (″)	0.3–8	0.5–2	2–8 keV	E_{50} (keV)	Quartile Ratio	Name CXO J	Name 2XMMi
AX J143148–6021 8239 2007-09-05 ACIS-S 2.62ks													
	J143148–6021_1	14:31:50.18	−60:22:08.3	0.97	0.6	0.9	$4.0^{+3.2}_{-1.9}$	$4.0^{+3.2}_{-1.9}$	$0.0^{+1.9}_{-0.0}$				
	J143148–6021_2	14:31:48.56	−60:21:44.5	0.56	0.5	0.8	10^{+4}_{-3}	$7.0^{+3.8}_{-2.6}$	$2.0^{+2.7}_{-1.3}$	1.1 ± 0.4	1.4 ± 0.9		
	J143148–6021_3	14:31:48.06	−60:19:59.5	1.19	0.3	0.8	146^{+13}_{-12}	51^{+8}_{-7}	95^{+11}_{-10}	2.7 ± 0.2	1.1 ± 0.1	143148.0–601959	
	J143148–6021_4	14:31:41.52	−60:19:55.2	1.56	0.6	0.9	$5.9^{+3.6}_{-2.4}$	$2.9^{+2.9}_{-1.6}$	$0.0^{+1.9}_{-0.0}$	0.6 ± 0.3	0.5 ± 0.4		
	J143148–6021_5	14:32:02.80	−60:18:57.4	2.81	0.7	1.0	20^{+6}_{-4}	$0.0^{+1.9}_{-0.0}$	20^{+6}_{-4}	4.4 ± 0.5	1.8 ± 0.2	143202.8–601857	
AX J144042–6001 9599 2008-05-04 HRC-I 1.18ks													
	J144042–6001_1	14:40:38.40	−60:01:36.8	0.56	0.3	0.8	326^{+19}_{-18}					144038.4–600136	

Notes.

[a] Details of the *Chandra* observation: the observation identification number (ID), the date of the observation (yyyy-mm-dd), the *Chandra* instrument used for the observation, and the exposure time of the observation in ks.

[b] The ChIcAGO source name. Those ChIcAGO sources marked with a * have a probability of false detection that is $>10^{-5}$. The ChIcAGO sources marked with a † fall in the chip gap between ACIS-S CCDs 6 and 7.

[c] The offset, in arcminutes, between the ChIcAGO source and the original AGPS source position published by Sugizaki et al. (2001).

[d] The ChIcAGO source position error information. wav: The 95% position error circle of the ChIcAGO source `wavdetect` position. This was calculated using Equation (5) of Hong et al. (2005). Total: The total 95% position error circle of the ChIcAGO source taking into account the `wavdetect` position error and the absolute astrometric accuracy of *Chandra*. Both errors are in arcseconds.

[e] The net number of counts in the 0.3–8.0, 0.5–2.0 and 2.0–8.0 keV energy ranges detected from each ChIcAGO source. The source counts were calculated using a source region with a radius equal to 95% of the PSF at 1.5 keV. The total counts have been background subtracted and the upper and lower 1σ confidence limits were calculated using Gehrels (1986) statistics.

[f] The values used in the quantile analysis (results in Tables 3 and 4). E_{50} is the 50% photon detected in the 0.3–8.0 keV energy band. The quartile ratio is the ratio of the E_{25} (energy of the 25% photon detected) and E_{75} (energy of the 75% photon detected) used in quantile analysis: $3\times(E_{25}-0.3)/(E_{75}-0.3)$. See Section 2.3.1 for further details.

[g] The corresponding *Chandra* Source Catalog name for each ChIcAGO source (Evans et al. 2010).

[h] The corresponding 2XMMi DR3 name for each ChIcAGO source (Watson et al. 2009).

(This table is available in its entirety in a machine-readable form in the online journal. A portion is shown here for guidance regarding its form and content.)

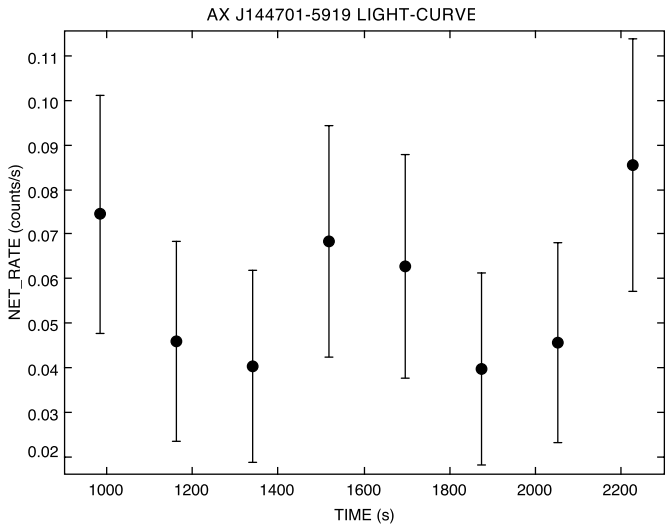

Figure 2. *Chandra* ACIS-S light curve of the ChIcAGO source AX J144701–5919 as output by ChIcAGO MAP. This ChIcAGO source does not exhibit evidence for short-term variability as its resulting $\chi^2 = 3.4$ for seven degrees of freedom is below the confidence threshold of 99.9%.

3. The new event file is filtered to only include photons with energies in the range 0.3–8.0 keV.
4. The CIAO tool `wavdetect` is used to detect all X-ray point sources (ChIcAGO sources) within 3′ of the AGPS position. A *Chandra* image is then created for each ChIcAGO source (for example, see the right image of Figure 1). If no sources are detected, ChIcAGO MAP ends.
5. The position, source counts, and associated errors are calculated for each ChIcAGO source detected. If the data set is an ACIS-S observation, then the total counts are obtained in the 0.3–8.0, 0.5–2.0, and 2.0–8.0 keV energy ranges, and the energy quartiles (E_{25}, E_{50}, and E_{75}), which are used in quantile analysis (see Section 2.3.1), are calculated.[21]
6. The CIAO tool `specextract` is run on ACIS-S data sets to obtain the source and background spectrum files and their corresponding redistribution matrix file (RMF) and the ancillary response file (ARF) for each ChIcAGO source. These files are used in quantile analysis and spectral modeling (see Section 2.3).
7. A timing analysis is conducted on each ChIcAGO source (detected with either the ACIS or HRC instruments) to search for short-term variability and periodicity.
   (a) A light curve with eight bins is constructed using the CIAO tool `dmextract`. The χ^2 is calculated for this light curve in order to test for short-term variability (e.g., Figure 2).
   (b) The Z_1^2 statistic is calculated to search for sinusoidal periodicity (Buccheri et al. 1983). This process creates a power spectrum and folded light curve (e.g., Figure 3), which predicts the most likely pulsed frequency, its corresponding power, and the probability that the power is random noise.
8. Multiwavelength follow-up and catalog searches are conducted to identify likely optical, infrared, and radio counterparts to each ChIcAGO source.
   (a) The U.S. Naval Observatory B Catalog, version 1.0 (USNO B1; Monet et al. 2003), Two Micron All Sky Survey (2MASS) Point Source Catalog (PSC; Skrutskie et al. 2006), and Galactic Legacy Infrared Mid-Plane Survey Extraordinaire (GLIMPSE) I and II catalogs (Benjamin et al. 2003) are accessed to obtain a list of all optical and infrared sources within 4″ of the ChIcAGO source's `wavdetect` position.
   (b) Small-sized (6′ × 6′) image cutouts, centered on the ChIcAGO source's `wavdetect` position, are obtained from the 2nd Digitized Sky Survey (Red: DSS2R, and Blue: DSS2B; McLean et al. 2000), 2MASS, and the GLIMPSE I and II surveys. A 30′ by 30′ radio image cutout is obtained from the Sydney University Molonglo Sky Survey (SUMSS; Bock et al. 1999). Examples of all the image cutouts can be found in Figures 4 and 5.

[21] The HRC instrument has very poor spectral resolution, so this and the following step are not conducted on those data sets.

ChIcAGO MAP first generates an image of the AGPS source as originally detected by the gas imaging spectrometer (GIS; Ohashi et al. 1996) on board *ASCA*. The GIS has a circular field of view with a 50′ diameter. The left image of Figure 1 shows the *ASCA* GIS detection of the AGPS source AX J144701–5919. We have chosen AX J144701–5919 as the example source for illustrating the output of ChIcAGO MAP because it was the first AGPS source observed with *Chandra* as part of the ChIcAGO survey, and it is also an interesting source with a bright counterpart (as demonstrated by its identification as an X-ray emitting Wolf–Rayet (WR) star in Anderson et al. 2011).

ChIcAGO MAP reprocesses all of the *Chandra* observations, both ACIS and HRC, using the CIAO `chandra_repro` script, which creates a new level = 2 event file and bad pixel file. The *Chandra* ACIS data are filtered to only include events with energies in the range 0.3–8.0 keV in order to avoid high-energy and cosmic ray particle backgrounds.

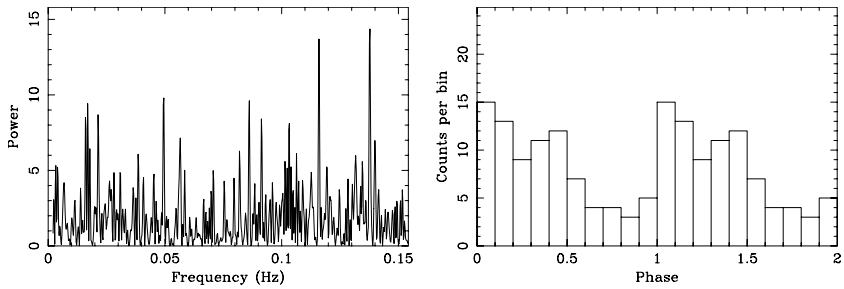

Figure 3. Power spectrum and folded light curve resulting from a Z_1^2 statistical search for periodicity from AX J144701–5919 as output by ChIcAGO MAP. Left: the power spectrum (power vs. frequency (Hz)) of AX J144701–5919. The power spectrum peaks at a value of $Z_1^2 = 14.4$ at a frequency of 0.1378 Hz. The probability of this power being random noise is 0.16. It is therefore unlikely to be a real signal. Right: the folded light curve (counts per bin vs. phase) that has been folded at 0.1378 Hz.

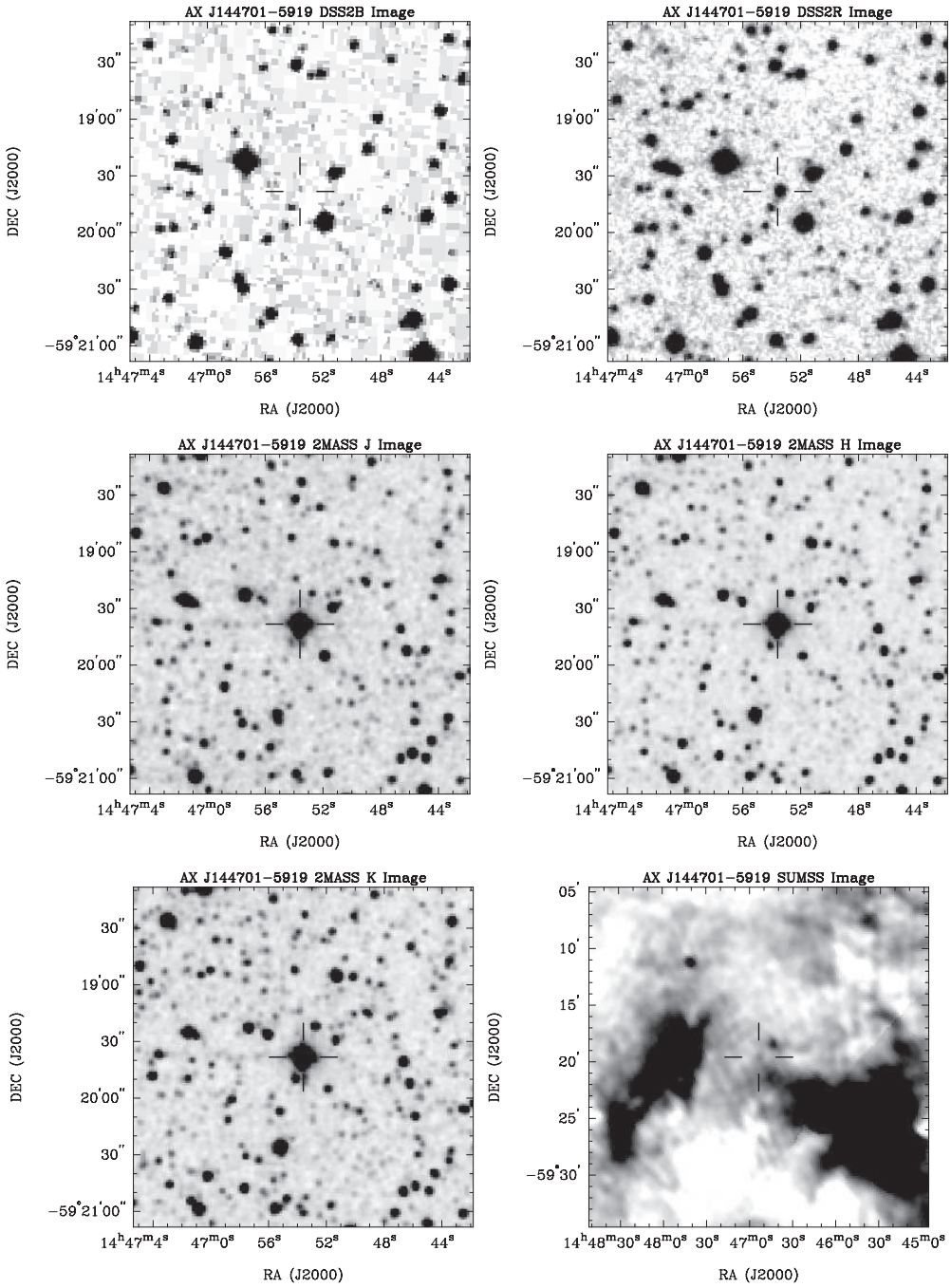

Figure 4. DSS2B, DSS2R, 2MASS, and SUMSS image cutouts of the region surrounding the AGPS source AX J144701–5919, which has been localized by *Chandra*, as output by ChIcAGO MAP. In all images the *Chandra* position of AX J144701–5919 is indicated by a black crosshair. The survey name and filter band of each image cutout are listed at the top of each plot.

We have chosen to optimize ChIcAGO MAP for the detection of point sources as our short *Chandra* observations (<10 ks) are not very sensitive to extended sources. ChIcAGO MAP uses the `CIAO` wavelet detection algorithm, `wavdetect`, which we have set to search for all sources with wavelet scales of radii of 1, 2, 4, 8, and 16 pixels. This does, however, introduce a source selection bias as it is possible that AGPS sources that were unresolved with the *ASCA* point-spread function (PSF) could be extended and therefore resolvable with *Chandra*. Rerunning ChIcAGO MAP using `wavdetect` with larger scales more appropriate for extended sources or using the `CIAO` Voronoi tessellation and percolation source detection algorithm `vtdetect` (Ebeling & Wiedenmann 1993) could be conducted in the future to detect extended sources in the ChIcAGO *Chandra* images.

ChIcAGO MAP utilizes `wavdetect` to detect all sources within 3′ of the original *ASCA* position (for example, see the *Chandra* detection of AX J144701–5919 in the right image of Figure 1). This search radius is based on the position accuracy and spatial resolution of *ASCA* and therefore is designed to ensure that the majority of contributing X-ray sources are encompassed. (However, it is also possible that there are associated X-ray sources beyond 3′ from the AGPS position. This could be due to the inaccuracy of the *ASCA* positions of those sources that are blended or near the edge of the field of

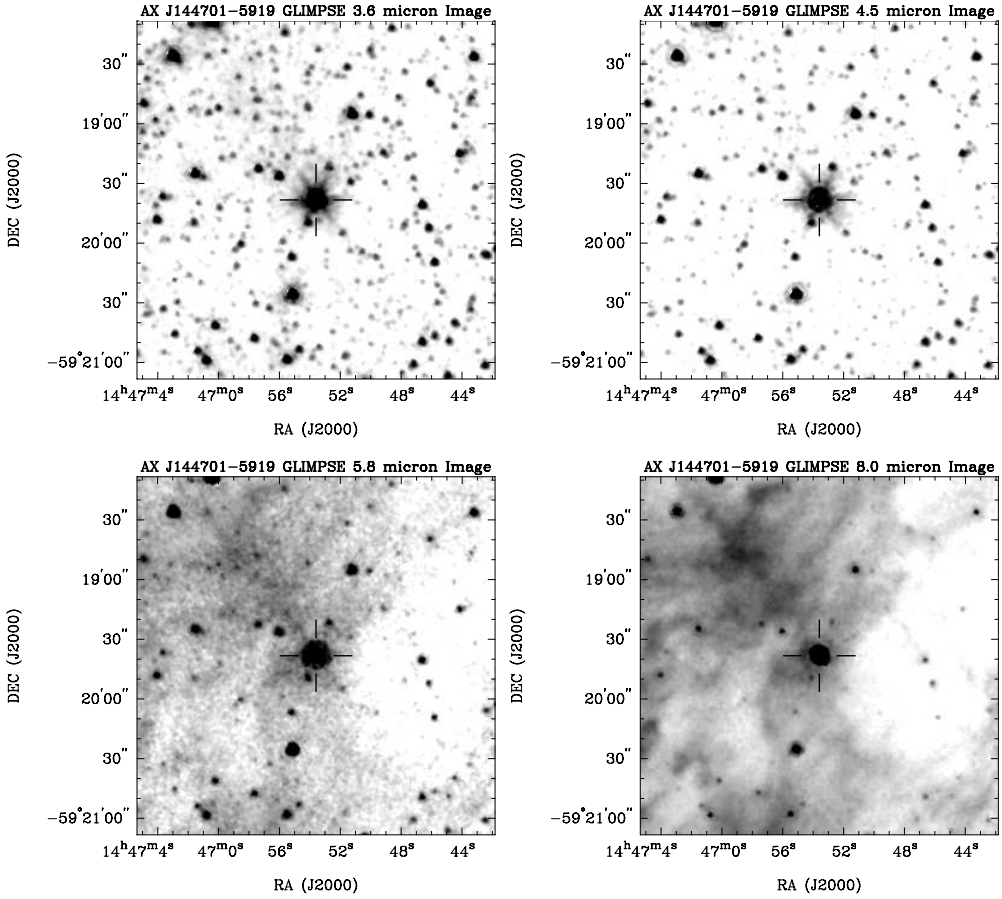

Figure 5. As for Figure 4, but showing the GLIMPSE 3.6, 4.5, 5.8, and 8.0 μm bands.

view. This is further explored in Section 3.1 and Appendix B.) In many cases more than one X-ray source could have been contributing to the total X-ray flux from an AGPS source originally detected with *ASCA*. (Note this is not the case for the example of AX J144701–5919.) The positional accuracy of `wavdetect` has been well investigated and tested in previous *Chandra* surveys (e.g., ChaMPlane; Hong et al. 2005).

The position of each ChIcAGO source as output by `wavdetect` is obtained, and Equation (5) of Hong et al. (2005) is used to calculate the 95% confidence position error circle.[22] This `wavdetect` error is then added in quadrature to the absolute astrometry error of *Chandra* to obtain the total position error of each ChIcAGO source.

The source regions used to calculate the total number of source counts, which are centered on the source position as output by `wavdetect`, have a radius equivalent to 95% of the PSF at 1.5 keV. The background subtraction is performed using an annulus whose size is between two and five times the above 95% PSF radius, centered on the source position. Given the low number of counts detected, usually <100, the 1σ lower and upper confidence limits of the total number of counts are calculated using the Gehrels (1986) statistics. The following energy-based analysis is then performed on the ACIS-S observations. The total number of counts are calculated for the 0.3–8.0, 0.5–2.0, and 2.0–8.0 keV energy ranges. ChIcAGO MAP then uses the extracted ACIS-S counts and corresponding energies to calculate the 25%, 50%, and 75% photon fractions (E_{25}, E_{50}, and E_{75}), the energies below which 25%, 50%, and 75% of the photon energies are found, respectively. These median (E_{50}) and quartile (E_{25} and E_{75}) values can immediately characterize the hardness of a source without using conventional hardness ratios, which are not versatile enough to account for diverse X-ray spectral types in the Galactic plane. These quartile fractions can then be used to employ quantile analysis (Hong et al. 2004), which uses a quantile based color–color diagram to classify spectral features and shapes of low-count sources (see Section 2.3.1).

The `CIAO` tool `specextract` is also run on the ACIS-S detected ChIcAGO sources to generate source and background spectrum files and their corresponding RMF and the ARF. These files are used to perform spectral interpolation with quantile analysis and to conduct spectral modeling and fitting with the `CIAO` package `Sherpa`. Further details on the spectral investigations of the ChIcAGO sources can be found in Section 2.3.

ChIcAGO MAP then performs a timing analysis on all the ChIcAGO sources detected with either the ACIS or HRC instrument to search for evidence of short-term variability and periodicity. In each case a light curve is extracted using `dmextract` where the counts are divided into eight bins (for example, see Figure 2). The Gehrels approximation to confidence limits for a Poisson distribution is used to estimate the errors as there are <20 X-ray counts in each bin. The χ^2 statistics are adopted to test for variability (for example, see Gaensler & Hunstead 2000). (It should be noted that as `dmextract` uses the upper (larger)

[22] This equation was constructed by running `wavdetect` on ACIS-I and ACIS-S data. It is therefore unknown whether this position error equation is applicable to the positions calculated from running `wavdetect` on HRC data sets. However, since the `wavdetect` algorithm is not instrument specific, it is likely that this equation estimates reasonable errors for sources detected in HRC observations.

Gehrels confidence limit to estimate the count rate errors, the resulting χ^2 output by ChIcAGO MAP may be underestimated.) For seven degrees of freedom, $\chi^2 \gtrsim 24.3$ is required for a source to be considered variable at 99.9% confidence.

After correcting the photon arrival times to the solar system barycenter, the target source is then investigated for evidence of periodicity using the Z_n^2 test (Buccheri et al. 1983), equivalent to the Rayleigh statistic when n, the chosen number of harmonics, is set to 1. ChIcAGO MAP uses $n = 1$ for the sake of simplicity and because such a test is sensitive to sinusoidal distributions. Z_1^2 has a probability density function equivalent to the χ^2 statistic with two degrees of freedom. ChIcAGO MAP searched for periodicity down to 6.48 s (twice the frame time resolution; Weisskopf et al. 2003) for sources detected with ACIS and down to 0.01s for sources detected with HRC.[23] A power spectrum (power versus frequency) and folded light curve (counts per bin versus phase) for each source are generated, predicting the pulsed frequency of the highest Z_1^2 power and the probability that this power was random noise for a given number of trials (for example, see Figure 3). A 99.9% confidence was required for a source to have a significant level of periodicity, which corresponds approximately to $Z_1^2 \gtrsim 26$ and $Z_1^2 \gtrsim 36$ for ACIS and HRC observations, respectively.

It is also possible that many of the AGPS sources are transient or undergo long-term variability and so have changed significantly in flux since the original *ASCA* observations. The detailed analysis of any periodic, variable, and transient sources is beyond the scope of this paper. We only flag those sources that may fit into one of the above categories for the purpose of future investigations.

The next step in the ChIcAGO identification process is to search for multiwavelength counterparts to the ChIcAGO sources. ChIcAGO MAP accesses the USNO B1 (visual magnitude bands B, R, and I; Monet et al. 2003), the 2MASS PSC (near-infrared magnitude bands J, H, and K_s; Skrutskie et al. 2006), and the GLIMPSE I and II Spring '07 Catalogs (highly reliable) and Archives (more complete, less reliable; infrared magnitude bands 3.6, 4.5, 5.8, and 8.0 μm; Benjamin et al. 2003) to obtain a list of all the optical and infrared sources within 4″ of the `wavdetect` position of each ChIcAGO source. The information extracted from these surveys includes the position of the source, the offset from the *Chandra* position, and the magnitudes listed in the given survey or data set.[24]

Small-sized image cutouts (6′ × 6′) from optical and infrared surveys, centered on the ChIcAGO source `wavdetect` position, are also downloaded to enable a visual inspection of likely counterparts and their surrounding environments. The B and R magnitude band images are obtained from DSS2B and DSS2R (McLean et al. 2000), and the J, H, and K magnitude band images are obtained from 2MASS. Image cutouts of infrared magnitude bands 3.6, 4.5, 5.8, and 8.0 μm are obtained from the GLIMPSE I and II, version 3.5, surveys.[25] A 30′ by 30′ image cutout of the 843 MHz radio sky is also generated from SUMSS, which is a survey conducted with the Molonglo Observatory Synthesis Telescope (MOST) and has a resolution of $43'' \times 43'' \, cosec \, |\mathrm{dec}|$ (Bock et al. 1999).[26] An example of all the image cutouts generated by ChIcAGO MAP for AX J144701–5919 can be seen in Figures 4 and 5.

2.3. ChIcAGO Source Spectral Investigation

Deducing the best spectral model fit to the ChIcAGO sources is difficult using standard X-ray spectral fitting techniques because of the small number of X-ray source counts detected in the *Chandra* observations (usually <100). We therefore implement two different techniques for predicting the best spectral parameters for the brighter (>20 X-ray counts) ChIcAGO sources. The first technique is "quantile analysis" (Hong et al. 2004), which has recently been developed to address some of the problems associated with spectral modeling of sources with low number statistics. Quantile analysis allows for the interpolation of likely spectral shapes of X-ray sources with as few as 10 counts. The second technique is utilizing the `CIAO` spectral fitting tool `Sherpa` to obtain best-fit spectral parameters using Cash (1979) statistics. These statistics are based on Poisson distributed data and are therefore ideal for modeling spectra with a limited number of source counts. Both methods are described in detail below.

2.3.1. Quantile Analysis

Quantile analysis uses predetermined fractions of the total number of energy source counts, such as the median (E_{50}) and quartile energies (E_{25} and E_{75}), to construct a quantile-based phase space that can be overlaid with grid patterns of common spectral models. This quantile phase space is more sensitive to the wide range of Galactic X-ray sources than those constructed from conventional hardness ratios. This is because there is no count-dependent sensitivity bias toward any spectral type, which is inherent in the choice of subenergy bands in the conventional spectral hardness or X-ray color analysis. In the ChIcAGO survey, quantile analysis is adopted to calculate potential spectral shapes of the ChIcAGO sources.

The ACIS-S detected ChIcAGO sources selected for quantile analysis have >20 (net) X-ray counts in the 0.3–8.0 keV energy band, as these are likely to be bright enough to be the original AGPS sources (see Section 2.1). The net counts were obtained by summing the total number of counts inside a source region that is six times the error radius in size and subtracting the background normalized counts calculated from an annulus that has an outer radius of ∼15″ with the source region subtracted. The three quartiles (E_{25}, E_{50}, and E_{75}) and their corresponding errors were calculated as outlined by Hong et al. (2004).

The quantile phase space, suggested by Hong et al. (2009, see their Figure 4) and used to calculate the likely spectral shapes, was constructed for each ChIcAGO source. This phase space consists of the normalized logarithmic median $(\log(E_{50}/E_{\mathrm{low}})/\log(E_{\mathrm{high}}/E_{\mathrm{low}}))$ and the normalized quartile ratio $(3 \times (E_{25} - E_{\mathrm{low}})/(E_{75} - E_{\mathrm{low}}))$, where $E_{\mathrm{low}} = 0.3$ keV and $E_{\mathrm{high}} = 8.0$ keV, equivalent to the energy range explored. The logarithmic median phase space takes advantage of the higher sensitivity at low energies in typical X-ray telescope CCDs, while keeping the spectral discernibility more or less uniform throughout the full range of the phase space. In order to compensate for the spatial change of the detector response in

[23] The lower limit of 0.01s for the HRC observations is chosen because a wiring error in the detector degrades the time resolution accuracy from 16 μs to the mean time between events. See http://cxc.harvard.edu/proposer/POG/html/chap7.html#sec:hrc_anom.

[24] The catalog information is downloaded via a generic URL from the VizieR Service (http://vizier.cfa.harvard.edu/viz-bin/VizieR) and the NASA/IPAC Infrared Science Archive (http://irsa.ipac.caltech.edu/).

[25] http://irsa.ipac.caltech.edu/data/SPITZER/GLIMPSE/

[26] The images from the DSS2R, DSS2B, 2MASS, and SUMSS surveys are downloaded using a generic URL from the virtual observatory SkyView, which is a service of the Astrophysics Science Division at NASA/GSFC and the High Energy Astrophysics Division of the Smithsonian Astrophysical Observatory (SAO), http://skyview.gsfc.nasa.gov/.

Chandra/ACIS, the RMF and the ARF appropriate to the observed location of each ChIcAGO source in the CCD are calculated using the CIAO tools.

The data points of the ChIcAGO sources in the quantile diagram were compared with simple power-law and thermal bremsstrahlung spectral models to extract the most plausible spectral parameter values for each source. It should be noted that quantile analysis cannot evaluate which model is more likely unless the estimated parameters of the model turn out to be unphysical (e.g., $\Gamma > 4$). The estimate of the spectral parameters is limited to $-2 \leqslant \Gamma \leqslant 4$ for a power-law model and 0.1 keV $\leqslant kT \leqslant$ 10 keV for a bremsstrahlung model. The explored extinction ($N_{\rm H}$) covers the range 0.01–100 $\times$ 10^{22} cm^{-2}. If the data point for a source in quantile phase space sits outside of the model grid set by these parameter ranges, the model is considered incompatible with the observed spectrum of the source. The quantile errors allow the spectral parameter uncertainties to be calculated for each ChIcAGO source (Hong et al. 2004).

2.3.2. Spectral Modeling

The spectral modeling of the ChIcAGO sources was conducted using the CIAO 4.5 spectral fitting package Sherpa with the statistics set to the XSpec (Dorman & Arnaud 2001) implementation of the Cash (1979) statistics. Cash statistics apply a maximum likelihood ratio test that can be performed on sources with a low number of source counts per bin. We chose to restrict all spectral modeling to those ChIcAGO sources with >50 X-ray counts as attempted modeling of those sources with fewer counts usually did not converge.

Cash statistics cannot be performed on a background-subtracted spectrum. The source and background spectrum must instead be modeled simultaneously. However, in the case of the *Chandra* observations of ChIcAGO sources the background is extremely low and cannot be described by a generic spectral model. As a result, attempting to model the background spectrum does not improve the overall spectral fit. We therefore only model the source spectrum of the ChIcAGO sources.

Both an absorbed power-law model and an absorbed thermal bremsstrahlung model are applied to the ChIcAGO source spectra so that they can be directly compared to the quantile analysis spectral interpolation results. The parameter errors are calculated using the Sherpa "projection" function, which estimates the 1σ confidence intervals. The absorbed and unabsorbed fluxes (plus errors) are calculated using the Sherpa function "sample_flux," which is new to CIAO 4.5. The overall goodness of fit measure is defined by the value of the Cash statistic divided by the number of degrees of freedom and should be of the order of one.

2.4. Multiwavelength Follow-up Observations

While the X-ray morphology and spectrum can provide information on the nature of a ChIcAGO source, the key to identification is usually through an extensive multiwavelength follow-up campaign. ChIcAGO MAP identifies the possible optical and infrared counterparts in existing multiwavelength Galactic plane surveys. There are, however, many cases where the counterparts are too faint to be detected in these surveys because of the high absorption in the Galactic plane. It is also possible that the high object density in the Galactic plane could result in confusion with nearby sources. In these cases, further optical and infrared photometric observations were conducted with large telescopes to obtain detections of faint counterpart candidates and to separate likely blends. If the first photometric observing attempt was unsuccessful at detecting or separating a counterpart candidate, then deeper imaging using longer exposure times was conducted. Those X-ray sources that remain undetected at optical and infrared wavelengths will need to be further investigated in the X-ray band or at other wavelengths.

The radio wavelength band is also a useful diagnostic for identifying X-ray sources in the Galactic plane. Comparing the X-ray source positions with radio surveys can indicate if there is a likely radio counterpart or whether the X-ray source lies in a diffuse region of radio emission in the Galactic plane. Interferometric radio observations of a small subset of ChIcAGO sources were obtained in order to resolve confusing regions of radio emission and to allow for the detection or confirmation of compact radio counterparts.

2.4.1. Optical and Near-infrared Observations with Magellan

The optical and NIR photometric observations presented in this paper were obtained using instruments on the 6.5 m, Baade Magellan telescope, located at Las Campanas Observatory, Chile. The NIR photometry, 1–2.5 μm, was obtained using Persson's Auxiliary Nasmyth Infrared Camera (PANIC; Martini et al. 2004; Osip et al. 2008) on Baade. PANIC was used primarily to detect the counterparts of ChIcAGO sources with no cataloged counterparts or to utilize this instrument's high angular resolution to eliminate possible blendings. Observations were obtained in the J, H, and K_s photometric bands, using short exposures (10–30 s) that were dithered to account for the high sky background inherent in NIR observations.

The PANIC NIR imaging data were reduced using the Image Reduction and Analysis Facility (IRAF; Tody 1986, 1993) and the PANIC Data Reduction Package for IRAF (Martini et al. 2004), taking into account the corresponding darks, sky flats, and bad pixel maps obtained for each respective night. The absolute astrometry for the PANIC observations was derived using the 2MASS PSC and the Graphical Astronomy and Image Analysis Tool (GAIA; Draper et al. 2009). The positional accuracy of the 2MASS PSC is 0.″1 (1σ; Skrutskie et al. 2006), and since there are usually many 2MASS sources in the field, a similar order of astrometric accuracy at the target positions was reached. SExtractor (Bertin & Arnouts 1996) was used for source detection, and the calibration of the photometry was performed by applying 2MASS PSC photometry to known 2MASS sources in the target fields. No correction to the atmospheric extinction was applied as this effect is very small in the NIR ($\sim$0.06 magnitudes in the H band). The errors were obtained by comparing the NIR magnitudes with 2MASS PSC magnitudes and reflected average deviations from the 2MASS catalog magnitudes.

Optical photometric observations of the counterparts were obtained utilizing several Magellan instruments depending on availability. These included the Inamori Magellan Areal Camera and Spectrograph (IMACS; Dressler et al. 2006; Osip et al. 2008) and the Raymond and Beverly Sackler Magellan Instant Camera (MagIC; Osip et al. 2008) on the Baade telescope. These instruments provide access to different photometric filters including Bessel B, V, and R and CTIO I.

The IMACS B, V, R, and I imaging data were reduced using IRAF, in which the data were trimmed, overscan corrected, and flat fielded. A dark current subtraction was not applied since the dark images showed it to be negligible. Standard stars were observed throughout in several bands, although the weather

during some of the observing nights varied. The absolute astrometry was again computed using GAIA with comparisons to the USNO B1 Catalog or the 2MASS PSC. The photometry of each counterpart was calculated using SExtractor and was calibrated using the USNO B1 Catalog.

MagIC observations were obtained in the *V*, *R*, and *I* bands. Short 30 s exposures were obtained in each filter, which were later combined to make sure that the brighter stars (used for astrometric referencing) were not saturated. These data were then reduced following standard procedures in IRAF: overscan subtraction for each amplifier, flat fielding using dome flats, and separate exposures combined. The astrometry was applied by referencing the observations to the 2MASS PSC, resulting in an rms residual of 0.″1 in each coordinate. Photometric calibration was derived using observations of the Stetson (2000) standard fields. The measured photometry for the air mass terms appropriate to Las Campanas Observatory were corrected, and the zero points with scatters of 0.02 mag in each filter were obtained. Similar to the PANIC and IMACS observations, the photometry of each counterpart was then measured using SExtractor.

2.4.2. Radio Follow-up and ATCA Observations

Radio survey data already exist for all of the AGPS source regions via the first and second epoch Molonglo Galactic Plane Surveys at 843 MHz (MGPS1 and MGPS2, respectively, $43'' \times 43'' \, cosec \, |\mathrm{dec}|$ resolution; Green et al. 1999; Murphy et al. 2007), the 90 cm Multi-configuration Very Large Array Survey of the Galactic Plane (42″ resolution; Brogan et al. 2006), the Multi-Array Galactic Plane Imaging Survey at 1.4 GHz (MAGPIS, 6″ resolution; Helfand et al. 2006), and the Very Large Array (VLA) Galactic Plane Survey at 1.4 GHz (VGPS, 1′ resolution; Stil et al. 2006). To search for possible radio counterparts, we first visually inspected the above surveys at the position of each ChIcAGO source. Any coincident radio emission was then categorized (see Section 3.4).

Follow-up ATCA observations were conducted to identify the nature of any radio counterparts to the ChIcAGO sources found through this visual inspection. The ATCA was also used to resolve any diffuse radio emission surrounding a ChIcAGO source, allowing the detection of any underlying compact radio counterpart. The high-resolution ATCA observations were instrumental in confirming a positional coincidence between the radio counterpart and the *Chandra* position of the ChIcAGO source to measure accurate radio fluxes and spectral indices, to broadly characterize variability with respect to earlier epochs, and to constrain the object's spatial extent. The *Chandra* positions of 10 ChIcAGO sources were observed with the ATCA on 2008 January 21 and on 2008 April 11. Each source was observed for ∼1 hr at each of 1.4, 2.4, 4.8, and 8.6 GHz over a 12 hr period with a 6 km baseline configuration.

3. RESULTS

3.1. Chandra Results

We present results on 93 AGPS sources that have been observed with *Chandra* as part of the ChIcAGO survey. In many cases more than one source was detected within 3′ of the original AGPS source positions, so as mentioned in Section 2.2, we will refer to these all as ChIcAGO sources. We therefore detected a total of 253 ChIcAGO sources in these 93 *Chandra* observations. The naming convention we have adopted is to call each source by the AGPS coordinate name, using ChI as the prefix, with a suffix between 1 and *i*, where *i* is equal to the number of sources detected in the 3′ field. (The source name order is based on the order that wavdetect detected and output the sources in ChIcAGO MAP.) For example, two ChIcAGO sources, ChI J165646–4239_1 and ChI J165646–4239_2, were detected with *Chandra* in the vicinity of the AGPS source AX J165646–4239. These two ChIcAGO sources are the black dots in Figure 6. The *ASCA* GIS detection of AX J165646–4239 is overlaid on Figure 6 in the form of contours, demonstrating that both ChI J165646–4239_1 and ChI J165646–4239_2 may have contributed to the X-ray emission originally detected for this source in the AGPS.

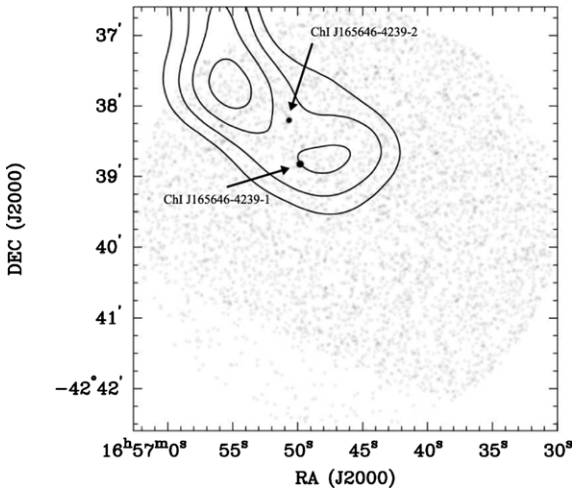

Figure 6. 3′ radius field of view of the *Chandra* observation of the AGPS source AX J165646–4239, which is centered on the position of AX J165646–4239 as listed by Sugizaki et al. (2001). Two ChIcAGO sources, ChI J165646–4239_1 and ChI J165646–4239_2, which are black dots indicated by arrows, were detected with *Chandra* and are labeled. The black contours represent the smoothed *ASCA* GIS detection of AX J165646–4239 at 65%, 75%, 85%, and 95% of the peak count rate.

The *Chandra* observations of the 93 AGPS sources are summarized in Table 1. This information includes the observation identification, the date of the observation, instrument (ACIS-S or HRC-I), and the exposure time. Table 1 also lists the ChIcAGO sources detected by ChIcAGO MAP within 3′ of the *ASCA* position and their corresponding wavdetect position, the offset of this position from the original AGPS position, the 95% wavdetect and total ChIcAGO source position errors, the background-corrected net counts in the 0.3–8.0, 0.5–2.0, and 2.0–8.0 keV energy ranges,[27] and the median energy quartile (E_{50}) and quartile ratio ($3 \times (E_{25} - 0.3)/(E_{75} - 0.3)$) used in quantile analysis (see Section 2.3.1).

The variability analysis performed by ChIcAGO MAP detected only one ChIcAGO source, ChI J170444–4109_1, with a χ^2 exceeding the 99.9% short-term variability threshold ($\chi^2 = 80.6$). However, this variability is not real as the ACIS-S detection of ChI J170444–4109_1 fell in the chip gap between the CCDs. This resulted in its light curve displaying the *Chandra* spacecraft's built-in dither as the source moved on and off the chip at regular intervals.[28] No other ChIcAGO source

[27] The net counts were calculated separately for each energy range, so there are several cases where the total number of counts in the 0.3–8.0 keV energy range is slightly different than the sum of counts detected in the 0.5–2.0 and 2.0–8.0 keV energy ranges. These differences are due to rounding errors, as well as the exclusion of very soft counts that were detected between 0.3 and 0.5 keV. (The 0.3–0.5 keV energy range was excluded as the 0.5–2 keV energy band is more commonly used than the 0.3–2 keV energy band.)

[28] http://cxc.harvard.edu/ciao/why/dither.html

had a χ^2 exceeding the 99.9% confidence threshold for short-term variability or periodicity. This does not, however, rule out the possibility that some of these sources are periodic as the Z_1^2 period search technique is extremely limited for <200 X-ray counts.

Several faint ChIcAGO sources were detected with `wavdetect` in the *Chandra* observations that are not suspected of being significant contributors to the *ASCA* counts detected in the AGPS. (All these faint sources are included in Table 1.) In order to determine the detection significance of these sources, we independently calculated the probability of a false detection (Pfd) for each source based on the Poisson statistics. We expect there to be ∼10,0000 trials in a 3′ radius ACIS CCD field of view if a detection cell size of a 1″ radius circle is assumed with two-dimensional Nyquist sampling (Weisskopf et al. 2007). (A generic detection cell size of 1″ for this detection significance calculation was suggested by Weisskopf et al. 2007 since the `CIAO` source detection algorithms usually use a detection cell size of between 40% and 80% of the PSF at a given energy.[29]) Pfd $= 10^{-5}$ implies that there is one false source in the 3′ radius ACIS *Chandra* field. The probability of a false detection was calculated for each source (see footnote 13 in Kashyap et al. 2010). Only 11 sources (out of 253) have a Pfd $> 10^{-5}$, but all have Pfd $< 7 \times 10^{-4}$. Several of these sources also have a likely optical and/or infrared counterpart, increasing the significance of these detections. As this technique for calculating source significance is highly theoretical (e.g., the effective detection cell size of ACIS is likely to be slightly smaller than the 1″ radius circles), without any consideration for possible counterparts, we will include these 11 marginally significant sources in Table 1 (denoted by an asterisk in the first column).

Several of the sources detected in these observations have also been listed in the *Chandra* Source Catalog (CSC; Evans et al. 2010). We assume that a CSC source and a ChIcAGO source are the same if the separation between their two positions is less than the quadratic sum of their 95% error radii plus a constant term of 0.″7, which accounts for the 95% absolute astrometry error of *Chandra* assuming the errors follow a Gaussian distribution[30] (see Equation (6) of Hong et al. 2005). We have conducted the same comparison with the fifth public release of the Second *XMM-Newton* Serendipitous Source Catalogue (2XMMi-DR3; Watson et al. 2009).[31] The CSC and 2XMMi-DR3 names that correspond to any ChIcAGO sources are listed in Table 1. Further analysis of the *XMM* observations will be conducted in future work.

The purpose of the ChIcAGO survey is to study those X-ray sources detected in the ChIcAGO *Chandra* observations that fall within the flux range of the AGPS sources ($F_x \sim 10^{-13}$ to 10^{-12} erg cm^{-2} s^{-1}). In 62 out of the 93 AGPS sources observed with *Chandra*, ChIcAGO MAP found 74 sources with >20 X-ray counts that fall within the investigated 3′ field of view that is centered on the AGPS positions. For the purposes of this study we will focus on these 74 ChIcAGO sources, listed in Table 2, as they are approximately within the original AGPS flux range. The detailed analysis of those 179 ChIcAGO sources with <20 counts will be deferred to future work. There were six AGPS sources where no ChIcAGO source was detected by *Chandra*: AX J165951–4209, AX J175331–2538, AX J180816–2021, AX J183607–0756, AX J185905+0333, and AX J191046+0917. At least three of these AGPS sources, AX J180816–2021, AX J185905+0333, and AX J191046+0917, may be transient given how bright they were in the original *ASCA* detections (Sugizaki et al. 2001). The remaining 25 AGPS fields observed with *Chandra* only have faint sources with <20 X-ray counts. There are also six AGPS sources, AX J144519–5949, AX J151005–5824, AX J154905–5420, AX J194310+2318, AX J194332+2323, and AX J195006+2628, where multiple ChIcAGO sources detected in each region (with $\lesssim$30 X-ray counts) sum to $\gtrsim$60 counts, which is close to the number of X-ray counts that were expected to be detected with *Chandra* from each AGPS source (see Section 2.1). Many of the ChIcAGO sources in these fields also have optical and/or infrared counterparts and may therefore be members of star clusters (see Section 4.1 for further discussion).

The contribution of X-ray emission beyond the 3′ search radius was also investigated using `wavdetect` to identify all the point sources with >20 X-ray counts in the *Chandra* observations that lie between 3′ and 5′ from the original AGPS position. Only 14 X-ray point sources were found in the 3′–5′ annulus surrounding 11 AGPS sources, which demonstrates that the 3′ search radius used by ChIcAGO MAP is reasonable and has likely allowed us to identify the majority of ChIcAGO sources. These 14 X-ray point sources are further discussed in Appendix B, where we explore the likelihood of whether they could be associated with their nearby AGPS source.

3.2. Quantile Analysis and Spectral Modeling Results

Quantile analysis and spectral modeling using Cash statistics were both techniques used to infer the most likely absorbed power-law and absorbed thermal bremsstrahlung spectra of the bright ChIcAGO sources detected by ACIS-S.[32] The spectral parameters and the absorbed and unabsorbed X-ray fluxes for absorbed power-law and absorbed thermal bremsstrahlung models are listed in Tables 3 and 4, respectively. There are also six HRC-I detected ChIcAGO sources with >20 counts (ChI J144042–6001_1, ChI J153818–5541_1, ChI J163252–4746_2, ChI J163751–4656_1, ChI J165420–4337_1, and ChI J172642–3540_1) that are not included in Tables 3 and 4 as their X-ray observations do not contain any spectral information. The possible counterparts to these six sources are, however, explored in detail in Section 3.3.

There is no measure of goodness for the quantile-analysis-derived absorbed power-law and absorbed bremsstrahlung spectral parameters listed for the ChIcAGO sources in Tables 3 and 4. Instead, a spectral interpolation is classified as unreasonable if the resulting parameters are outside $-2 < \Gamma < 4$ for a power-law model and $0.1 < kT < 10$ keV for a bremsstrahlung model. These parameter limits can allow for the grouping of the ChIcAGO sources into existing categories that are based on the physical understanding of X-ray sources that emit in the *Chandra* energy range (0.3–8 keV). While these selection criteria explicitly exclude the identification of new types of X-ray sources with unusual spectra, such an investigation is beyond the scope of this work. In all cases, if one of the quantile analysis spectral interpolations was disregarded for a given ChIcAGO source, the other is reasonable when considering the above criteria.

[29] See the `CIAO` detect manual at http://cxc.harvard.edu/ciao/download/doc/detect_manual/.

[30] The *Chandra* astrometric error is included in this calculation as the source positions listed in the CSC can be obtained from more than one data set.

[31] http://xmmssc-www.star.le.ac.uk/Catalogue/2XMMi-DR3/

[32] ChIcAGO sources with >20 X-ray counts for quantile analysis and >50 X-ray counts for spectral modeling.

Table 2
ChIcAGO Sources with >20 X-Ray Counts and Their Infrared Properties

ChIcAGO Source	NIR[a]	2MASS Name	Near-Infrared Magnitudes			PANIC Date	GLIMPSE Name	GLIMPSE Magnitudes[b]			
ChI	Data	2MASS J	J	H	K	(yyyy-mm-dd)	SSTGLMC G	$M_{3.6}$	$M_{4.5}$	$M_{5.8}$	$M_{8.0}$
J143148–6021_3	P		17.1 ± 0.1	16.3 ± 0.1	15.6 ± 0.1	2005-05-12					
J144042–6001_1	M	14403847-6001368	8.28 ± 0.02	7.88 ± 0.02	7.70 ± 0.02		316.1785+00.0060	7.65 ± 0.06	7.63 ± 0.05	7.64 ± 0.03	7.59 ± 0.03
J144519–5949_2	M	14452143-5949251	14.12 ± 0.04	10.95 ± 0.03	9.30 ± 0.03						
J144547–5931_1	M	14454369-5932050	9.23 ± 0.04	8.10 ± 0.03	7.52 ± 0.02		316.9656+00.1864	7.07 ± 0.05	6.89 ± 0.04	6.708 ± 0.03	6.63 ± 0.02
J144701–5919_1	M	14465358-5919382	8.93 ± 0.02	7.60 ± 0.04	6.82 ± 0.02		317.1882+00.3106	$6.70 \pm 0.09^{\dagger}$	$6.33 \pm 0.09^{\dagger}$	5.574 ± 0.03	5.32 ± 0.03

Notes. The `wavdetect` position of ChI J165646–4239_1 and the position of the quoted 2MASS source agree within 4σ. We have listed this 2MASS source as a possible counterpart as it is considered to be the same as the quoted GLIMPSE source, which does agree within 3σ of the `wavdetect` position. The quoted NIR magnitudes of ChI J181116–1828_2 and ChI J185643+0220_2, obtained with PANIC, are limits due to the counterparts being blended. The H-band PANIC observation of ChI J194152+2251_2 took place on 2007-07-31, whereas the other bands were observed on 2007-07-29.

[a] Data from which the counterpart near-infrared magnitudes were obtained. M = 2MASS Point Source Catalog (Skrutskie et al. 2006), P = PANIC Magellan observations. If three letters are listed this indicates that the magnitudes were obtained from different data sets. This order corresponds to the J, H and K_s magnitude order. Those data sets marked with * are likely blended or, particularly in the case of ChI J194152+2251_2, perhaps extended. Those data sets marked with ** means that the counterpart has a low sigma detection of $>1.5\sigma$ for the respective background plus rms estimate.

[b] $M_{3.6}$, $M_{4.5}$, $M_{5.8}$, and $M_{8.0}$ refer to the counterpart infrared magnitudes at 3.6, 4.5, 5.8, and 8.0 μm, respectively. Those magnitudes marked with † are from the GLIMPSE archives (more complete, less reliable) rather than the catalogs (which are more reliable). In these cases the GLIMPSE archive source's names begin with SSTGLMA G.

(This table is available in its entirety in a machine-readable form in the online journal. A portion is shown here for guidance regarding its form and content.)

Table 3
Quantile Analysis Power-law Interpolation and Cash Statistics Power-law Spectral Fit to ACIS *Chandra* Detections of the ChIcAGO Sources

ChIcAGO Source	Quantile Absorbed Power-law Interpolation[a]					Cash Statistics Absorbed Power-law Fit[b]				
ChI	Γ	$N_{\rm H}$	$F_{x,\rm abs}$	$F_{x,\rm unabs}$	$\chi^2_{\rm red}$	Γ	$N_{\rm H}$	$F_{x,\rm abs}$	$F_{x,\rm unabs}$	C
J143148–6021_3	$0.91^{+0.44}_{-0.35}$	$0.61^{+0.54}_{-0.34}$	9.12 ± 0.75	10.93 ± 0.90	0.3	$0.70^{+0.26}_{-0.25}$	$0.42^{+0.20}_{-0.17}$	$9.85^{+1.35}_{-1.15}$	$11.17^{+1.29}_{-1.31}$	0.5
J144547–5931_1						$4.98^{+1.06}_{-0.94}$	$4.53^{+1.25}_{-1.07}$	$2.38^{+0.45}_{-0.59}$	$1802.71^{+4414.31}_{-1388.60}$	1.0
J144701–5919_1						$3.39^{+0.67}_{-0.61}$	$2.70^{+0.73}_{-0.64}$	$5.55^{+1.15}_{-1.90}$	$177.46^{+157.69}_{-139.42}$	0.6
J150436–5824_1	$-0.37^{+0.17}_{-0.00}$	$0.01^{+0.06}_{-0.00}$	8.45 ± 0.71	8.47 ± 0.71	0.9	$-0.05^{+0.28}_{-0.27}$	$0.49^{+0.32}_{-0.27}$	$8.46^{+1.07}_{-0.84}$	$9.03^{+1.05}_{-0.98}$	1.2
J154122–5522_1	$2.53^{+0.62}_{-0.49}$	$0.14^{+0.14}_{-0.11}$	2.50 ± 0.27	4.46 ± 0.49	0.6	$2.35^{+0.43}_{-0.39}$	$0.15^{+0.10}_{-0.09}$	$2.86^{+0.38}_{-0.46}$	$4.82^{+0.99}_{-1.22}$	1.0
J154557–5443_1	$2.98^{+1.30}_{-0.70}$	$0.29^{+0.19}_{-0.17}$	0.17 ± 0.04	0.56 ± 0.12						
J155035–5408_3	$2.73^{+0.55}_{-0.46}$	$0.67^{+0.24}_{-0.21}$	2.90 ± 0.20	11.47 ± 0.80	0.9	$2.72^{+0.28}_{-0.27}$	0.61 ± 0.11	$2.88^{+0.36}_{-0.33}$	$11.33^{+3.17}_{-3.55}$	1.8
J155831–5334_1	$1.70^{+0.72}_{-0.63}$	$0.43^{+0.45}_{-0.34}$	3.62 ± 0.50	5.45 ± 0.76	0.4	$1.65^{+0.54}_{-0.49}$	$0.38^{+0.28}_{-0.22}$	$3.31^{+0.74}_{-0.63}$	$5.99^{+1.39}_{-2.16}$	1.0
J162011–5002_1	$0.88^{+1.00}_{-1.00}$	$2.50^{+2.8}_{-1.56}$	8.17 ± 1.11	11.73 ± 1.6	0.6	$0.75^{+0.83}_{-0.75}$	$2.59^{+2.02}_{-1.53}$	$7.62^{+2.09}_{-2.68}$	$12.82^{+1.50}_{-3.94}$	1.1
J162046–4942_1	$1.42^{+0.35}_{-0.31}$	$0.12^{+0.15}_{-0.10}$	3.35 ± 0.31	3.84 ± 0.35	1.4	$1.71^{+0.31}_{-0.29}$	$0.31^{+0.13}_{-0.11}$	$3.32^{+0.61}_{-0.53}$	$5.01^{+0.72}_{-0.85}$	2.7
J165105–4403_1	$0.84^{+0.37}_{-0.31}$	$0.34^{+0.36}_{-0.25}$	12.6 ± 1.03	14.19 ± 1.15	0.8	$0.97^{+0.28}_{-0.27}$	$0.58^{+0.22}_{-0.19}$	$13.42^{+1.59}_{-1.83}$	$16.43^{+2.16}_{-1.68}$	1.1
J165217–4414_1	$1.63^{+0.47}_{-0.49}$	$0.64^{+0.41}_{-0.34}$	5.97 ± 0.57	9.32 ± 0.9	0.7	$1.29^{+0.31}_{-0.29}$	$0.38^{+0.18}_{-0.15}$	$6.48^{+1.14}_{-1.06}$	$8.66^{+1.01}_{-1.56}$	0.9
J165646–4239_1						$3.93^{+0.40}_{-0.36}$	0.22 ± 0.06	$4.99^{+0.36}_{-0.39}$	$27.34^{+18.76}_{-13.30}$	2.8
J165646–4239_2	$1.49^{+0.79}_{-0.62}$	$0.31^{+0.48}_{-0.30}$	2.27 ± 0.30	2.98 ± 0.39	0.4	$1.28^{+0.44}_{-0.41}$	$0.22^{+0.21}_{-0.17}$	$2.37^{+0.49}_{-0.36}$	$3.18^{+0.35}_{-0.56}$	0.7
J165707–4255_1	$3.91^{+1.07}_{-1.25}$	$0.22^{+0.21}_{-0.20}$	2.5 ± 0.32	13.51 ± 1.73	2.1	$3.17^{+0.79}_{-0.60}$	$0.07^{+0.12}_{-0.07}$	$3.05^{+0.53}_{-0.59}$	$7.05^{+4.82}_{-2.67}$	2.6
J170017–4220_1	$-1.89^{+1.14}_{-0.10}$	$1.00^{+5.60}_{-0.99}$	19.25 ± 2.37	19.91 ± 2.45	1.0	$0.24^{+1.10}_{-0.98}$	$14.01^{+8.49}_{-6.85}$	$11.36^{+5.90}_{-7.08}$	$29.98^{+6.53}_{-8.94}$	1.0
J170052–4210_1						$4.89^{+1.98}_{-1.45}$	$0.37^{+0.31}_{-0.23}$	$0.81^{+0.23}_{-0.22}$	$32.64^{+152.63}_{-26.84}$	3.6
J170444–4109_1	$3.38^{+0.86}_{-0.65}$	$0.16^{+0.18}_{-0.13}$	9.01 ± 0.73	27.22 ± 2.21	1.7	$3.17^{+0.38}_{-0.35}$	0.23 ± 0.09	$8.35^{+1.04}_{-1.16}$	$28.45^{+14.82}_{-8.65}$	2.1
J170444–4109_2	$0.31^{+1.60}_{-1.37}$	$1.70^{+3.10}_{-1.69}$	2.10 ± 0.50	2.51 ± 0.59						
J170536–4038_1	$2.88^{+0.79}_{-0.63}$	$0.26^{+0.19}_{-0.15}$	6.54 ± 0.61	19.03 ± 1.79	1.0	$2.09^{+0.33}_{-0.31}$	0.14 ± 0.08	$8.50^{+1.05}_{-1.15}$	$12.81^{+2.24}_{-1.93}$	1.7
J171910–3652_2						$3.25^{+0.49}_{-0.44}$	$0.14^{+0.08}_{-0.07}$	$2.64^{+0.38}_{-0.29}$	$6.78^{+3.77}_{-2.33}$	3.3
J171922–3703_1	$-0.75^{+0.49}_{-0.55}$	$1.15^{+1.85}_{-1.03}$	6.83 ± 0.56	7.27 ± 0.60	0.6	$-0.26^{+0.41}_{-0.39}$	$2.19^{+1.12}_{-0.92}$	$5.79^{+1.10}_{-1.32}$	$7.09^{+0.84}_{-1.65}$	1.4
J172050–3710_1						$4.70^{+0.39}_{-0.37}$	$0.54^{+0.08}_{-0.07}$	$2.07^{+0.11}_{-0.18}$	$67.55^{+49.73}_{-32.05}$	1.8
J172550–3533_1	$0.14^{+1.93}_{-1.40}$	$6.60^{+11.9}_{-5.3}$	2.8 ± 0.43	4.11 ± 0.63	0.4					
J172550–3533_2	$3.28^{+1.49}_{-1.00}$	$0.38^{+0.38}_{-0.25}$	0.44 ± 0.06	2.28 ± 0.34	0.6					
J172550–3533_3	$3.17^{+1.11}_{-0.79}$	$0.28^{+0.30}_{-0.22}$	0.55 ± 0.09	2.11 ± 0.33						
J172623–3516_1	$2.94^{+2.04}_{-1.28}$	$0.46^{+0.84}_{-0.40}$	1.07 ± 0.16	4.44 ± 0.68	0.6	$1.63^{+0.52}_{-0.47}$	$0.13^{+0.17}_{-0.13}$	$1.64^{+0.61}_{-0.35}$	$2.49^{+0.41}_{-0.54}$	1.4
J172642–3504_1	$0.84^{+0.75}_{-0.70}$	$2.30^{+2.00}_{-1.25}$	2.86 ± 0.31	4.01 ± 0.43	0.2	$0.64^{+0.55}_{-0.51}$	$2.40^{+1.18}_{-0.98}$	$3.02^{+0.57}_{-1.03}$	$4.28^{+0.52}_{-1.61}$	0.6
J173548–3207_1	$2.04^{+0.67}_{-0.47}$	$0.20^{+0.22}_{-0.15}$	1.65 ± 0.24	2.54 ± 0.37	3.5	$2.17^{+0.60}_{-0.55}$	$0.32^{+0.22}_{-0.19}$	$1.64^{+0.35}_{-0.48}$	$3.80^{+1.86}_{-1.69}$	3.3
J180857–2004_1	$2.84^{+1.86}_{-1.28}$	$5.40^{+4.60}_{-2.80}$	1.16 ± 0.17	14.45 ± 2.18						
J180857–2004_2	$3.45^{+1.28}_{-0.93}$	$6.20^{+3.00}_{-2.00}$	1.94 ± 0.22	80.67 ± 9.02	0.7	$2.71^{+0.72}_{-0.67}$	$4.35^{+1.32}_{-1.15}$	$1.96^{+0.40}_{-0.59}$	$23.39^{+17.88}_{-13.91}$	1.7
J181116–1828_2	$2.00^{+1.38}_{-1.09}$	$2.20^{+2.20}_{-1.50}$	2.77 ± 0.39	7.66 ± 1.07	1.6	$1.52^{+0.68}_{-0.61}$	$1.13^{+0.75}_{-0.58}$	$2.24^{+0.58}_{-0.88}$	$5.14^{+1.53}_{-2.33}$	2.3
J181213–1842_7	$-0.16^{+0.55}_{-0.52}$	$0.52^{+0.73}_{-0.50}$	10.49 ± 0.98	11.03 ± 1.03	0.5	$0.37^{+0.42}_{-0.39}$	$1.62^{+0.77}_{-0.65}$	$10.12^{+1.67}_{-1.96}$	$12.47^{+1.70}_{-1.92}$	0.5
J181213–1842_9	$3.63^{+1.35}_{-1.07}$	$0.20^{+0.31}_{-0.19}$	0.35 ± 0.09	1.48 ± 0.36						
J181852–1559_2	$0.77^{+1.11}_{-0.82}$	$2.50^{+3.20}_{-1.59}$	6.00 ± 0.94	8.34 ± 1.30	1.1	$-0.18^{+0.88}_{-0.77}$	$1.24^{+2.19}_{-1.24}$	$5.22^{+3.02}_{-3.62}$	$6.48^{+3.14}_{-3.06}$	0.7
J181915–1601_2	$1.32^{+0.49}_{-0.37}$	$0.70^{+0.50}_{-0.33}$	3.79 ± 0.52	5.20 ± 0.71	1.5	$2.14^{+0.69}_{-0.63}$	$1.46^{+0.71}_{-0.58}$	$2.97^{+0.89}_{-0.94}$	$9.40^{+7.92}_{-4.37}$	2.0
J181915–1601_3	$1.21^{+0.46}_{-0.34}$	$0.67^{+0.48}_{-0.31}$	5.35 ± 0.62	7.03 ± 0.81	1.2	$1.61^{+0.52}_{-0.48}$	$1.38^{+0.59}_{-0.50}$	$5.25^{+1.04}_{-1.29}$	$10.99^{+2.77}_{-4.17}$	1.6
J182435–1311_1						$4.77^{+0.78}_{-0.70}$	$1.44^{+0.34}_{-0.30}$	$0.45^{+0.09}_{-0.13}$	$60.30^{+99.63}_{-51.18}$	3.4
J182509–1253_1						$3.40^{+0.57}_{-0.52}$	$0.44^{+0.14}_{-0.13}$	$0.57^{+0.12}_{-0.09}$	$4.49^{+3.81}_{-2.67}$	2.2
J182509–1253_3	$-0.05^{+1.65}_{-0.84}$	$3.00^{+7.50}_{-2.66}$	1.96 ± 0.28	2.40 ± 0.34	1.9	$-0.08^{+1.15}_{-0.99}$	$2.98^{+4.05}_{-2.55}$	$1.25^{+0.79}_{-0.96}$	$1.84^{+0.74}_{-0.69}$	2.5
J182530–1144_2	$0.14^{+0.38}_{-0.37}$	$0.55^{+0.33}_{-0.31}$	9.44 ± 0.61	10.13 ± 0.66	1.0	$0.43^{+0.24}_{-0.23}$	$1.01^{+0.32}_{-0.28}$	$9.37^{+0.71}_{-1.22}$	$10.83^{+1.04}_{-1.16}$	1.7
J182651–1206_4	$1.80^{+0.89}_{-0.70}$	$0.28^{+0.42}_{-0.27}$	0.34 ± 0.08	0.49 ± 0.12						
J183116–1008_1	$2.28^{+0.70}_{-0.55}$	$4.80^{+1.80}_{-1.30}$	5.66 ± 0.61	28.9 ± 3.13	1.4	$3.28^{+0.86}_{-0.79}$	$8.15^{+2.26}_{-1.97}$	$5.33^{+1.11}_{-2.67}$	$373.72^{+629.26}_{-273.72}$	1.7
J183206–0938_1	$0.91^{+0.47}_{-0.46}$	$1.50^{+0.90}_{-0.71}$	29.85 ± 2.40	39.86 ± 3.20	0.7	$0.86^{+0.36}_{-0.35}$	$1.81^{+0.58}_{-0.51}$	$33.04^{+3.69}_{-7.94}$	$47.45^{+5.54}_{-11.41}$	1.4
J183345–0828_1	$2.63^{+1.40}_{-1.03}$	$2.60^{+2.00}_{-1.35}$	0.65 ± 0.10	4.04 ± 0.64						
J183356–0822_2	$2.38^{+2.60}_{-1.75}$	$18.0^{+17.00}_{-10.20}$	2.06 ± 0.25	26.08 ± 3.14	1.0	$0.82^{+1.30}_{-1.13}$	$10.46^{+7.15}_{-5.41}$	$1.65^{+0.90}_{-1.21}$	$5.80^{+0.95}_{-1.38}$	1.2
J183356–0822_3	$1.28^{+1.28}_{-1.11}$	$1.80^{+2.40}_{-1.61}$	0.43 ± 0.11	0.69 ± 0.17						
J184652–0240_1	$2.88^{+0.96}_{-0.70}$	$1.50^{+0.80}_{-0.56}$	4.14 ± 0.45	28.0 ± 3.02	1.0	$2.92^{+0.55}_{-0.51}$	$1.51^{+0.44}_{-0.38}$	$3.93^{+0.79}_{-0.71}$	$35.73^{+24.49}_{-19.70}$	1.8
J184738–0156_1	$2.35^{+1.79}_{-1.14}$	$12.0^{+9.00}_{-5.20}$	19.56 ± 1.76	178.36 ± 16.08	1.2	$0.53^{+0.57}_{-0.53}$	$5.13^{+2.14}_{-1.75}$	$21.11^{+4.10}_{-8.53}$	$35.70^{+3.87}_{-12.23}$	2.2
J184741–0219_3	$-1.62^{+1.86}_{-0.38}$	$1.00^{+12.00}_{-0.99}$	2.57 ± 0.46	2.67 ± 0.47						
J185608+0218_1						$3.83^{+0.44}_{-0.40}$	0.33 ± 0.08	$6.97^{+0.66}_{-0.74}$	$50.56^{+47.69}_{-22.77}$	1.8
J185643+0220_2	$0.00^{+0.63}_{-0.44}$	$0.97^{+1.53}_{-0.81}$	3.27 ± 0.39	3.59 ± 0.43	1.3	$0.75^{+0.70}_{-0.64}$	$3.22^{+1.83}_{-1.47}$	$3.03^{+0.53}_{-1.35}$	$4.97^{+0.63}_{-0.80}$	1.6

Table 3
(Continued)

ChIcAGO Source	Quantile Absorbed Power-law Interpolation[a]					Cash Statistics Absorbed Power-law Fit[b]				
ChI	Γ	$N_{\rm H}$	$F_{x,\rm abs}$	$F_{x,\rm unabs}$	$\chi^2_{\rm red}$	Γ	$N_{\rm H}$	$F_{x,\rm abs}$	$F_{x,\rm unabs}$	C
J185750+0240_1	$0.25^{+0.74}_{-0.58}$	$0.32^{+1.08}_{-0.31}$	4.20 ± 0.63	4.43 ± 0.66	0.5	$0.31^{+0.60}_{-0.52}$	$0.30^{+0.61}_{-0.30}$	$4.01^{+0.78}_{-1.45}$	$4.28^{+1.01}_{-0.97}$	0.4
J190534+0659_1	$2.28^{+1.35}_{-0.96}$	$0.52^{+0.68}_{-0.43}$	0.73 ± 0.19	1.70 ± 0.45						
J190749+0803_1	$1.74^{+0.93}_{-0.75}$	$4.80^{+3.00}_{-2.00}$	6.12 ± 0.64	17.21 ± 1.80	0.2	$0.75^{+0.55}_{-0.51}$	$2.73^{+1.24}_{-1.04}$	$6.79^{+0.99}_{-1.89}$	$10.52^{+1.11}_{-2.06}$	0.6
J190814+0832_2	$2.66^{+0.62}_{-0.56}$	$0.73^{+0.37}_{-0.27}$	0.9 ± 0.14	3.41 ± 0.53	1.0	$3.22^{+0.86}_{-0.74}$	$0.74^{+0.36}_{-0.29}$	$0.73^{+0.18}_{-0.21}$	$5.83^{+6.28}_{-3.54}$	0.7
J190818+0745_1	$1.32^{+0.28}_{-0.25}$	$0.20^{+0.15}_{-0.12}$	10.45 ± 0.89	12.38 ± 1.05	0.7	$1.35^{+0.26}_{-0.25}$	$0.22^{+0.11}_{-0.10}$	$10.35^{+1.30}_{-1.38}$	$12.91^{+1.55}_{-1.30}$	1.2
J194152+2251_2	$0.38^{+0.56}_{-0.69}$	$0.82^{+0.58}_{-0.63}$	6.07 ± 0.72	6.84 ± 0.81	0.3	$0.36^{+0.50}_{-0.46}$	$0.91^{+0.72}_{-0.55}$	$5.96^{+1.36}_{-2.02}$	$7.02^{+1.39}_{-1.88}$	0.3
J194939+2631_1	$0.67^{+0.69}_{-0.49}$	$2.30^{+1.90}_{-1.15}$	16.71 ± 1.57	22.28 ± 2.09	0.9	$-0.10^{+0.38}_{-0.35}$	$0.67^{+0.57}_{-0.43}$	$18.24^{+2.62}_{-4.08}$	$20.06^{+2.18}_{-3.87}$	1.5

Notes. The quantile analysis spectral interpolation and Cash statistics spectral modeling are performed on those ChIcAGO sources with >20 and >50 X-ray counts, respectively.

[a] The quantile analysis interpolated absorbed power law model parameters including the spectral index, Γ, and absorption column density $N_{\rm H}$ (10^{22} cm^{-2}), as well as the absorbed and unabsorbed X-ray fluxes, $F_{x,\rm abs}$ and $F_{x,\rm unabs}$ (10^{-13} erg cm^{-2} s^{-1}), respectively, in the 0.3–8.0 keV energy range. The quoted $\chi^2_{\rm red}$ value is what is expected if these interpolated spectral parameters are used to fit the X-ray spectrum of the source.

[b] The absorbed power law fit model parameters using Cash (1979) statistics including the spectral index, Γ, and absorption column density $N_{\rm H}$ (10^{22} cm^{-2}), as well as the absorbed and unabsorbed X-ray fluxes, $F_{x,\rm abs}$ and $F_{x,\rm unabs}$ (10^{-13} erg cm^{-2} s^{-1}), respectively, in the 0.3–8.0 keV energy range. The quoted C value is the reduced Cash statistic, which is the observed statistic divided by the number of degrees of freedom. A good fit is indicated by a C value of the order of one.

As a way to further explore the goodness of the spectral interpolations, the CIAO spectral fitting tool Sherpa was used to fit the X-ray spectrum of each ChIcAGO source with spectral parameters derived from quantile analysis in Tables 3 and 4. The $\chi^2_{\rm red}$ was calculated for each ChIcAGO source where >40 X-ray counts were detected with ACIS-S. In many cases we found $\chi^2_{\rm red} < 1$, which is not unexpected given the low number of X-ray counts detected, indicating that any reasonable model is a decent fit. However, there are also a few cases where $\chi^2_{\rm red} > 2$, indicating that the spectral parameters do not adequately describe the spectrum. The values of $\chi^2_{\rm red}$ corresponding to the quantile interpolated spectral parameters are included in Tables 3 and 4.

The parameters and fluxes resulting from the absorbed power-law and absorbed thermal bremsstrahlung spectral modeling of the ChIcAGO sources have also been included in Tables 3 and 4 so that they can be directly compared to the quantile analysis results. Best-fit absorbed power-law parameters were obtained for all the ACIS-S detected ChIcAGO sources with >50 X-ray counts (see Table 3). However, there were several cases where the absorbed thermal bremsstrahlung fitting was unsuccessful as the Sherpa modeling algorithm hit the hard maximum limit on the kT parameter (10 keV). These unsuccessful fits were not included in Table 4.

All of the parameters and absorbed fluxes derived from the Cash statistics spectral fitting agree within 3σ of those derived from the quantile analysis spectral interpolation, the majority of which agree within 1σ errors. The only exception is the kT parameter value for ChI J171910–3652_2. However, the unabsorbed fluxes were far less agreeable between the two techniques as there were several ChIcAGO sources for which this value differed by $>3\sigma$. These include ChI J183356–0822_2 and ChI J184738–0156_1 from the power-law spectral analysis and ChI J144547–5931_1, ChI J144701–5919_1, ChI J165646–4239_1, ChI J171910–3652_2, ChI J172050–3710_1, and ChI J185608+0218_1 from the bremsstrahlung spectral analysis. Both techniques therefore appear to be successful in constraining the spectral parameters and absorbed fluxes for each of the investigated ChIcAGO sources but less successful in constraining the unabsorbed fluxes. It should also be noted that the majority of the reduced Cash statistics from the spectral modeling were systematically higher than the corresponding $\chi^2_{\rm red}$ derived from the spectral parameters interpolated through quantile analysis.

3.3. Infrared and Optical Counterparts

Infrared and optical follow-up were primarily performed on those ChIcAGO sources with >20 X-ray counts (see Table 2). In order to determine which optical and infrared sources are counterparts to ChIcAGO sources, we used a technique similar to that described by Zhao et al. (2005), using their Equation (11). If the separation between a ChIcAGO source's wavdetect position and its possible counterpart is less than the quadratic sum of their 3σ position errors and the 3σ *Chandra* pointing error,[33] then the X-ray and optical (or infrared) sources are likely to be associated. The 1σ position errors for all sources in 2MASS PSC and the GLIMPSE[34] catalogs are 0.″1 (Skrutskie et al. 2006) and 0.″3, respectively. USNO B has an astrometric accuracy of <0.″25 (Monet et al. 2003). We have assumed that the error distributions of the *Chandra* observations, *Chandra* pointing, and USNO B Catalog are all Gaussian for the purposes of identifying possible counterparts to the ChIcAGO sources. While this assumption is not necessarily correct in every case, the full examination required to obtain the Gaussian errors would involve a very complicated approach. However, other *Chandra* Galactic plane X-ray surveys that search for multiwavelength counterparts assuming Gaussian errors for cross-correlation purposes have had successful results (e.g., ChaMPlane; Zhao et al. 2005). On the basis of these results we feel that Gaussian errors are an acceptable assumption for the purpose of identifying optical and infrared counterparts to the ChIcAGO sources.

The infrared properties, such as the names and magnitudes of any likely 2MASS or GLIMPSE counterparts, together with the NIR magnitudes (J, H, and K) obtained from Magellan PANIC observations, are listed in Table 2 along with the date of each observation. We assume that those ChIcAGO sources with no listed 2MASS (or PANIC) counterpart have 2MASS PSC limiting magnitudes $J > 15.8$, $H > 15.1$,

[33] http://cxc.harvard.edu/cal/ASPECT/celmon/

[34] See GLIMPSE documents at http://www.astro.wisc.edu/sirtf/docs.html.

Table 4
Quantile Analysis Bremsstrahlung Spectral Interpolation and Cash Statistic Bremsstrahlung Spectral Fit to ACIS *Chandra* Detections of the ChIcAGO Sources

ChIcAGO Source	Absorbed Bremsstrahlung Interpolation[a]					Cash Statistics Absorbed Bremsstrahlung Fit[b]				
ChI	kT	$N_{\rm H}$	$F_{x,\rm abs}$	$F_{x,\rm unabs}$	$\chi^2_{\rm red}$	kT	$N_{\rm H}$	$F_{x,\rm abs}$	$F_{x,\rm unabs}$	C
J144519–5949_2	$1.38^{+2.15}_{-0.65}$	$4.80^{+3.60}_{-2.2}$	2.17 ± 0.44	21.59 ± 4.37						
J144547–5931_1	$0.84^{+0.30}_{-0.21}$	$4.10^{+1.20}_{-0.9}$	2.56 ± 0.31	57.74 ± 6.95	0.9	$1.01^{+0.37}_{-0.23}$	$3.27^{+0.86}_{-0.74}$	$1.93^{+0.68}_{-1.24}$	$37.28^{+9.98}_{-22.51}$	0.9
J144701–5919_1	$1.00^{+0.70}_{-0.39}$	$3.50^{+1.90}_{-1.2}$	5.49 ± 0.60	74.01 ± 8.12	0.6	$2.04^{+0.95}_{-0.54}$	$1.93^{+0.49}_{-0.43}$	$5.78^{+1.16}_{-2.03}$	$23.52^{+4.04}_{-7.51}$	0.9
J154122–5522_1	$1.88^{+0.96}_{-0.70}$	$0.04^{+0.09}_{-0.03}$	2.35 ± 0.26	2.72 ± 0.3	0.6	$2.62^{+1.68}_{-0.80}$	$0.05^{+0.06}_{-0.05}$	$2.46^{+0.45}_{-0.47}$	$3.08^{+0.47}_{-0.70}$	1.0
J154557–5443_1	$1.38^{+1.32}_{-0.73}$	$0.14^{+0.15}_{-0.1}$	0.16 ± 0.03	0.25 ± 0.05						
J154557–5443_2	$1.77^{+96.43}_{-1.33}$	$24.0^{+46.0}_{-15.8}$	0.63 ± 0.16	17.65 ± 4.49						
J154557–5443_3	$0.10^{+0.30}_{-0.00}$	$0.97^{+1.23}_{-0.88}$	0.11 ± 0.03	224.95 ± 51.46						
J155035–5408_1	$0.35^{+0.18}_{-0.18}$	$0.14^{+0.38}_{-0.14}$	0.18 ± 0.05	0.56 ± 0.14						
J155035–5408_3	$2.14^{+0.91}_{-0.72}$	$0.43^{+0.21}_{-0.1}$	2.73 ± 0.19	5.29 ± 0.37	0.9	$2.17^{+0.55}_{-0.38}$	$0.42^{+0.08}_{-0.07}$	$2.81^{+0.28}_{-0.37}$	$5.43^{+0.45}_{-0.85}$	1.8
J155331–5347_1	$0.31^{+0.31}_{-0.16}$	$0.70^{+0.85}_{-0.39}$	1.25 ± 0.15	30.92 ± 3.67	2.2					
J155831–5334_1	$9.04^{+89.16}_{-5.99}$	$0.34^{+0.30}_{-0.22}$	3.54 ± 0.49	4.73 ± 0.66	0.4					
J162046–4942_1						$8.37^{+16.53}_{-3.50}$	$0.24^{+0.09}_{-0.08}$	$3.48^{+0.50}_{-0.61}$	$4.48^{+0.56}_{-0.89}$	2.7
J165646–4239_1	$0.35^{+0.13}_{-0.10}$	$0.25^{+0.15}_{-0.10}$	4.06 ± 0.25	20.59 ± 1.26	1.8	$0.78^{+0.14}_{-0.11}$	0.03 ± 0.03	$5.06^{+0.53}_{-0.64}$	$6.62^{+0.49}_{-0.99}$	2.8
J165707–4255_1	$0.71^{+0.21}_{-0.31}$	$0.05^{+0.16}_{-0.04}$	2.53 ± 0.32	3.39 ± 0.43	2.1	$0.87^{+0.24}_{-0.16}$	<0.02	$2.69^{+0.24}_{-0.53}$	$2.78^{+0.24}_{-0.57}$	3.3
J170052–4210_1	$0.31^{+0.35}_{-0.16}$	$0.25^{+0.45}_{-0.22}$	0.84 ± 0.14	4.93 ± 0.82		$0.51^{+0.42}_{-0.19}$	$0.13^{+0.17}_{-0.13}$	$0.84^{+0.18}_{-0.27}$	$1.98^{+0.69}_{-0.80}$	3.9
J170444–4109_1	$0.97^{+0.28}_{-0.29}$	$0.01^{+0.10}_{0.00}$	9.28 ± 0.75	9.85 ± 0.80	1.8	$1.54^{+0.42}_{-0.30}$	$0.03^{+0.06}_{-0.03}$	$8.51^{+0.66}_{-0.88}$	$10.48^{+0.92}_{-1.02}$	2.4
J170536–4038_1	$1.46^{+1.11}_{-0.55}$	$0.13^{+0.14}_{-0.10}$	6.09 ± 0.57	9.33 ± 0.88	1.1	$3.95^{+2.79}_{-1.29}$	$0.05^{+0.06}_{-0.05}$	$8.65^{+0.81}_{-1.65}$	$9.68^{+1.46}_{-1.40}$	1.8
J171910–3652_2	$0.17^{+0.07}_{-0.06}$	$0.61^{+0.39}_{-0.24}$	1.81 ± 0.17	136.22 ± 12.59	1.1	$1.23^{+0.25}_{-0.20}$	<0.03	$2.59^{+0.30}_{-0.26}$	$2.71^{+0.25}_{-0.20}$	4.00
J172050–3710_1	$0.38^{+0.08}_{-0.06}$	$0.37^{+0.09}_{-0.09}$	1.77 ± 0.10	12.78 ± 0.72	1.1	$0.67^{+0.09}_{-0.08}$	$0.24^{+0.05}_{-0.04}$	$2.03^{+0.13}_{-0.28}$	$6.06^{+0.75}_{-0.98}$	2.1
J172550–3533_2	$1.14^{+1.35}_{-0.55}$	$0.20^{+0.25}_{-0.16}$	0.41 ± 0.06	0.81 ± 0.12	0.6					
J172550–3533_3	$1.28^{+1.14}_{-0.56}$	$0.10^{+0.21}_{-0.09}$	0.55 ± 0.09	0.79 ± 0.12						
J172623–3516_1	$1.56^{+6.01}_{-1.10}$	$0.28^{+0.69}_{-0.26}$	1.0 ± 0.15	1.93 ± 0.29	0.6					
J173548–3207_1	$4.00^{+6.00}_{-2.30}$	$0.12^{+0.21}_{-0.09}$	1.58 ± 0.23	1.95 ± 0.29	3.6	$3.67^{+5.98}_{-1.59}$	$0.21^{+0.15}_{-0.13}$	$1.57^{+0.42}_{-0.70}$	$2.13^{+0.68}_{-0.59}$	3.3
J175404–2553_3	$2.56^{+95.64}_{-1.85}$	$33.00^{+40.00}_{-18.00}$	1.34 ± 0.27	28.13 ± 5.69						
J180857–2004_1	$3.19^{+19.41}_{-1.77}$	$4.40^{+3.20}_{-2.00}$	1.12 ± 0.17	4.19 ± 0.63						
J180857–2004_2	$2.21^{+1.68}_{-0.82}$	$4.90^{+1.90}_{-1.40}$	1.88 ± 0.21	10.23 ± 1.14	0.6	$4.03^{+4.75}_{-1.50}$	$3.37^{+0.88}_{-0.78}$	$1.78^{+0.55}_{-1.13}$	$5.52^{+1.58}_{-3.43}$	1.9
J181116–1828_2	$6.52^{+91.68}_{-4.45}$	$1.85^{+1.55}_{-0.85}$	2.7 ± 0.38	5.36 ± 0.75	1.5					
J181213–1842_9	$0.84^{+0.79}_{-0.49}$	$0.04^{+0.27}_{-0.03}$	0.35 ± 0.09	0.45 ± 0.11						
J181915–1601_2						$5.44^{+17.68}_{-2.61}$	$1.15^{+0.49}_{-0.40}$	$3.25^{+0.55}_{-0.99}$	$5.92^{+1.18}_{-1.37}$	2.1
J182435–1311_1	$0.84^{+0.19}_{-0.17}$	$0.82^{+0.18}_{-0.15}$	0.47 ± 0.05	2.54 ± 0.27	1.7	$0.74^{+0.21}_{-0.15}$	$0.99^{+0.24}_{-0.21}$	$0.44^{+0.08}_{-0.21}$	$3.90^{+0.91}_{-2.11}$	3.3
J182509–1253_1	$0.76^{+0.38}_{-0.23}$	$0.26^{+0.17}_{-0.12}$	0.49 ± 0.05	1.4 ± 0.15	1.6	$1.37^{+0.56}_{-0.34}$	$0.20^{+0.09}_{-0.08}$	$0.54^{+0.09}_{-0.19}$	$1.03^{+0.21}_{-0.22}$	2.7
J182538–1214_1	$0.38^{+0.90}_{-0.26}$	$0.37^{+1.13}_{-0.36}$	0.52 ± 0.10	3.86 ± 0.72						
J182651–1206_4	$6.31^{+91.89}_{-4.17}$	$0.20^{+0.28}_{-0.19}$	0.32 ± 0.08	0.42 ± 0.10						
J183116–1008_1	$5.26^{+7.89}_{-2.28}$	$4.10^{+1.30}_{-1.00}$	5.55 ± 0.60	15.35 ± 1.67	1.5	$2.96^{+2.26}_{-0.96}$	$6.37^{+1.54}_{-1.35}$	$5.18^{+1.52}_{-2.86}$	$26.82^{+7.42}_{-13.83}$	1.9
J183345–0828_1	$3.26^{+13.04}_{-1.77}$	$2.00^{+1.40}_{-0.90}$	0.62 ± 0.10	1.64 ± 0.26						
J183356–0822_2	$6.31^{+91.89}_{-4.64}$	$16.0^{+13.0}_{-6.6}$	2.05 ± 0.25	10.44 ± 1.26	1.0					
J184652–0240_1	$2.21^{+2.00}_{-0.86}$	$1.10^{+0.55}_{-0.37}$	3.9 ± 0.42	10.29 ± 1.11	0.9	$2.21^{+1.06}_{-0.59}$	$1.14^{+0.31}_{-0.27}$	$3.66^{+0.79}_{-1.46}$	$10.87^{+1.81}_{-3.90}$	1.8
J184738–0156_1	$5.47^{+92.73}_{-3.33}$	$11.0^{+6.00}_{-4.20}$	19.34 ± 1.74	83.9 ± 7.56	1.2					
J185608+0218_1	$0.42^{+0.17}_{-0.11}$	$0.31^{+0.15}_{-0.12}$	5.66 ± 0.41	30.15 ± 2.16	1.3	$0.96^{+0.21}_{-0.16}$	$0.10^{+0.05}_{-0.04}$	$6.82^{+0.72}_{-0.83}$	$11.02^{+1.91}_{-2.17}$	2.0
J190534+0659_1	$3.12^{+41.53}_{-1.91}$	$0.37^{+0.45}_{-0.30}$	0.69 ± 0.18	1.12 ± 0.30						
J190814+0832_2	$2.21^{+1.75}_{-0.72}$	$0.52^{+0.27}_{-0.19}$	0.84 ± 0.13	1.71 ± 0.26	0.8	$1.46^{+1.00}_{-0.48}$	$0.50^{+0.25}_{-0.21}$	0.77		0.4
J194310+2318_5	$0.55^{+0.29}_{-0.25}$	$0.12^{+0.22}_{-0.1}$	0.69 ± 0.13	1.42 ± 0.26						
J195006+2628_2	$0.48^{+1.01}_{-0.32}$	$0.29^{+0.81}_{-0.28}$	0.22 ± 0.04	0.97 ± 0.20						

Notes. The quantile analysis spectral interpolation and Cash statistics spectral modeling are performed on those ChIcAGO sources with >20 and >50 X-ray counts, respectively. The `CIAO` task `sample_flux` failed for ChI J190814+0832_2 and so the quoted flux is taken from the best fit model parameters.

[a] The quantile analysis interpolated absorbed thermal bremsstrahlung model parameters including the temperature, kT (keV), and absorption column density $N_{\rm H}$ (10^{22} cm^{-2}), as well as the absorbed and unabsorbed X-ray fluxes, $F_{x,\rm abs}$ and $F_{x,\rm unabs}$ (10^{-13} erg cm^{-2} s^{-1}), respectively, in the 0.3–8.0 keV energy range. The quoted $\chi^2_{\rm red}$ value is what is expected if these interpolated spectral parameters are used to fit the X-ray spectrum of the source.

[b] The absorbed thermal bremsstrahlung fit model parameters using Cash (1979) statistics including the temperature, kT (keV), and absorption column density $N_{\rm H}$ (10^{22} cm^{-2}), as well as the absorbed and unabsorbed X-ray fluxes, $F_{x,\rm abs}$ and $F_{x,\rm unabs}$ (10^{-13} erg cm^{-2} s^{-1}), respectively, in the 0.3–8.0 keV energy range. The quoted C value is the reduced Cash statistic, which is the observed statistic divided by the number of degrees of freedom. A good fit is indicated by a C value of the order of one.

Table 5
Properties of Optical Counterparts, Where They Exist, for All ChIcAGO Sources with >20 X-Ray Counts

ChIcAGO Source	USNO Name	Optical[a]	Optical Magnitudes[b]				MagIC or IMACS Date[c]
ChI	USNO-B1.0	Data Source	*B*	*V*	*R*	*I*	(yyyy-mm-dd)
J143148–6021_3	0296–0521275	U,A,A,A	19.71 ± 0.3	20.49 ± 0.03	19.31 ± 0.03	18.27 ± 0.03	2008-05-13
J144042–6001_1	0299–0503336	U	10.26 ± 0.3		9.36 ± 0.3	8.99 ± 0.3	
J144547–5931_1	0304–0487344	U	20.54 ± 0.3		15.79 ± 0.3	12.30 ± 0.3	
J144701–5919_1	0306–0492632	U			16.61 ± 0.3	12.95 ± 0.3	
J154122–5522_1	0346–0518164	U	13.17 ± 0.3		11.87 ± 0.3	10.87 ± 0.3	
J154557–5443_1	0352–0535858	U	16.16 ± 0.3		15.10 ± 0.3	14.67 ± 0.3	
J154557–5443_3	0352–0535969	U	17.91 ± 0.3		16.51 ± 0.3	15.42 ± 0.3	
J155035–5408_1	0358–0537979	U	11.40 ± 0.3		10.71 ± 0.3	10.43 ± 0.3	
J155035–5408_3	0358–0538167	U	15.81 ± 0.3		13.96 ± 0.3	13.09 ± 0.3	
J155331–5347_1	0361–0529851	U	14.38 ± 0.3		12.93 ± 0.3	12.74 ± 0.3	
J155831–5334_1	0364–0530109	U	16.99 ± 0.3		16.37 ± 0.3	16.15 ± 0.3	
J162046–4942_1	0402–0531543	U	15.03 ± 0.3		12.48 ± 0.3	10.71 ± 0.3	
J163252–4746_2		A		>25	>25	21.93 ± 0.05	2008-05-13
J163751–4656_1	0430–0573746	U	15.27 ± 0.3		14.94 ± 0.3	15.07 ± 0.3	
J165217–4414_1	0457–0509597	U,A,A,A	19.03 ± 0.3	19.73 ± 0.03	18.74 ± 0.03	17.80 ± 0.03	2008-05-13
J165420–4337_1	0463–0473777	U,A,A,A	17.62 ± 0.3	19.88 ± 0.03	19.01 ± 0.03	17.82 ± 0.03	2008-05-13
J165646–4239_1	0473–0602564	U	14.49 ± 0.3		12.46 ± 0.3	10.89 ± 0.3	
J165646–4239_2		A		22.69 ± 0.06	21.76 ± 0.05	20.83 ± 0.04	2008-05-13
J165707–4255_1	0470–0567106	U	14.15 ± 0.3		12.37 ± 0.3	11.04 ± 0.3	
J170017–4220_1		I,A,A,A	>23.5 ± 0.3	>25	>25	>23.4 ± 0.3	I:2008-07-30,A:2008-05-13
J170052–4210_1	0478–0576746	U	15.02 ± 0.3		13.57 ± 0.3	11.83 ± 0.3	
J170444–4109_1	0488–0491640	U	16.68 ± 0.3		15.07 ± 0.3	13.01 ± 0.3	
J170536–4038_1	0493–0497837	U	11.65 ± 0.3		10.89 ± 0.3	10.33 ± 0.3	
J172050–3710_1	0528–0624586	U	11.97 ± 0.3		11.62 ± 0.3	11.47 ± 0.3	
J172550–3533_2	0544–0498651	U	16.04 ± 0.3		14.84 ± 0.3	14.97 ± 0.3	
J172550–3533_3	0544–0498592	U	11.82 ± 0.3		11.16 ± 0.3	10.89 ± 0.3	
J172623–3516_1	0547–0493410	U	14.26 ± 0.3		11.86 ± 0.3	10.82 ± 0.3	
J172642–3540_1	0543–0502139	U	11.62 ± 0.3		9.98 ± 0.3	9.16 ± 0.3	
J173548–3207_1	0578–0723476	U	15.19 ± 0.3		14.67 ± 0.3	14.45 ± 0.3	
J181116–1828_2		A(blend)		20.08 ± 0.03	18.93 ± 0.03	17.84 ± 0.03	2008-05-13
J181213–1842_7		I		>23.5 ± 0.5			2008-07-30
J181213–1842_9	0713–0551349	U	13.43 ± 0.3			12.76 ± 0.3	
J181915–1601_2	0739–0563199	U	16.15 ± 0.3		13.66 ± 0.3	11.23 ± 0.3	
J182435–1311_1	0768–0532899	U	13.08 ± 0.3		11.01 ± 0.3	9.92 ± 0.3	
J182509–1253_1	0771–0546066	U	12.64 ± 0.3		11.36 ± 0.3	10.74 ± 0.3	
J182538–1214_1	0777–0567961	U	14.33 ± 0.3		13.00 ± 0.3	12.89 ± 0.3	
J182651–1206_4	0778–0569793	U	16.62 ± 0.3		13.97 ± 0.3	14.10 ± 0.3	
J183116–1008_1	0798–0402571	U	16.79 ± 0.3		13.38 ± 0.3		
J183206–0938_1	0803–0434604	U			16.59 ± 0.3	11.35 ± 0.3	
J184652–0240_1	0873–0550754	U	19.50 ± 0.3		15.44 ± 0.3	12.41 ± 0.3	
J185608+0218_1	0922-0521590	U	10.36 ± 0.3		9.48 ± 0.3	9.12 ± 0.3	
J190534+0659_1	0969–0463844	U	14.67 ± 0.3		11.98 ± 0.3	10.46 ± 0.3	
J190814+0832_2	0985–0428114	U	16.05 ± 0.3		14.32 ± 0.3	12.78 ± 0.3	
J190818+0745_1	0977–0515881	U	18.04 ± 0.3		16.74 ± 0.3	16.54 ± 0.3	
J194310+2318_5	1132–0447077	U	9.63 ± 0.3		9.08 ± 0.3	8.85 ± 0.3	
J194939+2631_1	1165–0456015	U,I,I,NA	20.20 ± 0.3	20.1 ± 0.1	19.1 ± 0.1		2008-07-30

Notes. ChI J170017–4220_1 was observed with both MagIC and IMACS. The dates of both observations are listed and prefixed by the corresponding data set symbol described below. The MagIC observation of ChI J181116–1828_2 shows that it may be a blend.

[a] Catalog or observations from which the counterpart optical magnitudes were obtained. U = USNO B1 Catalog (Monet et al. 2003), A = MagIC Magellan observations, I = IMACS Magellan observations, NA = no data for the corresponding magnitude. If four symbols are listed this indicates that the magnitudes were obtained from different data sets. This order corresponds to the *B*, *V*, *R* and *I* magnitude order.

[b] The USNO-B1.0 *B* and *R* band magnitudes listed are the second epoch *B* and *R* magnitudes (Monet et al. 2003)

[c] Date of the MagIC and IMACS observations: yyyy-mm-dd.

and $K > 14.3$ (Skrutskie et al. 2006). In Table 5, optical magnitudes have also been provided for those 44 ChIcAGO sources with >20 X-ray counts that have optical counterparts in the USNO B1 Catalog or in one of the IMACS or MagIC Magellan observations. Two other ChIcAGO sources (ChI J170017–4220_1 and ChI J181213–1842_7) with magnitude limits obtained with either IMACS or MagIC are also included in Table 5.

Of the 74 ChIcAGO sources with >20 X-ray counts listed in Table 2, 59 have a NIR counterpart, 44 of which are 2MASS sources and 15 of which were detected in PANIC observations. Looking into the mid-infrared wavelength bands, we find that 41 of these 2MASS sources and 3 of the PANIC sources also have GLIMPSE counterparts. NIR magnitude limits were obtained for 4 other PANIC-observed ChIcAGO sources since

any possible counterparts were too faint to be detected or, in the case of ChI J181116–1828_2 and ChI J185643+0220_2, the counterpart appeared to be blended. (ChI J181116–1828_2 does, however, have a unique GLIMPSE counterpart.) If we include ChI J181116–1828_2 and ChI J185643+0220_2, for which we have detected a counterpart but the magnitudes are only an upper limit because of blending, then 89% of our PANIC observations of ChIcAGO sources have yielded a detection in one of more of the J, H, or K filter bands. There are also a few ChIcAGO sources where the 2MASS counterpart magnitudes are listed as 95% confidence upper limits due to a nondetection or inconsistent deblending. We were therefore able to use PANIC to obtain more accurate magnitudes for four ChIcAGO sources that have limited 2MASS magnitude information in one or more bands. (These four ChIcAGO sources can be identified as those with three letters listed in the "Data" column of Table 2.)

All 46 ChIcAGO sources listed in Table 5 (44 ChIcAGO sources with optical counterparts and 2 with limiting magnitudes obtained with Magellan instruments) have NIR counterparts detected with either 2MASS or PANIC. Of the 44 with optical counterparts, 41 have USNO B1 counterparts, and for 4 of those, extra magnitude measurements were obtained with one of the two Magellan optical imagers. A further 3 ChIcAGO sources, not cataloged in USNO B1, were also detected in the optical with these Magellan instruments. Of the 74 ChIcAGO sources with >20 X-ray counts, 14 do not have a detected optical, NIR, or IR counterpart.

We conducted an experiment similar to that outlined in Kaplan et al. (2004) to quantify the probability that the optical and infrared survey counterparts quoted in Tables 2 and 5 are a random chance association with the >20 X-ray count ChIcAGO source with which they are coincident. We searched for all 2MASS, GLIMPSE, and USNO B1 sources brighter than the possible counterpart listed in Tables 2 and 5 within 10′ of each ChIcAGO source position. (We only searched for survey sources that have a brighter K_s, 3.6 μm, and second epoch R band magnitude for the 2MASS, GLIMPSE, and USNO B1 surveys, respectively.) We then used the resulting statistics to determine the number of survey sources brighter than the listed counterpart that are likely to be detected within a region the same size as the ChIcAGO source's 95% position error circle. We did this for each ChIcAGO source individually as the density of sources can vary dramatically across the Galactic plane. In most cases the resulting chance of a random association is very low (<0.01). Those ChIcAGO sources that have a random chance of association >0.01 in either 2MASS or GLIMPSE are listed in Table 6. For each ChIcAGO source the chance of a random association with a USNO B1 is <0.01.

We refer to the ChIcAGO sources that have <20 counts as "secondary" sources. In Table 7 we list the names of any USNO B1, 2MASS, and GLIMPSE sources that appear to be coincident with a secondary ChIcAGO source on the basis of our position agreement criteria outlined in Section 2.4.1. Table 7 also includes the offset in arcseconds between the secondary ChIcAGO source's `wavdetect` position and the position of the coincident survey source. (Only those secondary ChIcAGO sources that have a coincident survey source have been included in Table 7.) A summary of the fraction of ChIcAGO sources with a coincident source in the 2MASS, GLIMPSE, and USNO B1 catalogs can be found in Table 8, which includes the fraction of the total number of ChIcAGO sources, as well the fraction of just the >20 X-ray count ChIcAGO sources, with a coincident survey source. (Note that we assume the survey sources coincident with the >20 X-ray count ChIcAGO sources are counterparts based on the very low chance of random associations, as demonstrated by Table 6.)

Table 6
Chance of a Random Association between the Listed ChIcAGO Sources (All of Which Have >20 X-Ray Counts) and a 2MASS and GLIMPSE Source

ChIcAGO Source ChI	2MASS $N(<K_s)$[a] ($\times 10^{-2}$)	GLIMPSE $N(<M_{3.6})$[b] ($\times 10^{-2}$)
J155831–5334_1	1.76	
J163751–4656_1	1.67	3.16
J165420–4337_1		2.29
J172550–3533_2	1.08	1.71
J173548–3207_1	1.22	3.02
J181116–1828_2		3.15
J183345–0828_1	1.25	
J190818+0745_1		1.17

Notes. Only those ChIcAGO sources where the chance of random alignment with a survey source is >0.01 are listed.
[a] Chance of finding a 2MASS source with a K_s magnitude brighter than the counterpart listed in Table 2 within the ChIcAGO source's 95% position error circle.
[b] Chance of finding a GLIMPSE source with a 3.6 μm magnitude brighter than the counterpart listed in Table 2 within the ChIcAGO source's 95% position error circle.

3.4. Radio Counterparts

As mentioned in Section 2.4.2, the position of each ChIcAGO source (above and below 20 X-ray counts) was visually inspected for any possibly associated radio emission in the MGPS, MAGPIS, VGPS, and the 90 cm Multi-configuration Very Large Array Survey of the Galactic Plane. The results of this inspection are listed in Table 9. ChIcAGO source position comparisons were also made with the Green (2009) catalog of Galactic SNRs. Any possible counterparts that are known objects, such as SNRs, H II regions, infrared dark clouds (IRDCs; Peretto & Fuller 2009), CWBs, or massive stars, are listed in Table 9 in the "Type" column. However, if the radio sources are uncataloged, they have instead been flagged as being possibly compact, diffuse, or arc/shell structured diffuse emission. Two ChIcAGO sources, ChI J181116–1828_5 and ChI J184741–0219_3, appear to be previously unidentified AGNs as their coincident radio sources show core–lobe morphologies in the MAGPIS 1.4 GHz survey images.

Each of the ChIcAGO sources with a possible radio association is then listed in Table 9 as being either coincident with, adjacent to, or on the limb of the radio source (such as on the limb of a SNR, diffuse emission, or H II region). If a ChIcAGO source is listed as either coincident with or on the limb of a SNR, then this means it is within the extent of the SNR based on the SNR's size quoted in the Green (2009) catalog. In the cases of the two candidate AGNs, these ChIcAGO sources appear to be directly coincident with the core of the AGN. The name of each radio source and the corresponding reference are listed in Table 9.

The 10 ChIcAGO sources observed with the ATCA are also included in Table 9. The ATCA-detected compact radio counterparts to both ChI J144701–5919_1 and ChI J163252–4746_2 aided in their identification as X-ray emitting massive stars or CWBs (see Anderson et al. 2011). No radio counterparts were detected for the other 8 ChIcAGO sources observed with the ATCA.

Table 7
Likely Optical and Infrared Counterparts of Secondary (<20 X-Ray Counts) ChIcAGO Sources

ChIcAGO Source ChI	USNO Name USNO-B1.0	Offset[a] (arcsec)	2MASS Name 2MASS J	Offset[a] (arcsec)	GLIMPSE Name[b] SSTGLMC G	Offset[a] (arcsec)
J143148–6021_1	0296–0521300	0.4	14315021–6022087	0.56	G315.0382+00.1212	0.41
J143148–6021_2	0296–0521279	0.35	14314859–6021444	0.25	G315.0377+00.1287	0.36
J143148–6021_4	0296–0521208	0.32	14314161–6019552	0.7	G315.0358+00.1622	0.56
J144519–5949_1			14451506–5949286	0.51	G316.7879-00.0504	0.61
J144519–5949_4	0301–0471052	0.36	14451937–5948007	0.47	G316.8065-00.0321	0.64

Notes.
[a] The offset, in arcseconds, between the catalogs and ChIcAGO source position for the likely USNO B1, 2MASS and GLIMPSE counterparts, respectively.
[b] Those GLIMPSE counterpart names marked with a * are from the archives (more complete, less reliable) rather than the catalogs (more reliable). In these cases the archival GLIMPSE source's names begins with "SSTGLMA G."

(This table is available in its entirety in a machine-readable form in the online journal. A portion is shown here for guidance regarding its form and content.)

Table 8
Summary of the Fraction of ChIcAGO Sources with a Coincident Cataloged Source from 2MASS, GLIMPSE, and USNO B1

ChIcAGO Source Samples	2MASS Fraction (%)	GLIMPSE Fraction (%)	USNO B1 Fraction (%)
Total (253 sources)	57	61	47
>20 X-ray counts (74 sources)	59	61	55

Note. These fractions are for the total number of ChIcAGO sources and for the ChIcAGO sources with >20 X-ray counts.

In summary, Table 9 shows there are 16 ChIcAGO sources from the *Chandra* observations of 8 different AGPS source regions that are coincident with or on the limb of nine SNRs. There are 54 ChIcAGO sources from 7 different AGPS source regions that fall within the extent of 6 H II regions. There are also four massive stars, all of which are confirmed or candidate CWBs (see Anderson et al. 2011; Motch et al. 2010), with radio counterparts. Only two ChIcAGO sources, both toward the same single AGPS target, are coincident with an IRDC.

Several ChIcAGO sources also fall within regions of uncataloged extended radio emission. These include 15 ChIcAGO sources from 5 different AGPS source regions falling within the extent of 5 regions of diffuse radio emission. Of these 15 ChIcAGO sources, there are 6 (from 3 different AGPS source regions) that are coincident with uncataloged diffuse emission with an arc or shell structure. Excluding the two AGN candidates, there is only one other ChIcAGO source coincident with an unidentified compact radio source.

There are 74 ChIcAGO sources (14 sources with >20 X-ray counts and 60 with <20 X-ray counts), out of the 253 detected, with no optical or infrared counterparts, making them possible compact object candidates and therefore potentially detectable in the radio. We therefore searched for any possible pulsar counterparts in the Australia Telescope National Facility Pulsar Catalogue (version 1.44[35]; Manchester et al. 2005), but no known pulsars exist within 0.′6 of the `wavdetect` position of any of the 74 sources.

4. DISCUSSION

4.1. Unidentified ChIcAGO Sources with Radio Counterparts

Table 9 lists 16 ChIcAGO sources that fall within the extent of 9 SNRs. X-ray point sources within SNRs could be associated compact objects. Identification of an optical or infrared counterpart discounts such a possibility since the optical/IR counterparts to NSs and other compact objects are expected to be very faint (for the details on this approach, see Kaplan et al. 2004). Those SNR coincident ChIcAGO sources with a random chance of association >0.01 in the USNO B1 and GLIMPSE catalogs are listed in Table 10. (The chance of a random association between one of these 16 ChIcAGO sources and a 2MASS catalog source is <0.01.)

Of the 16 ChIcAGO sources inside SNRs, only 5 have no optical or infrared counterparts. These five X-ray sources are all very faint, with <8 X-ray counts detected for each in the ChIcAGO *Chandra* observations. These are ChI J145732–5901_2 in SNR G318.2+0.1 (Whiteoak & Green 1996), ChI J182435–1311_2,3,4 in SNR G18.1–0.1 (Helfand et al. 2006; Brogan et al. 2006), and ChI J184447–0305_1 in SNR G29.3667+0.1000 (Helfand et al. 2006). Bocchino et al. (2001) has already reported on three X-ray sources within SNR G318.2+0.1 but not at the position of ChI J145732–5901_2. Both SNR G18.1–0.1 and SNR G29.3667+0.1000 are newly discovered SNRs, so little X-ray analysis has been done on these objects. Further investigation is required to determine if any of these five ChIcAGO sources are compact objects and if they are associated with the surrounding SNRs.

There are 54 ChIcAGO sources coincident with 6 different H II regions that were detected in the ChIcAGO *Chandra* observations of 7 AGPS sources (see Table 9). On the basis of the results from X-ray observations of other H II regions (for example, see Broos et al. 2007) it is possible that many of these 54 ChIcAGO sources could be pre-main-sequence (PMS) stars, massive OB and WR stars, and CWBs. Simpson & Cotera (2004) also found optically obscured star clusters in 2MASS images within 1′ of three of these AGPS sources; AX J144519–5949, AX J151005–5824, and AX J162208–5005, which supports a H II region and young and massive star interpretation for these *ASCA* sources. Of these 54 ChIcAGO sources, 43 have optical and/or infrared counterparts, supporting a possible stellar origin (see Tables 2, 5, and 7). In most cases the chance of random association with a field source is low (<0.01). Those H II region coincident ChIcAGO sources for which the chance of random

[35] http://www.atnf.csiro.au/research/pulsar/psrcat

Table 9
Radio Counterparts to ChIcAGO Sources

ChIcAGO Source (ChI)[a]	Survey[b]	Radio Source	Type[c]	Location[d]	Reference[e]
J144042–6001_1	MGPS	SNR G316.3–0.0	SNR	L	1
J144519–5949_(1–6)	MGPS	GAL 316.8–00.1	H II	C	2
J144701–5919_1	ATCA	AX J144701–5919	MS	C	3
J145732–5901_(1–2)	MGPS	SNR G318.2+0.1	SNR	L	4,5
J151005–5824_(1–11)	MGPS	G320.3–0.3	H II	C	6
J153818–5541_1	ATCA		ND		7
J154905–5420_(1–11)	MGPS	G326.96+0.03	H II	A	8
J155331–5347_1	ATCA		ND		7
J155331–5347_2	ATCA		ND		7
J162208–5005_(1–3)	MGPS	G333.6–0.2	H II	C	6
J163252–4746_1	ATCA		ND		7
J163252–4746_2	ATCA	AX J163252–4746	CWB	C	3
J163751–4656_1	ATCA		ND		7
J165217–4414_1	MGPS	Uncataloged	Arc	C	
J165420–4337_1	ATCA		ND		7
J165420–4337_2	ATCA		ND		7
J165646–4239_(1–2)	MGPS	SDC G343.306+0.161	IRDC	C	9
J165707–4255_(1–2)	MGPS	Uncataloged	Arc	C	
J170052–4210_1	ATCA		ND		7
J172550–3533_(1–3)	MGPS	Uncataloged	Arc	L	
J180857–2004_1,2	90, MAGPIS	MAGPIS 10.3139–01417	D	C	10
J181116–1828_5	MAGPIS	MAGPIS 11.97095+0.19155	AGN	K	10
J181213–1842_1,8	90, MAGPIS	SNR G11.8–0.2	SNR	L	11
J181213–1842_2,5	90, MAGPIS	SNR G12.0–0.1	SNR	A	12
J181705–1607_(1–7)	90, MAGPIS	MAGPIS 14.6167+0.0667	D	L	10
J182435–1311_(1–4)	90, MAGPIS	SNR G18.1–0.1	SNR	C	10,11
J182538–1214_1	90, MAGPIS	SNR G19.1+0.2	SNR	L	11
J183206–0938_1	MAGPIS	MAGPIS 22.15394–0.15414	CWB	C	10,13
J183356–0822_6,7	MAGPIS	SNR 23.5667–0.0333	SNR	L	10
J184400–0355_1	MAGPIS	SNR G28.6–0.1	SNR	L	14
J184447–0305_1	MAGPIS	SNR 29.3667+0.1000	SNR	C	10
J184738–0156_1	MAGPIS	NVSS 184736–015632	CWB	C	3,15
J184741–0219_3	MAGPIS	MAGPIS 30.43741–0.20625	AGN	K	10
J194310+2318_(1–10)	VGPS	G59.5–0.2	H II	C	6
J194332+2323_(1–8)	VGPS	G59.5–0.2	H II	C	6
J194622+2436_1	VGPS	NVSS 194620+243514	Com	L	15
J195006+2628_(1–5)	VGPS	G62.9+0.1	H II	C	6,16

Notes.
[a] The names of the ChIcAGO sources with radio counterparts. If all the ChIcAGO sources in a *Chandra* observation of an AGPS source are coincident with the radio counterpart, then the range of suffixes are listed in parentheses. If only a subset of the ChIcAGO sources detected in a given *Chandra* observation are coincident with the radio counterpart, then only those suffixes are listed.
[b] The radio Galactic plane surveys or observations visually inspected—MGPS: Molonglo Galactic Plane Survey; 90: 90 cm Multi-configuration Very Large Array survey of the Galactic Plane; MAGPIS: the Multi-Array Galactic Plane Imaging Survey; VGPS: VLA Galactic Plane Survey; ATCA: Australia Telescope Compact Array observations obtained for radio follow-up of ChIcAGO sources (see Sections 2.4.2 and 3.4).
[c] Type of radio source—SNR: supernova remnant; H II: H II region; MS: massive star; CWB: colliding wind binary; IRDC: Infrared Dark Cloud; AGN: likely active galactic nuclei based on a core–lobe morphology; D: diffuse; Arc: diffuse emission with an arc or shell morphology; Com: compact; ND: no detection in the case of the ATCA observations.
[d] Position of the ChIcAGO source relative to the radio source—C: coincident; A: adjacent; L: limb (usually the limb or edge of a SNR, arc/shell structured diffuse emission or H II region); K: core of a possible AGN given the apparent core–lobe morphology.
[e] Many additional references to the SNRs are compiled in Green (2009).
References. (1) Shaver & Goss 1970; (2) Haverkorn et al. 2006; (3) Anderson et al. 2011; (4) Whiteoak & Green 1996; (5) Bocchino et al. 2001; (6) Kuchar & Clark 1997; (7) This paper; (8) McClure-Griffiths et al. 2001; (9) Peretto & Fuller 2009; (10) Helfand et al. 2006; (11) Brogan et al. 2006; (12) Caswell et al. 1975; (13) Motch et al. 2010; (14) Helfand et al. 1989; (15) Condon et al. 1998; (16) Ramos-Larios et al. 2010.

association with a 2MASS or GLIMPSE source is >0.01 are listed in Table 11.

The possible nature of these H II region coincident ChIcAGO sources could be further investigated by comparing their luminosities to those of PMS stars, massive OB and WR stars, and CWBs. A spectral analysis of the 54 ChIcAGO sources is extremely difficult given that they all have ⩽32 X-ray counts. However, the primary goal is to obtain a wide-band flux that can then be converted into a luminosity. Quantile analysis was therefore performed to obtain absorbed Mewe–Kaastra–Liedahl

Table 10
Chance of a Random Association between the Listed ChIcAGO Sources Coincident with SNRs and a USNO B1 and GLIMPSE Source

ChIcAGO Source ChI	USNO B1 $N(<R)$[a] ($\times 10^{-2}$)	GLIMPSE $N(<M_{3.6})$[b] ($\times 10^{-2}$)
J181213–1842_1		1.15
J181213–1842_2	3.05	7.15
J181213–1842_5	4.04	
J182435–1311_1		3.17
J183356–0822_6	1.68	

Notes. Only those ChIcAGO sources where the chance of random alignment with a survey source is >0.01 are listed.
[a] Chance of finding a USNO source with a R magnitude brighter than the counterpart listed in Table 7 within the ChIcAGO source's 95% position error circle.
[b] Chance of finding a GLIMPSE source with a 3.6 μm magnitude brighter than the counterpart listed in Tables 2 or 7 within the ChIcAGO source's 95% position error circle.

(Mekal; Mewe et al. 1985, 1986; Kaastra 1992; Liedahl et al. 1995) spectral interpolations of all the H II region coincident ChIcAGO sources with $\geqslant$5 X-ray counts. A Mekal model was chosen as thin thermal plasma emission is expected from hot X-ray emitting stars (for example, see Wolk et al. 2005; Sana et al. 2006). The absorbed Mekal spectral interpolations can be found in Table 11.

The luminosities of these ChIcAGO sources were calculated using kinematic distance estimates to the H II regions with which they are coincident. Kinematic distances calculated by Russeil (2003) were used to calculate luminosities for the ChIcAGO sources coincident with G320.3–0.3, G333.6–0.2, and G59.5–0.2. (Note that there is a more distant kinematic distance estimate of 6.3 kpc to G59.5–0.2 calculated by Kuchar & Bania 1994, but we have decided to use the more recent estimate from Russeil 2003.) The kinematic distances used in the luminosity calculations for G326.96+0.03 and G62.9+0.1 were obtained from McClure-Griffiths et al. (2001) and Fich & Blitz (1984), respectively. The kinematic distance to the massive young stellar object G316.8112–00.0566 (Busfield et al. 2006), likely embedded within GAL 316.8–00.1, was used in the luminosity calculations for those ChIcAGO sources coincident with this H II region. (The distance from Busfield et al. 2006 agrees reasonably well with the near kinematic distance to GAL 316.8–00.1 calculated by Caswell & Haynes 1987 when revised for a modern Galactic center distance of 8.5 kpc.) Table 11 lists the kinematic distance and corresponding absorbed and unabsorbed luminosities calculated for each H II region coincident ChIcAGO source.

The range of absorbed luminosities calculated for all the ChIcAGO sources coincident with the 6 H II regions span the range 30.6 erg s^{-1} < log $L_{x,\mathrm{abs}}$ < 32.4 erg s^{-1} (0.3–8 keV). This absorbed luminosity range is similar to that observed from the H II region M17 (29.3 erg s^{-1} < log $L_{x,\mathrm{abs}}$ < 32.8 erg s^{-1} (0.5–8 keV); Broos et al. 2007). With the exception of ChI J151005–5824_8, the H II region coincident ChIcAGO sources in Table 11 have unabsorbed luminosities between $L_{x,\mathrm{unab}} \sim 10^{31}$ and 10^{35} erg s^{-1}. The unabsorbed luminosities of these ChIcAGO sources cover the ranges of what has been observed from flaring PMS stars ($L_{x,\mathrm{unab}} \sim 10^{30}$ to 10^{33} erg s^{-1}; Favata et al. 2005; Wolk et al. 2005), single and binary massive O-type stars ($L_{x,\mathrm{unab}} \sim 10^{31}$ to 10^{33} erg s^{-1}; Oskinova 2005; Sana et al. 2006), WR stars ($L_{x,\mathrm{unab}} \sim 10^{31}$ to 10^{34} erg s^{-1}; Oskinova 2005; Mauerhan et al. 2010), and CWBs ($L_{x,\mathrm{unab}} \sim 10^{32}$ to 10^{34} erg s^{-1}; Oskinova 2005; Mauerhan et al. 2010). In fact, we were able to identify ChI J194310+2318_5, which is within G59.5–0.2, as the O7V((f))-type star HD 344784 (Walborn 1973) using the SIMBAD Astronomical Database. It is therefore likely that the AGPS sources AX J144519–5949, AX J151005–5824, AX J154905–5420, AX J162208–5005, AX J194310+2318, AX J194332+2323, and AX J195006+2628 are young and massive stars within H II regions. Deeper X-ray, radio, and IR observations are required to determine the precise nature of the individual ChIcAGO sources.

4.2. Unidentified ChIcAGO Sources with Infrared Counterparts

The X-ray and infrared population statistics performed in this section are conducted using just those ChIcAGO sources with >20 X-ray counts, therefore concentrating on the persistent populations that fall within the AGPS flux range ($F_x \sim 10^{-13}$ to 10^{-11} erg cm^{-2} s^{-1}). However, discarding the ChIcAGO sources with <20 X-ray counts limits our analysis as we are excluding the populations of sources that exhibit long-term variability or transient behavior. Sources with <20 X-ray counts will need to be investigated in future work using archival X-ray observations at different epochs.

4.2.1. X-ray and Infrared Populations Statistics

Using the X-ray and infrared properties of the unidentified ChIcAGO sources, it is possible to classify some of the sources detected in the AGPS into possible populations. We chose to focus on the IR counterparts as this wave band is less affected by interstellar extinction when compared to the optical band. This group of sources therefore makes up a larger subset of the unidentified ChIcAGO sources than those with optical counterparts (see Section 3.3). For those unidentified ChIcAGO sources observed with the *Chandra* HRC instrument (for which there is no spectral information), we generated fake spectra, using `XSpec` and the `CIAO` spectral fitting tool `Sherpa`. These spectra are based on the absorbed power-law fits reported in Sugizaki et al. (2001), allowing the absorbed X-ray flux and median energy (E_{50}) of the unidentified ChIcAGO source in question to be calculated. These values are used in the statistical plots described below.

To help identify possible distinct populations in the statistical plots, we have also included both archival sources (those AGPS source that were identified by Sugizaki et al. 2001 or in the literature and so were not observed with *Chandra* as part of the ChIcAGO survey) and the previously identified ChIcAGO sources (for example, those investigated by Anderson et al. 2011, 2012). Fake spectra were generated using `Sherpa` and `XSpec` for these archival sources, using spectral fits in the literature, to determine their absorbed X-ray fluxes and E_{50} values for the energy ranges investigated. All archival AGPS sources are summarized and tabulated in Section 4.5 (see Table 12) and are individually described in Appendix A.

The identified sources were divided into the following categories: AGNs, CVs, CWBs, high-mass X-ray binaries (HMXBs), magnetars, massive stars, and stars. The "AGN" category includes ChI J184741–0219_3, which we identified by positional comparison with MAGPIS radio data (for the radio identification and further details on this source, see Sections 3.4 and 4.3.15, respectively). The "CWB" category includes AX J163252–4746 and AX J184738–0156, which were identified in Anderson et al. (2011, listed as ChI J163252–4746_2

Table 11
Quantile Spectral Interpolations and Luminosity Estimates for All ChIcAGO Sources within H II Regions That Have $\gtrsim$5 X-Ray Counts

ChIcAGO Source	Absorbed Mekal Interpolation[a]				Distance[b]		Luminosities[c]		False Associations ($\times 10^{-2}$)[d]	
ChI	kT	$N_{\rm H}$	$F_{x,\rm abs}$	$F_{x,\rm unabs}$	(kpc)	Ref	log $L_{x,\rm abs}$	log $L_{x,\rm unabs}$	2MASS $N(<K_s)$	GLIMPSE $N(<M_{3.6})$
J144519–5949_2	$1.52^{+1.38}_{-0.73}$	$5.00^{+3.60}_{-2.10}$	23.70 ± 4.80	218.44 ± 44.20	2.8	1	32.35	33.31		
J144519–5949_3	$0.78^{+2.69}_{-0.57}$	$22.00^{+51.00}_{-15.00}$	13.05 ± 4.73	7207.60 ± 2610.31	2.8	1	32.09	34.83		
J144519–5949_5	>1.94	$0.14^{+0.68}_{-0.14}$	3.37 ± 2.29	3.98 ± 2.71	2.8	1	31.50	31.57		
J151005–5824_1	$0.90^{+1.80}_{-0.77}$	$7.60^{+27.40}_{-4.60}$	0.74 ± 0.45	47.76 ± 28.64	4.7	2	31.29	33.10		
J151005–5824_2	82.45	$2.80^{+0.00}_{-2.07}$	1.72 ± 0.85	2.92 ± 1.45	4.7	2	31.66	31.89		
J151005–5824_3	$0.21^{+1.42}_{-0.11}$	$1.60^{+1.30}_{-1.35}$	0.18 ± 0.12	65.24 ± 44.33	4.7	2	30.68	33.24		
J151005–5824_4	82.45	$2.20^{+-0.10}_{-1.53}$	1.21 ± 0.73	1.96 ± 1.18	4.7	2	31.51	31.71		
J151005–5824_5	82.45	$1.80^{+0.00}_{-1.50}$	1.14 ± 0.68	1.76 ± 1.06	4.7	2	31.48	31.67		
J151005–5824_6	>0.1	$2.50^{+10.50}_{-2.49}$	0.44 ± 0.18	452.64 ± 182.20	4.7	2	31.07	34.08		
J151005–5824_7	>2.21	$21.00^{+11.00}_{-17.00}$	6.46 ± 1.94	36.97 ± 11.10	4.7	2	32.23	32.99		
J151005–5824_8	$0.17^{+0.33}_{-0.07}$	$33.00^{+28.00}_{-21.00}$	0.96 ± 0.48	$218762449.44 \pm 108233831.76$	4.7	2	31.41	39.76		
J151005–5824_9	>2.49	$0.01^{+0.25}_{0.00}$	0.41 ± 0.28	0.42 ± 0.28	4.7	2	31.04	31.04		3.15
J151005–5824_10	>5.26	$1.20^{+1.00}_{-1.16}$	1.39 ± 0.69	2.00 ± 0.99	4.7	2	31.56	31.72		1.71
J151005–5824_11	>0.1	$0.38^{+0.87}_{-0.38}$	0.64 ± 0.43	0.79 ± 0.54	4.7	2	31.23	31.32		
J154905–5420_1	$0.61^{+0.81}_{-0.33}$	$11.50^{+12.50}_{-5.60}$	1.49 ± 0.68	743.78 ± 340.69	3.7	3	31.39	34.09		
J154905–5420_2	>2.63	$2.30^{+3.30}_{-0.80}$	4.07 ± 1.35	6.63 ± 2.20	3.7	3	31.82	32.04		
J154905–5420_3	$0.74^{+1.54}_{-0.56}$	$15.50^{+39.50}_{-9.50}$	0.99 ± 0.67	397.68 ± 270.25	3.7	3	31.21	33.81	2.40	2.21
J154905–5420_4	$1.80^{+3.04}_{-1.69}$	$0.01^{+1.29}_{0.00}$	0.40 ± 0.24	0.41 ± 0.25	3.7	3	30.82	30.83	1.62	1.88
J154905–5420_5	>0.1	$0.01^{+0.42}_{0.00}$	1.66 ± 0.71	1.69 ± 0.72	3.7	3	31.44	31.44		
J154905–5420_7	>16.3	$1.05^{+0.35}_{-1.04}$	1.89 ± 0.87	2.66 ± 1.22	3.7	3	31.49	31.64		
J154905–5420_8	>4.63	$1.20^{+1.10}_{-1.19}$	1.09 ± 0.74	1.57 ± 1.07	3.7	3	31.25	31.41		3.02
J154905–5420_9	>0.1	$0.01^{+0.60}_{0.00}$	0.70 ± 0.38	0.71 ± 0.38	3.7	3	31.06	31.07		
J154905–5420_10	>0.1	$0.01^{+0.66}_{0.00}$	0.46 ± 0.31	0.47 ± 0.32	3.7	3	30.88	30.89	3.25	5.29
J154905–5420_11	>0.63	$0.46^{+1.39}_{-0.45}$	1.24 ± 0.47	2.05 ± 0.78	3.7	3	31.31	31.53		
J162208–5005_1	>1.91	$2.40^{+3.60}_{-1.10}$	23.73 ± 6.53	42.69 ± 11.74	3.1	2	32.44	32.69		
J162208–5005_3	>6.52	$2.60^{+2.30}_{-1.40}$	6.75 ± 4.59	11.30 ± 7.68	3.1	2	31.89	32.11		
J194310+2318_1	$2.28^{+6.97}_{-1.86}$	$0.01^{+1.04}_{0.00}$	5.31 ± 1.46	5.47 ± 1.50	2.6	2	31.63	31.65		
J194310+2318_4	$0.12^{+19.33}_{-0.02}$	$0.67^{+0.00}_{-0.66}$	1.06 ± 0.72	253.21 ± 172.07	2.6	2	30.93	33.31		1.06
J194310+2318_5	$0.14^{+3.33}_{-0.03}$	$0.76^{+-0.03}_{-0.75}$	5.97 ± 1.08	1446.16 ± 262.87	2.6	2	31.68	34.07		
J194310+2318_6	$0.76^{+1.38}_{-0.62}$	$1.75^{+3.85}_{-1.05}$	5.33 ± 1.41	94.55 ± 24.98	2.6	2	31.63	32.88		
J194310+2318_7	>0.19	$1.60^{+10.90}_{-1.59}$	1.70 ± 0.92	909.74 ± 491.76	2.6	2	31.14	33.87		
J194310+2318_8	82.45	$0.94^{+0.26}_{-0.93}$	3.77 ± 2.56	5.22 ± 3.55	2.6	2	31.48	31.63		
J194310+2318_9	$0.10^{+1.28}_{0.00}$	$1.70^{+1.40}_{-1.69}$	0.99 ± 0.59	18914.51 ± 11342.64	2.6	2	30.90	35.18		
J194332+2323_1	$2.91^{+7.09}_{-2.56}$	$0.13^{+1.52}_{-0.12}$	1.65 ± 0.55	2.10 ± 0.69	2.6	2	31.13	31.23		
J194332+2323_3	$0.22^{+0.33}_{-0.11}$	$3.00^{+4.60}_{-1.30}$	0.64 ± 0.35	1053.73 ± 569.60	2.6	2	30.72	33.93		
J194332+2323_5	>0.1	$1.15^{+10.35}_{-1.14}$	3.81 ± 1.32	24.79 ± 8.57	2.6	2	31.49	32.30		
J194332+2323_6	>0.1	$0.01^{+2.49}_{0.00}$	0.70 ± 0.38	0.73 ± 0.39	2.6	2	30.76	30.77	1.35	1.38
J194332+2323_7	$0.15^{+0.55}_{-0.05}$	$0.58^{+.15}_{-0.57}$	0.64 ± 0.29	51.52 ± 23.60	2.6	2	30.72	32.62		
J195006+2628_1	$0.10^{+0.04}_{0.00}$	$1.25^{+2.35}_{-0.73}$	0.70 ± 0.38	3815.10 ± 2062.27	2.3	4	30.65	34.38		
J195006+2628_2	$1.74^{+2.02}_{-1.62}$	$0.01^{+1.49}_{0.00}$	2.74 ± 0.55	2.83 ± 0.57	2.3	4	31.24	31.25		
J195006+2628_3	$2.70^{+16.75}_{-2.59}$	$0.23^{+1.87}_{-0.22}$	0.61 ± 0.42	$.88 \pm .60$	2.3	4	30.59	30.75		
J195006+2628_4	$0.40^{+1.23}_{-0.29}$	$2.10^{+3.50}_{-1.37}$	0.63 ± 0.34	58.70 ± 31.73	2.3	4	30.60	32.57		
J195006+2628_5	$0.11^{+1.76}_{-0.01}$	$1.55^{+1.35}_{-1.54}$	0.74 ± 0.28	5807.00 ± 2211.85	2.3	4	30.67	34.57		

Notes.

[a] The quantile analysis interpolated absorbed Mekal model parameters including the temperature, kT, and absorption column density $N_{\rm H}$ (10^{22} cm^{-2}), as well as the absorbed and unabsorbed X-ray fluxes, $F_{x,\rm abs}$ and $F_{x,\rm unabs}$ (10^{-14} erg cm^{-2} s^{-1}), respectively, in the 0.3–8.0 keV energy range. (If $kT = 82.45$ then this indicates that the spectral interpolation of this ChIcAGO source has hit the hard limit for this parameter.)

[b] The distances used to estimate the absorbed and unabsorbed luminosities. The corresponding reference is also listed.

[c] The log of the absorbed and unabsorbed luminosities, $L_{x,\rm abs}$ and $L_{x,\rm unabs}$ (erg s^{-s}), respectively, in the 0.3–8.0 keV energy range.

[d] Chance of finding a 2MASS (or GLIMPSE) source with a K_s (or 3.6 μm) magnitude brighter than the counterpart listed in Tables 2 or 7, within the ChIcAGO source's 95% position error circle. This value is only quoted for the ChIcAGO sources where the chance of random alignment with a survey source is >0.01.

References. (1) Busfield et al. 2006; (2) Russeil 2003; (3) McClure-Griffiths et al. 2001; (4) Fich & Blitz 1984.

and ChI J184738–0156_1 in Table 1, respectively), and AX J183116–1008 and AX J183206–0938, which were identified in the XGPS (Motch et al. 2010, listed as ChI J183116–1008_1 and ChI J183206–0938_1 in Table 1, respectively). The "HMXB" category includes the archival AGPS sources that are supergiant HMXBs (McClintock & Remillard 2006), supergiant fast X-ray

Table 12
Confirmed and Tentative Identifications of the AGPS Sources, Including Both Literature and ChIcAGO Survey Identifications

AGPS ID	ChIcAGO ID[a]	Type[b]	ID[c]	Reference[d]	Flag[e]
AX J143148–6021	ChI J143148–6021_3	U		1	n,R,n
AX J143416–6024		RS CVn	HD 127535	2,3*	n,n,n
AX J144042–6001	ChI J144042–6001_1	PMS	HD 128696	2*	n,n,n
AX J144519–5949	ChI J144519–5949_2(1,3-6)	WR and H II	GAL 316.8–00.1	1	T,T,N
AX J144547–5931	ChI J144547–5931_1	OIf$^+$		4,4	I,I,n

Notes.
[a] The equivalent ChIcAGO name of the AGPS source. All ChIcAGO sources with >20 X-ray counts are listed. In a few cases there is more than one ChIcAGO source listed for a given AGPS source. For a given identified H II region, all of the ChIcAGO sources contributed to the X-ray emission originally detected with *ASCA* in the AGPS. In these cases the ChIcAGO source name suffixes are listed in parentheses. If a suffix is listed before the parentheses then this ChIcAGO source corresponds to an X-ray source whose stellar type is listed in column three, before the H II classification.
[b] The source type abbreviations are ASC: active stellar corona, AGN: active galactic nucleus, CV: cataclysmic variable, CWB: colliding wind binary, H II: young and massive stars in the H II region named in the "ID" column; HMXB: high-mass X-ray binary, LBV: luminous blue variable, LMXB: low-mass X-ray binary, Magnetar: magnetar, MS: massive star, MS-O: massive O-type star, ND: no ChIcAGO sources detected in the *Chandra* observation (no detection), PMS: pre-main sequence star, PSR: X-ray emission from a rotation-powered pulsar, PWN: pulsar wind nebula, SNR: supernova remnant, SyXB: symbiotic X-ray binary, U: unknown, and WR: Wolf–Rayet star. The other abbreviations are the spectral type of the stellar counterpart.
[c] The most commonly used name
[d] The * and ** symbols indicate those AGPS sources that were correctly and incorrectly identified by Sugizaki et al. (2001), respectively. Those archival AGPS sources and identified ChIcAGO sources used in the statistical analysis in Section 4.2 have two references in this Table, the first being the paper describing an X-ray fit from which we derived an absorbed X-ray flux, and the second being the paper from which the NIR counterpart (J, H, and K_s magnitudes) information was obtained. All the longer-wavelength IR counterpart information (3.6, 4.5, 5.8, and 8.0 μm magnitudes) was gathered from the GLIMPSE catalogs and archives.
[e] Flags that correspond to the identification properties of the AGPS and ChIcAGO sources. One flag is listed for each of the first three columns. I: identified sources through work in the ChIcAGO survey; T: tentatively identified sources using the X-ray and infrared population statistics in Section 4.2; F: AGPS sources for which only ChIcAGO sources with $\leqslant$20 X-ray counts were detected. These include AGPS sources where no sources were detected in the corresponding ChIcAGO *Chandra* observations but excludes those AGPS sources that have been identified as H II regions. R: Figure 8 Region iv sources; N: unconfirmed classification type; n: no flag.
References. (1) This paper; (2) Sugizaki et al. 2001; (3) Skrutskie et al. 2006; (4) Anderson et al. 2011; (5) Degenaar et al. 2012; (6) Bernardini et al. 2011; (7) Israel et al. 2009; (8) Torres et al. 2006; (9) Tomsick et al. 2006; (10) Anderson et al. 2012; (11) Rodriguez et al. 2006; (12) Walter et al. 2006; (13) Nazé et al. 2008; (14) Combi et al. 2006; (15) Bodaghee et al. 2006; (16) Funk et al. 2007; (17) Hamaguchi et al. 2005; (18) Kaur et al. 2010; (19) Markwardt et al. 2010; (20) Chakrabarty et al. 2002; (21) Combi et al. 2010; (22) Lazendic et al. 2005; (23) Gaensler et al. 2008; (24) Giacani et al. 2009; (25) De Becker et al. 2004; (26) Yamauchi et al. 2008; (27) Rho et al. 2004; (28) Mereghetti et al. 2005; (29) Israel et al. 2005; (30) Brogan et al. 2006; (31) Kargaltsev & Pavlov 2007; (32) Gotthelf & Halpern 2007; (33) Israel et al. 2004; (34) Mereghetti et al. 2012; (35) Helfand et al. 2003a; (36) Bassani et al. 2009; (37) Motch et al. 2010; (38) Kargaltsev et al. 2012; (39) Kaplan et al. 2007; (40) Gotthelf & Halpern 2008; (41) Paron et al. 2012; (42) Morii et al. 2003; (43) Bamba et al. 2001; (44) Helfand et al. 2003b; (45) Pooley et al. 2007; (46) Chen et al. 2004; (47) Yamaguchi et al. 2004; (48) Gotthelf & Halpern 2005; (49) Petre et al. 2002; (50) Yamauchi et al. 2011; (51) Safi-Harb et al. 2005; (52) Pavan et al. 2011; (53) Hwang et al. 2000; (54) Kohoutek & Wehmeyer 1997; (55) Zolotukhin & Chilingarian 2011.

(This table is available in its entirety in a machine-readable form in the online journal. A portion is shown here for guidance regarding its form and content.)

transients (SFXTs; Sguera et al. 2006), and SyXBs (Masetti et al. 2007). The infrared and X-ray fluxes from magnetars are variable and correlated (Durant & van Kerkwijk 2005), so the fluxes we used in the "magnetar" category are from infrared and X-ray observations that occurred close together in time. PSR J1622–4950, which was determined through the ChIcAGO *Chandra* observation to be the main contributor to AX J162246–4946, has also been included as an identified magnetar (see Anderson et al. 2012 and Section 4.3.6 for further details). The sources included in the "massive star" category are massive stars that are WR, luminous blue variable (LBV) stars, and massive O-type stars, which emit X-rays through instability-driven wind shocks (Lucy & White 1980; Lucy 1982) and possibly through colliding winds in a CWB. These include AX J144547–5931 and AX J144701–5919, which were identified by Anderson et al. (2011, listed as ChI J144547–5931_1 and ChI J144701–5919_1 in Table 1, respectively). All other nondegenerate stars are in the "star" category and most likely correspond to ASCs or PMS stars.

We first investigated the relationship between the X-ray and infrared flux of the ChIcAGO sources by comparing these properties to those of known stars and AGNs. Figure 5 of Gelfand & Gaensler (2007) shows the X-ray versus K_s-band flux of sources from the *Chandra* Orion Ultradeep Project (COUP; Getman et al. 2005) and XBootes Survey (Jannuzi et al. 2004; Kenter et al. 2005), which are stars (predominantly in the PMS) and AGNs, respectively. In Figure 7 we create a similar plot that includes the unidentified ChIcAGO sources (U ChIcAGO; red data points) along with the COUP stars (blue crosses) and the XBootes Survey AGNs (magenta diamonds; for further details on the data from these surveys see Gelfand & Gaensler 2007, and references therein). The X-ray flux ($F_{x,2-7\,\mathrm{keV}}$) is over the 2.0–7.0 keV energy range, and the K_s band flux ($F_{Ks} = \lambda F_{\lambda,Ks}$) is derived from $F_{\lambda,Ks}$ (erg cm^{-2} s^{-1} μm^{-1}) where the effective wavelength is $\lambda = 2.159\,\mu$m. The archival sources and the identified ChIcAGO sources with K-band counterparts have also been included in Figure 7 in order to further distinguish between possible X-ray populations.

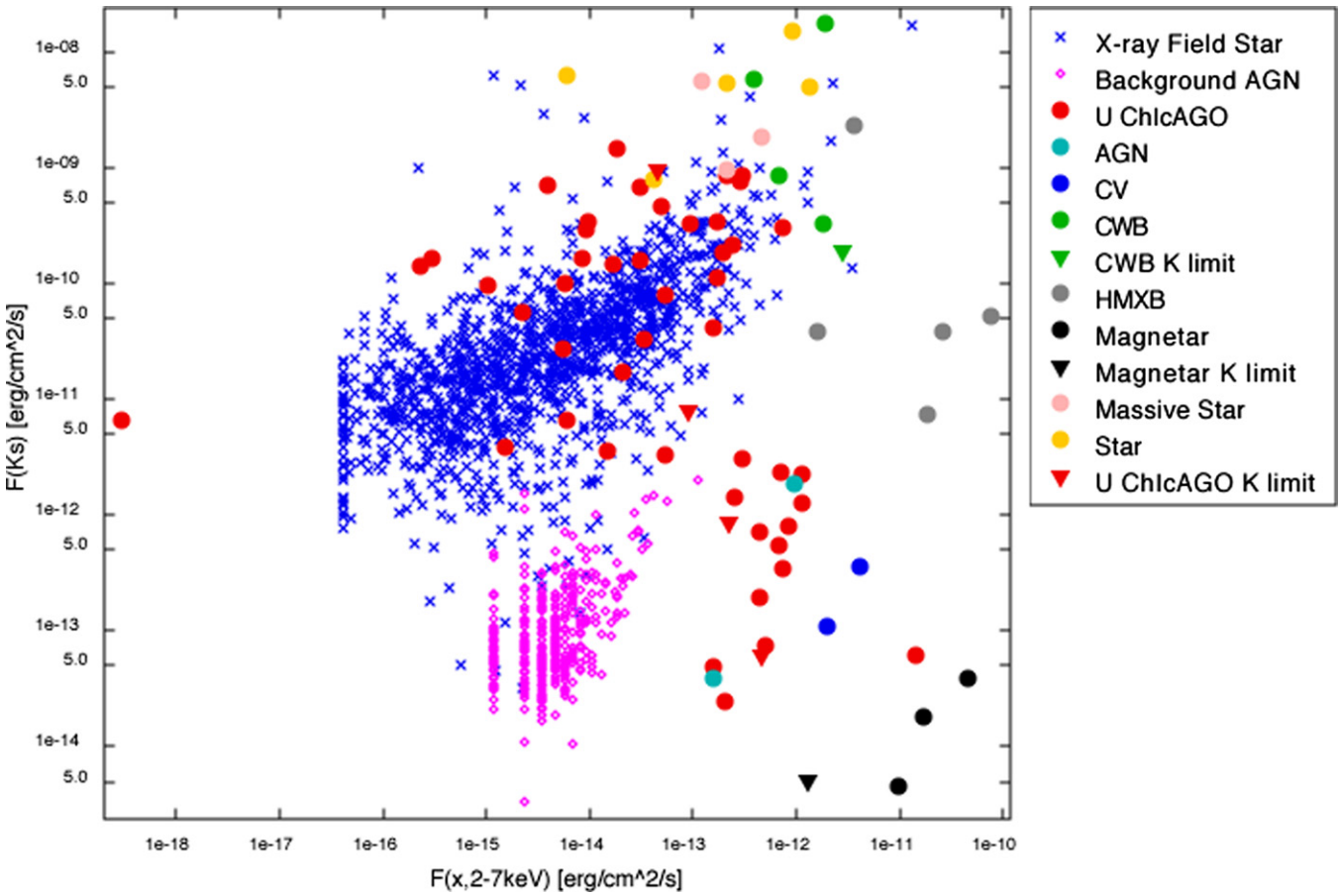

Figure 7. Observed K_s-band flux (F_{Ks}) vs. absorbed 2–7 keV X-ray flux ($F_{x,2-7\,\mathrm{keV}}$) of unidentified ChIcAGO sources ("U ChIcAGO": red points) and identified ChIcAGO and archival sources. Triangular data points represent those sources that only have upper limits on their K_s-band fluxes. The *Chandra* Orion Ultradeep Project sources (blue crosses) and the XBootes Survey sources (magenta diamonds), which are predominantly PMS stars and background AGNs, respectively, are also included. The lone red data point on the far left of the diagram (ChI J154557–5443_3) should be treated as an X-ray flux upper limit as *Chandra* detected very few hard X-ray counts (>2 keV) from this source. This plot is based upon Figure 5 of Gelfand & Gaensler (2007).

(A color version of this figure is available in the online journal.)

Two groups and two outliers are apparent in Figure 7 among the unidentified ChIcAGO sources: group 1, those coincident with the COUP stars, and group 2, which sits to the right of the AGN detected in the XBootes survey. The two outliers are ChI J154557–5443_3, on the very left of Figure 7 with a hard X-ray flux limit of $F_{x,2-7\,\mathrm{keV}} \lesssim 3 \times 10^{-19}$ erg cm^{-2} s^{-1},[36] and the source on the bottom right, ChI J153818–5541_1, with an X-ray flux of $F_{x,2-7\,\mathrm{keV}} \sim 1 \times 10^{-11}$ erg cm^{-2} s^{-1}, located near the identified magnetars.

Group 1 is distributed similar to the COUP stars, following a "track" indicating an increase in K-band flux with X-ray flux. This comparison demonstrates that a large number of the ChIcAGO stellar population could be PMS stars. While the overall Galactic X-ray population is dominated by field stars, we would expect that the ChIcAGO survey (and the AGPS) is biased toward PMS stars as such objects are brighter and harder X-ray emitters (for example, see Wolk et al. 2005). The identified ChIcAGO and archival sources that have been categorized as massive stars (light pink dots) and CWBs (green data points) congregate near the top right of group 1, beyond most of the COUP stars. These massive stars and CWBs are composed of massive late-type WR stars in the nitrogen sequence that are hydrogen rich (WNH; Smith et al. 2008) or their massive O star progenitors (Of; Crowther et al. 1995), all of which are expected to be bright in the infrared and potentially harder in X-rays than other types of X-ray emitting stars (yellow data points). (See Anderson et al. 2011 for further details on these WR and massive O stars.) It is therefore possible that the unidentified ChIcAGO sources located near these massive stars and CWBs in Figure 7 could be similar objects. It should also be noted that the identified AGPS HMXBs sit to the right of group 1, with no unidentified ChIcAGO sources near their positions with which to draw a comparison.

Group 2 sits at a similar K_s-band flux but higher X-ray flux than the AGN from the XBootes survey. The identified ChIcAGO and archival AGNs are coincident with the unidentified ChIcAGO sources in group 2, indicating that at least part of this group could also be AGNs. Such AGNs would have to be very X-ray bright in order to be detected through the high foreground column density in the Galactic plane. The identified archival CVs sit adjacent to group 2, at a slightly higher X-ray flux, indicating another possible population identification.

The unidentified ChIcAGO source ChI J154557–5443_3 has a K-band flux similar to the COUP stars but has an extremely faint hard X-ray flux. No identified ChIcAGO or archival sources are located near ChI J154557–5443_3 in Figure 7 that suggest

[36] The majority of X-ray counts that *Chandra* detected from ChI J154557–5443_3 were soft (<2 keV). This hard flux is therefore an upper limit.

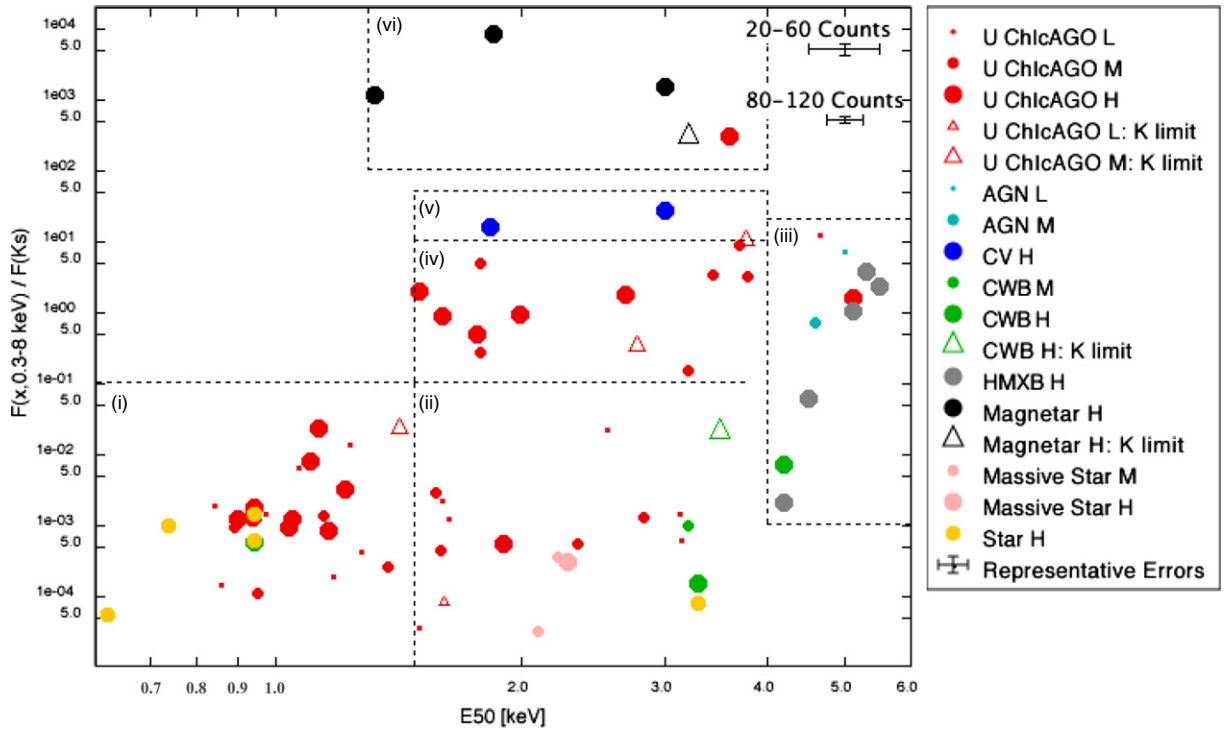

Figure 8. Observed X-ray to K_s-band flux ratio ($F_{x,0.3–8\ \mathrm{keV}}/F_{Ks}$) vs. median energy ($E_{50}$ keV) of unidentified ChIcAGO sources and the identified ChIcAGO and AGPS sources. The different sizes of data points represent whether a given source has a low count rate (L as listed in the legend), a medium count rate (M), or a high count rate (H). The unidentified ChIcAGO sources ("U ChIcAGO") are represented by red data points, and the identified ChIcAGO and archival sources are in other colors. The triangles represent those sources that only have upper limits on their K_s-band fluxes, implying lower limits on their F_x/F_{Ks} ratios. The representative error bars demonstrate the sizes of errors expected from a 20–60 count X-ray source or an 80–120 count X-ray source. This plot has been divided into six regions, indicated by the dashed lines and roman numerals, in order to further explore the source populations (see Section 4.2).

(A color version of this figure is available in the online journal.)

a clue to its nature. ChI J154557–5443_3 is discussed further in Section 4.3.4.

The unidentified ChIcAGO source that sits at the bottom right of Figure 7, ChI J153818–5541_1, is very faint in the near-infrared but bright in high energy X-rays. It is therefore very similar in both X-ray and K_s-band fluxes to the identified archival magnetars, suggesting a similar identification that warrants further investigation. ChI J153818–5541_1 is further discussed in Section 4.3.3.

In order to further identify the possible populations that make up the above-described groups, we created a statistical plot that also takes into account the hardness of each of the unidentified ChIcAGO sources. Figure 8 plots the X-ray to K_s-band flux ratio ($F_{x,0.3–8.0\ \mathrm{keV}}/F_{Ks}$) versus the median energy (E_{50} keV), in the 0.3–8.0 keV energy band, of each unidentified ChIcAGO source ("U ChIcAGO"; red data points). We further separated the ChIcAGO sources into the categories "low," "medium," and "high" on the basis of their ACIS-S and HRC-I X-ray count rates, using symbol sizes to distinguish these categories. The smallest data points (low) have count rates of <15 counts s^{-1}, the medium-sized data points (medium) have count rates between 15 and 40 counts s^{-1}, and the largest data points (high) have count rates of >40 counts s^{-1}. The identified ChIcAGO and archival sources, also divided into categories on the basis of the X-ray count rate expected from a *Chandra* ACIS-S observation, have also been included in Figure 8. As the X-ray fluxes and median energy errors are fundamentally based on the number of X-ray counts detected in the *Chandra* observations, we show two representative error bars for the low-count ChIcAGO sources (20–60 counts) and the high-count ChIcAGO sources (80–120 counts). The error associated with the K_s-band flux is greater for PANIC magnitudes than for 2MASS magnitudes. We therefore adopt the PANIC K_s-band flux errors so that the vertical error bars represent the maximum possible error in the F_x/F_{Ks} ratio for low- and high-count unidentified ChIcAGO sources.

In Figure 8, group 1 and source ChI J154557–5443_3 from Figure 7 have flux ratios $F_x/F_{Ks} < 0.1$ but have a wide range of median energies. Group 2 is harder than group 1, with $E_{50} > 1.5$ keV but with a flux ratio $0.1 < F_x/F_{Ks} < 20$. The unidentified ChIcAGO source ChI J153818–5541_1 from Figure 7 is quite hard ($E_{50} > 3$ keV), with $F_x/F_{Ks} \approx 300$. Using Figure 7 as a guide, as well as the relative positions between the unidentified ChIcAGO sources and the identified ChIcAGO and archival sources in Figure 8, we divided the groups and isolated sources from Figure 7 into six different population regions. These regions are marked by dashed lines and labeled with Roman numerals in Figure 8. The region boundaries in this plot are based on the observed X-ray properties and K_s band flux. If these values were extinction and absorption corrected, both the F_x/F_{Ks} and E_{50} region boundaries would lower.

Region i ($E_{50} < 1.5$ keV and $F_x/F_{Ks} < 0.1$) in Figure 8 contains unidentified ChIcAGO sources with low, medium, and high count rates. The majority of the low-count-rate unidentified ChIcAGO sources included in Figure 8 fall into this region. These low-count-rate sources could be very nearby objects that were only detected because of their close proximity to the solar system, or they are simply a more distant version of the medium- and high-count-rate sources in Region i. All unidentified ChIcAGO sources in this region are unlikely to be extragalactic given their softer X-ray spectra and bright

K_s-band counterparts compared to the XBootes AGNs in Figure 7. Within this region are three of the archival X-ray stars (yellow data points), of which there is an RS CVn star, a PMS star, and a multiple system. The unidentified ChIcAGO sources in Region i are therefore likely to be soft X-ray stars with ASCs or PMS stars, similar to the three archival stars but at a variety of distances in the Galaxy.

The sources in Region ii ($E_{50} > 1.5$ keV and $F_x/F_{Ks} < 0.1$) of Figure 8 have similar F_x/F_{Ks} ratios but slightly harder X-ray emission compared to those in Region i. This region also has fewer unidentified ChIcAGO sources than Region i, implying that it may contain a slightly rarer X-ray source population. The majority of the unidentified ChIcAGO sources in Region ii have low or medium count rates, with only one in the high-count-rate category. The identified ChIcAGO and archival sources in this region are CWBs (green data points) and massive stars (pink dots), all of which sit at the top of the stellar track in Figure 7. We defined $E_{50} > 1.5$ keV as the lower-energy cutoff of Region ii by looking at the unidentified ChIcAGO sources closest to the CWBs and massive stars in Figure 7. The CWBs and massive stars are WNH and Of stars, which produce X-rays through instability-driven wind shocks but can also, in the case of CWBs, produce hard X-rays due to colliding winds (for example, see Anderson et al. 2011). It is therefore likely that many of the unidentified ChIcAGO sources in Region ii are WR and Of stars, some of which may also be CWBs.

Region iii ($E_{50} > 4.0$ keV and $1 \times 10^{-3} < F_x/F_{Ks} < 20$) in Figure 8 encompasses the archival HMXBs (gray dots) and the archival and identified ChIcAGO AGNs (cyan dots). The only two unidentified ChIcAGO sources in this region are ChI J170017–4220_1 (high) and ChI J172550–3533_1 (low) and are therefore quite hard X-ray sources, making HMXB or AGN identifications a strong possibility.

Region iv (1.5 keV $< E_{50} <$ 4.0 keV and $0.1 < F_x/F_{Ks} <$ 10) in Figure 8 contains 12 medium- and high-count-rate unidentified ChIcAGO sources. However, there are no identified ChIcAGO or archival sources in this region that could indicate any likely source populations. The best clue comes from Figure 7, which shows that these unidentified sources are in the same region of the plot as the identified ChIcAGO and archival AGNs. In the Galactic plane, the $\log N$–$\log S$ relation of X-ray sources in the 2.0–10.0 keV energy range (see Figure 15 of Hands et al. 2004) demonstrates that within the X-ray flux range $1 \times 10^{-13} < F_x < 2 \times 10^{-12}$ of Region iv, between 0.06 and 8 extragalactic sources are expected per square degree. These number densities are consistent with more recent $\log N$–$\log S$ modeling conducted by Mateos et al. (2008), who used 1129 *XMM* observations at $|b| > 20^\circ$ to demonstrate that sources in the 2–10 keV energy range at high Galactic latitudes agree with AGN models to better than 10%. As the ChIcAGO sources in Region iv have a number density <8 deg^{-2}, it is not unreasonable to speculate that many of the unidentified ChIcAGO sources in this region could be AGNs. However, we compared the $N_{\rm H}$ values of the Region iv ChIcAGO sources calculated from the power-law quantile analysis and spectral fits in Table 3 to the Galactic column densities in their direction from surveys conducted by Kalberla et al. (2005) and Dickey & Lockman (1990).[37] In all but four cases the ChIcAGO sources have $N_{\rm H}$ values an order of a magnitude lower than the Galactic $N_{\rm H}$, suggesting a possible Galactic origin. ChIcAGO sources ChI J181116–1828_2, ChI J181213–1842_7, ChI J190749+0803_1, and ChI J194152+2251_2 have $N_{\rm H}$ values of the same order as the Galactic column density ($N_{\rm H} = 1.2 \times 10^{22}$, 1.3×10^{22}, 1.5×10^{22}, and 1.1×10^{22} cm^{-2}, respectively; Kalberla et al. 2005), which is more indicative of an extragalacitc origin and therefore an AGN identification. *XMM* detections of ChI J181116–1828_2 and ChI J181213–1842_7 were also investigated by Cackett et al. (2006, who referred to these sources by their AGPS names AX J1811.2–1828 and AX J1812.2–1842). They derived absorbed power law spectral fits from these data and obtained parameters that agree within the 1σ errors that we derived from quantile analysis and Cash statistics spectral modeling to the *Chandra* data. However, their bestfit $N_{\rm H}$ values are lower than ours and therefore lower than the Galactic value. Cackett et al. (2006) therefore suggested a Galactic origin for these two sources proposing a possible HMXB, low-mass X-ray binary (LMXB) or CV identification for AX J1811.2–1828 (ChI J181116–1828_2) and a possible CV origin for AX J1812.2–1842 (ChI J181213–1842_7). Further multi-wavelength investigations are required to confirm the nature of the Region iv population.

Region v (1.5 keV $< E_{50} <$ 4.0 keV and $10 < F_x/F_{Ks} <$ 50) of Figure 8 encompasses the two identified archival CVs and the lower F_x/F_{Ks} ratio limit of unidentified ChIcAGO source ChI J181852–1559_2. As its flux ratio is only a lower limit (corresponding to an upper limit on the K-band flux), it is possible that ChI J181852–1559_2 may instead be a member of Region vi (described below).

Region vi (1.3 keV $< E_{50} <$ 4.0 keV and $F_x/F_{Ks} > 1 \times 10^2$) contains four identified archival magnetars. The only unidentified ChIcAGO source that sits within this region is ChI J153818–5541_1. On the basis of its proximity to these magnetars, it is possible that ChI J153818–5541_1 could also be a magnetar; however, its X-ray emission is much harder in comparison. Regardless, the position of ChI J153818–5541_1 in Figure 8 indicates that this source is definitely worthy of further study.

4.2.2. Infrared Population Statistics

In order to further refine the possible populations within Figure 8, we investigated the infrared colors of the unidentified ChIcAGO sources, once again drawing comparisons with the identified ChIcAGO and archival sources. As mentioned above, there is strong evidence in Figure 8 that some of the unidentified ChIcAGO sources in Region ii could be massive stars such as WR and Of stars and perhaps even CWBs. It is also possible that many of the ChIcAGO sources, particularly in Region i, are PMS stars given their X-ray to infrared flux ratio is similar to that of the COUP stars in Figure 8. However, for the purposes of this paper we have chosen to concentrate on the selection criteria for the hard X-ray emitting massive stars. We therefore leave the investigation of the PMS star population in the ChIcAGO survey for future work (for infrared selection criteria for PMS stars, see Favata et al. 2005; Maercker & Burton 2005; Maercker et al. 2006).

Hadfield et al. (2007) created a selection criterion for WR stars using GLIMPSE and 2MASS magnitudes that was further refined by Mauerhan et al. (2011). Figures 9(a) and (b) are recreations of the Hadfield et al. (2007) [3.6]–[4.5] versus [3.6]–[8.0] and $J - K_s$ versus $K_s -$ [8.0] color–color plots, showing the unidentified ChIcAGO sources. (The numbers in brackets correspond to the effective wavelength in microns of the GLIMPSE magnitude bands.) The dashed lines in Figures 9(a) and (b) indicate the color space used by Mauerhan et al. (2011)

[37] The Galactic column densities were obtained using the online HEASARC calculator. http://heasarc.gsfc.nasa.gov/cgi-bin/Tools/w3nh/w3nh.pl

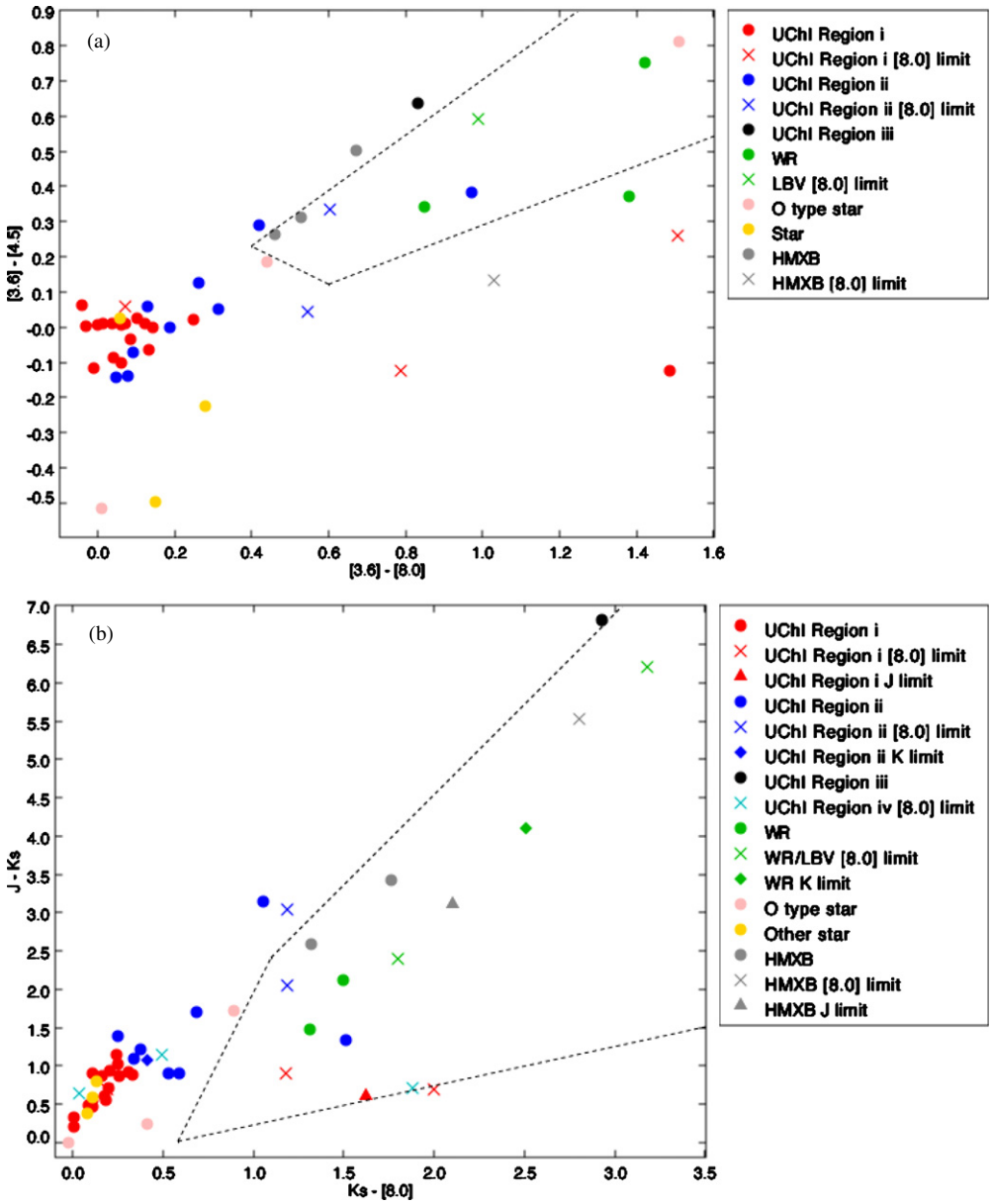

Figure 9. Infrared and near-infrared color–color diagrams illustrating the selection criteria of Hadfield et al. (2007) and Mauerhan et al. (2011) for WR stars. (a) 3.6–4.5 μm vs. 3.6–8.0 μm. (b) $J - K_s$ vs. $K_s - 8.0\,\mu$m. In both plots the dashed lines indicated the WR color space used by Mauerhan et al. (2011). The unidentified ChIcAGO sources ("UChI") are represented by red, blue, and black for Regions i, ii, and iii, respectively. The identified ChIcAGO and archival AGPS sources that are WRs and LBVs (green), massive O-type stars (pink), all other nondegenerate stars (yellow), and HMXBs (gray) are also represented. The dots represent those sources that have accurate photometric information in the magnitude bands plotted. The crosses indicate those source for which we have used their GLIMPSE 5.8 μm magnitude in the absence of a GLIMPSE 8.0 μm detection. The Region iv sources in Figure 9(b) (cyan crosses) were not detected at 5.8 or 8.0 μm, so their 4.5 μm magnitudes were used instead. The triangles mark sources for which the J magnitude is a lower limit. The diamonds mark sources for which the K_s magnitude is a lower limit.

(A color version of this figure is available in the online journal.)

to select WR candidates. These color spaces indicate where WR stars are expected to fall in comparison to field stars because of the infrared excess of WR stars resulting from free-free emission generated in their strong, dense stellar winds (see Mauerhan et al. 2011, and references therein).

In Figures 9(a) and (b), the unidentified ChIcAGO sources (UChI) have been separated into different colored symbols based on whether they are in Region i (red), Region ii (blue), or Region iii (black). In both plots, the majority of unidentified ChIcAGO sources, particularly from Region i, do not have an infrared excess, so they cluster together near the origin where Hadfield et al. (2007) state the general stellar locus is located. These unidentified ChIcAGO sources are therefore unlikely to have strong stellar winds, so they are more likely to have ASCs. There are, however, several Region ii sources and three Region i sources that have more unusual colors, falling within, very close to, or below the indicated WR color spaces. (It should be noted that many of these unusually colored unidentified ChIcAGO sources only have magnitude lower limits in one or more of the filter bands, making their positions in these color–color diagrams uncertain. See Figures 9(a) and (b) for details on these magnitude-limited sources.)

Rather than keeping the original identified source categories, we have instead separated the identified ChIcAGO and archival massive stars and CWBs into categories based on their dominant stellar components. These categories are WR and LBVs (green data points), massive O-type stars (pink data points), and all other nondegenerate stars (yellow data points). The HMXBs are still indicated by gray data points.

The identified WR stars fall within one or both of the Mauerhan et al. (2011) WR color spaces in Figures 9(a) and (b). On the basis of their positions within one or both WR color spaces, it is possible that unidentified Region ii ChIcAGO sources ChI J181915–1601_2, ChI J180857–2004_2, and ChI J183345–0828_1 may also be WR stars. In fact, using this color space technique, Hadfield et al. (2007) identified the 2MASS counterpart of ChI J181915–1601_2, 2MASS J18192219-1603123, as a WR star and further classified it as a WN7o star using spectroscopy. There are also three Region i unidentified ChIcAGO sources, ChI J154557–5443_1, ChI J154557–5443_3, and ChI J172550–3533_2, whose magnitude limits fall within the WR color space of Figure 9(b) and below the WR color space of Figure 9(a), which may also be worth further investigation.

The identified ChIcAGO source AX J144547–5931 (an Of-type star, which is also shown as a pink dot in Figures 7 and 8; see Anderson et al. 2011) sits to the left of both WR color spaces in Figures 9(a) and (b). Unidentified Region ii ChIcAGO sources ChI J182435–1311_1, ChI J182651–1206_4, ChI J183356–0822_3, and ChI J184652–0240_1 are also located in the same vicinity as AX J144547–5931 in one or both plots (within $0.2 < [3.6] - [8.0] < 0.5$ in Figure 9(a) and within $0.5 < K_s - [8.0] < 1.2$ in Figure 9(b)). While these four unidentified ChIcAGO sources have unusual infrared colors, they are not as extreme as those of typical WR stars. Given their proximity in Figure 9 to the Of star AX J144547–5931, it is possible that these unidentified ChIcAGO sources could be similar massive O-type stars. The remaining Region ii ChIcAGO sources lie within the general stellar locus of Figures 9(a) and (b), so they could be massive stars, ASCs, or PMS stars.

The archival HMXBs also have unusual infrared colors as they fall within or above the top edge of the WR color spaces in Figures 9(a) and (b). These infrared colors may be due to intrinsic absorption (for example, see Rodriguez et al. 2006). Several unidentified Region ii ChIcAGO sources also lie close to the HMXBs in these plots, but as they have much softer median X-ray energies (see Figure 8), such an identification is unlikely. ChI J170017–4220_1 is the only Region iii source with sufficient infrared magnitude information to be displayed in Figures 9(a) and (b). This unidentified ChIcAGO source falls within the vicinity of the HMXBs in Figure 8 but has much more extreme infrared colors and lies above the WR color space in both color–color plots. Further investigation is required to confirm the X-ray binary nature of ChI J170017–4220_1.

None of the 11 unidentified Region iv ChIcAGO sources have been detected at 8 μm, with only 3, ChI J163751–4656_1, ChI J165420–4337_1, and ChI J190818+0745_1, detected with GLIMPSE at 3.6 and 4.5 μm, all of which are likely to be Galactic in origin (see Section 4.2.1). In Figure 9(b) we have plotted these three unidentified ChIcAGO sources using their 4.5 μm magnitude in place of 8 μm magnitude. Only ChI J165420–4337_1 falls within the WR color space. Given the extreme uncertainties associated with the $K_s - [8.0]$ color of ChI J165420–4337_1, no conclusions can be drawn about its possible nature.

4.3. Further Discussion of Interesting ChIcAGO and AGPS Sources

We have flagged several of the unidentified ChIcAGO sources as interesting and worthy of future follow-up on the basis of their X-ray and infrared properties explored in Section 4.2. These population statistics have also allowed us to make some tentative identifications. The details of these sources are described below. There are several unidentified ChIcAGO sources that are not detailed in this section but are listed, along with their tentative identification based on the population statistics, in Table 12.

4.3.1. ChI J144519–5949_2

ChI J144519–5949_2 is one of the six ChIcAGO sources detected within the H II region GAL 316.8–00.1 (see Table 9). As it does not have a GLIMPSE counterpart, it is not included in Figures 9(a) and (b). However, its 2MASS counterpart, 2MASS 14452143-5949251, has unusual colors and falls within the WR color space of the $J-H$ versus $H - K_s$ plot in Figure 1 of Mauerhan et al. (2011). We therefore tentatively identify ChI J144519–5949_2 as a candidate WR star. Given the location of ChI J144519–5949_2 in Region ii of Figure 8, particularly near two identified CWBs, it is very likely that this star has very strong winds that are generating X-rays through instability-driven wind shocks. This object could even possibly be a CWB (for example, see Anderson et al. 2011).

4.3.2. ChI J150436–5824_1

Several unidentified AGPS sources have been investigated by Degenaar et al. (2012) using the X-Ray Telescope (XRT) on the *Swift* satellite (Gehrels et al. 2004). Degenaar et al. (2012) suggest that ChI J150436–5824_1 (which they publish under the AGPS name AX J1504.6–5824) could possibly be associated with a main sequence star that falls within the 90% XRT error circle. However, the ChIcAGO *Chandra* observation of ChI J150436–5824_1 demonstrates that there is no cataloged counterpart within the $<1''$ position error circle of this X-ray source, arguing against this tentative identification.

4.3.3. ChI J153818–5541_1

In Figure 7, ChI J153818–5541_1 has properties that are clearly not consistent with the stellar or AGN populations. It sits near the bottom right-hand corner of Figure 7, having X-ray and infrared fluxes similar to the archival magnetars (black data points). ChI J153818–5541_1 also falls within Region vi in Figure 8 along with these same magnetars, further indicating a possible magnetar nature. However, during the writing of this paper, recent studies with *Swift* have indicated that ChI J153818–5541_1 (published under its AGPS name AX J1538.3–5541) may in fact be a LMXB (Degenaar et al. 2012). If this is the case, then X-ray and infrared statistical analysis is not a foolproof diagnostic. That being said, this same statistical analysis has allowed us to show that interesting and unusual Galactic X-ray sources fall within Region vi of Figure 8. (It should be noted that a magnetar identification for this source has not been completely ruled out.)

4.3.4. ChI J154557–5443_3

ChI J154557–5443_3 is a soft X-ray source as demonstrated by its isolated position in Figure 7. Only 2 X-ray counts, from a total of 22 detected with *Chandra*, had an energy >2 keV, but otherwise, the source's median energy ($E_{50} = 0.8$ keV) is

consistent with the other sources in Region i of Figure 8. The X-ray to optical flux ratio for this source is $\log[F_{(x,0.3-8\ \mathrm{keV})}/F_R] = -2.5$ (where $F_R = \lambda F_{R,\lambda}$ using the R magnitude band), which is consistent with what is expected from stars and normal galaxies (Mainieri et al. 2002). An unusual property of this source is its position in WR color space in Figure 9(b), but this may result from using its 5.8 μm GLIMPSE magnitude in place of a lacking 8.0 μm magnitude. An optical or infrared spectrum would likely reveal the identity of this source. ChI J154557–5443_3 is therefore unlikely to be related to AX J154557–5443 as *ASCA* only detected hard counts (>2 keV) from this AGPS source.

4.3.5. ChI J162011–5002_1

Degenaar et al. (2012) tentatively identified ChI J162011–5002_1 (published under its AGPS name AX J1620.1–5002) as a candidate accreting magnetized white dwarf on the basis of its hard X-ray spectrum described by a flat power law and lack of any cataloged optical/infrared counterpart. The power-law index obtained using quantile spectral interpolation (see Table 3) agrees with the result from Degenaar et al. (2012) and is consistent with the spectra of magnetically accreting white dwarfs ($\Gamma < 1$; Muno et al. 2003). However, our analysis resulted in a column density higher than the value calculated by Degenaar et al. (2012, $N_{\mathrm{H}} \lesssim 3 \times 10^{21}$ cm^{-2}). Deep imaging in the H band with PANIC resulted in the detection of a faint counterpart ($H = 17.01 \pm 0.14$). Further follow-up is required to confirm this classification.

4.3.6. AX J162246–4946

The newly discovered radio and X-ray emitting magnetar, PSR J1622–4950 (also known as CXOU J162244.8–495054; Evans et al. 2010; Levin et al. 2010), was not cataloged by ChIcAGO MAP. This is because it lies 4′ from the position of AX J162246–4946 and is therefore outside the 3′ radius for which ChIcAGO MAP searches for X-ray point sources. However, PSR J1622–4950 was detected in this ChIcAGO *Chandra* observation, and further investigation in Anderson et al. (2012) demonstrates that this magnetar may have contributed up to 75% of the X-ray emission originally detected by *ASCA* from AX J162246–4946. We therefore identify AX J162246–4946 as PSR J1622–4950, and this source has been included as an identified magnetar in Figures 7 and 8. (For further discussion on X-ray point sources detected beyond the 3′ search radius surrounding the AGPS position, see Appendix B.)

4.3.7. AX J165951–4209

While Sugizaki et al. (2001) reported an absorbed flux of $F_x = 4.04 \times 10^{-12}$ erg cm^{-2} s^{-1} from AX J165951–4209 in the 0.7–10.0 keV band, this AGPS source was not detected in the ChIcAGO *Chandra* observation on 2008 June 21, with an upper limit on any X-ray flux of $F_x \sim 5 \times 10^{-14}$ erg cm^{-2} s^{-1} (0.3–8 keV). AX J165951–4209 was also not detected with the *Swift* XRT on 2008 January 23 (Degenaar et al. 2012) at a flux level of $F_x \sim 3 \times 10^{-13}$ erg cm^{-2} s^{-1} (0.3–10 keV). While variability of several orders of magnitude (in this case a factor of ~100) is typical behavior of both Be X-ray binaries (BeXs; Reig 2011) and black hole transients (McClintock & Remillard 2006), the hard power-law index calculated from the *ASCA* spectrum of this source ($\Gamma \sim 0.47$; Sugizaki et al. 2001) is quite hard. This power-law index is harder than what is usually observed from black hole transients (McClintock & Remillard 2006) but is consistent with spectra from BeXs (for example, see Haberl et al. 2008). We therefore suggest that AX J165951–4209 could be a transient BeX.

4.3.8. ChI J170017–4220_1

ChI J170017–4220_1 (also known as AX J1700.2–4220) has long been assumed to be a HMXB (see Liu et al. 2006; Bird et al. 2007; Krivonos et al. 2007; Bird et al. 2010). This is, however, unconfirmed and is partly based upon the assumption that the Be star HD 153295 (2MASS J17002524-4219003) is the counterpart to ChI J170017–4220_1 (Negueruela & Schurch 2007). The ChIcAGO *Chandra* observation shows that HD 153295 is actually the counterpart to ChI J170017–4220_2 (see Table 7) and that ChI J170017–4220_1 has no 2MASS counterpart. The main clue to the nature of ChI J170017–4220_1 comes from Markwardt et al. (2010), who detected a 54 s X-ray pulse period and 44 day orbital period using archival *XMM* and *Rossi X-ray Timing Explorer* data. These period values are suggestive of a Be HMXB (Markwardt et al. 2010).

We obtained PANIC NIR observations of ChI J170017–4220_1 and identified its GLIMPSE counterpart, allowing this ChIcAGO source to be represented in Figures 7, 8, and 9. ChI J170017–4220_1 is part of Group 2 in Figure 7 and is therefore consistent with an AGN, but this source is also situated in the same region as the archival HMXBs in Figure 8. Its placement on Figures 9(a) and (b) demonstrates that it has very unusual infrared colors, even more extreme than the archival HMXBs, which could indicate strong winds or a large amount of circumstellar absorption. Further investigation is required to determine the true nature of ChI J170017–4220_1.

4.3.9. ChI J172050–3710_1

Degenaar et al. (2012) suggested that ChI J172050–3710_1 (also known as AX J1720.8–3710) may be associated with the NIR source 2MASS J17205180-3710371, which has colors similar to a main sequence star. They also suggested that the low absorption inferred from a power-law X-ray fit indicates that ChI J172050–3710_1 may be a foreground star. We agree that this 2MASS source is the likely counterpart to ChI J172050–3710_1 on the basis of the position obtained with the ChIcAGO *Chandra* observation (see Table 2). We also agree that the counterpart colors are unremarkable (see Figures 9(a) and (b)), given that they are consistent with the general stellar locus depicted in Figure 1 of Hadfield et al. (2007). Our quantile thermal bremsstrahlung spectral interpolation of ChI J172050–3710_1 (see Table 4) also predicts a low value of N_{H}. This, combined with the unremarkable colors of 2MASS J17205180-3710371 and the fact that this ChIcAGO source is situated in Region i of Figure 8 with the other soft X-ray emitting stars, supports the claim by Degenaar et al. (2012) that ChI J172050–3710_1 is likely a foreground main sequence star. We therefore argue that the likely source of X-ray emission from ChI J172050–3710_1 is generated in an ASC.

4.3.10. ChI J180857–2004_2

ChI J180857–2004_2 falls within the inner edge of the infrared dust bubble CN 148 (Churchwell et al. 2007). Such bubbles are formed by the stellar winds of young hot stars impacting the interstellar medium (Churchwell et al. 2006). The morphology of the dust cloud immediately surrounding ChI J180857–2004_2 demonstrates a shell-type structure. This could indicate that its stellar winds are impacting the environment and generating a small secondary bubble within CN 148.

If this is the case, then ChI J180857–2004_2 could be a young massive star with strong stellar winds. This is already indicated by its position within the WR color spaces in Figures 9(a) and (b) and by the detection of hard X-ray emission with *Chandra*, indicated by its position within Region ii of Figure 8. ChI J180857–2004_2 could therefore be a WR star, for which the X-ray emission is generated through instability-driven wind shocks, or in a CWB (see Anderson et al. 2011).

4.3.11. ChI J181116–1828_5

ChI J181116–1828_5 is a faint point source detected in the *Chandra* observation of AX J181116–1828, so it is unlikely to be the main contributor of X-ray emission to this AGPS source. This source is, however, quite hard, with all but one count having an energy >2 keV, and is coincident with a MAGPIS radio source with a core–lobe morphology (see Section 3.4). Given the morphology of its likely radio counterpart, along with the detection of predominately hard X-rays ($E_{50} = 3.4$ keV), we tentatively identify ChI J181116–1828_5 as an AGN.

4.3.12. ChI J181852–1559_2

During the writing of this paper, ChI J181852–1559_2 (also known as AX J1818.8–1559) was proposed as a magnetar candidate through the analysis of several X-ray observations (Mereghetti et al. 2012). This proposed identification is encouraging as the lower limit of ChI J181852–1559_2 in Figure 8 is consistent with the archival magnetars in Region vi, demonstrating the usefulness of this statistical plot for identifying interesting sources.

4.3.13. ChI J181915–1601_2

As mentioned in Section 4.2.2, Hadfield et al. (2007) identified 2MASS J18192219–1603123 (the counterpart to ChI J181915–1601_2; see Table 2) as a WR star of type WN7o using the same selection criteria that we have adopted in Figures 9(a) and (b). The mechanism behind the production of X-ray emission is still unknown but is likely caused by massive stellar winds, as demonstrated by the position of ChI J181915–1601_2 within Region ii of Figure 8. Further investigation is required to determine if this WR star is mainly producing X-ray emission through instability-driven wind shocks or if it is part of a CWB.

4.3.14. ChI J183345–0828_1

Kargaltsev et al. (2012) identified 2MASS J18334038–0828304 as the counterpart to ChI J183345–0828_1 (also known as CXOU J183340.3–082830), but the nature of this X-ray source is still unknown. ChI J183345–0828_1 falls within an extended X-ray source in SNR G23.5+0.1, which Kargaltsev et al. (2012) have tentatively identified as the PWN powered by PSR B1830–08. It is possible that both this PWN and ChI J183345–0828_1 may have contributed to the X-ray emission originally detected by *ASCA* from AX J183345–0828. While ChI J183345–0828_1 is unlikely to be associated with the PWN, given the relative brightness of its IR counterpart, it does fall within the WR color space in Figure 9(b). ChI J183345–0828_1 could therefore be a massive star with strong stellar winds.

4.3.15. ChI J184741–0219_3

As mentioned in Section 3.4, ChI J184741–0219_3 is coincident with a MAGPIS radio source that has a core–lobe morphology. Deep PANIC observations also allowed the detection of its infrared counterpart ($K = 18.46$), which places it in Region iii of Figure 8 (represented by the smallest cyan data point) along with the other archival AGN AX J183039–1002 (Bassani et al. 2009), which is the medium-sized cyan data point. (We obtained the NIR magnitudes $J > 20.6 \pm 0.3$, $H = 17.3 \pm 0.2$ and $K_s = 14.3 \pm 0.2$ on 2007 July 29 for AX J183039–1002 using PANIC.) As ChI J184741–0219_3 had by far the highest count rate of all sources detected in the 3′ *Chandra* region around the aimpoint for this target (see Table 1), it is likely the main contributor to the X-ray emission detected from AX J184741–0219 in the AGPS.

ChI J184741–0219_3 has a hard X-ray spectrum (see Table 3) where the resulting absorbed X-ray flux from the power-law spectral interpolation is $F_x = 2.6 \pm 0.5 \times 10^{-13}$ erg cm^{-2} s^{-1} in the 0.3–8 keV energy band. Using the same spectral interpolation parameters and the *ASCA* count rates (Sugizaki et al. 2001), *Chandra* PIMMS estimates that ChI J184741–0219_3 had an absorbed X-ray flux of $F_x \approx 1 \times 10^{-12}$ erg cm^{-2} s^{-1} during the 1999 AGPS observation. Degenaar et al. (2012) also observed the field of ChI J184741–0219_3 with the *Swift* XRT in 2007 March but only obtained an absorbed X-ray flux upper limit of $F_x < 1 \times 10^{-13}$ erg cm^{-2} s^{-1} (0.3–10 keV). These flux measurements suggest likely long-term variability from this source. We therefore tentatively identify ChI J184741–0219_3 as an X-ray variable AGN.

4.3.16. AX J185905+0333

Suzaku observations have demonstrated that AX J185905+0333 is likely an X-ray luminous cluster of galaxies behind the Galactic plane (Yamauchi et al. 2011). The extended nature of this source is the likely reason it was not detected in the short ChIcAGO *Chandra* observation.

4.3.17. AX J191046+0917

AX J191046+0917 (also known as AX J1910.7+0917), although not detected in the ChIcAGO *Chandra* observation, has been detected intermittently in a small number of *ASCA*, *XMM*, and *Integral* observations, allowing Pavan et al. (2011) to identify it as a likely HMXB candidate. Further X-ray observations are required to confirm such an identification and further refine its class.

4.3.18. ChI J194939+2631_1

During the writing of this paper, ChI J194939+2631_1 (also known as AX J194939+2631) was identified as a CV by Zolotukhin & Chilingarian (2011) using the ChIcAGO *Chandra* observation and the Isaac Newton Telescope Photometric Hα Survey of the northern Galactic plane (IPHAS; Drew et al. 2005). Further follow-up is required to confirm their tentative intermediate polar (IP) classification.

4.4. ChIcAGO Sources Identified with SIMBAD

We were also able to identify four of the bright (>20 X-ray counts) ChIcAGO sources using the SIMBAD Astronomical Database. These four ChIcAGO sources are described below. We also discuss the secondary ChIcAGO source ChI J165420–4337_2.

4.4.1. ChI J144042–6001_1

The position obtained with the ChIcAGO *Chandra* observation confirms the Sugizaki et al. (2001) identification of ChI J144042–6001_1 (also known as AX J144042–6001) as the

PMS star HD 128696. This source appears as an identified star (yellow data point) in group 1 of Figure 7, in Region i of Figure 8, and is consistent with the general stellar locus in Figures 9(a) and (b).

4.4.2. ChI J165420–4337_2

Sugizaki et al. (2001) identified AX J165420–4337 as the K5-type star HD 326426. After observing the *ASCA* position of AX J165420–4337 with *Chandra* HRC, we detected two ChIcAGO sources, ChI J165420–4337_1 (123 X-ray counts detected) and ChI J165420–4337_2 (16 X-ray counts detected). As ChI J165420–4337_1 is by far the brightest of the ChIcAGO sources detected in this *Chandra* observation, it is therefore likely to be the main source of X-ray emission originally detected in the AGPS. The fainter (secondary) ChIcAGO source in the field, ChI J165420–4337_2, is in fact the X-ray counterpart to HD 326426 on the basis of position comparisons using SIMBAD. Therefore, the identification of AX J165420–4337 as HD 326426 by Sugizaki et al. (2001) is incorrect.

4.4.3. ChI J172550–3533_2

Using the position obtained with the ChIcAGO *Chandra* observation, we identified ChI J172550–3533_2 as the dwarf nova V478 Sco (Vogt & Bateson 1982). ChI J172550–3533_2 has a soft X-ray spectrum, as indicated by its position within Region i of Figure 8, but it has quite unusual infrared colors on the basis of its position below the WR color spaces in Figures 9(a) and (b).

4.4.4. ChI J172642–3540_1

Using SIMBAD, we identified ChI J172642–3540_1 as the X-ray counterpart to the K2V-type star CD-35 11565 (Torres et al. 2006). ChI J172642–3540_1 is soft, like the other stars in Region i of Figure 8. Its position in Figures 9(a) and (b) is also consistent with the general stellar population.

4.4.5. ChI J194310+2318_5

ChI J194310+2318_5 is one of the 18 ChIcAGO sources detected within the H II region G59.5–0.2 (see Section 4.1 and Table 9). Using SIMBAD and the *Chandra* position for this source, we determined that ChI J194310+2318_5 is the X-ray counterpart to the O7V((f))-type star HD 344784 (Walborn 1973). This source is quite soft (within Region i of Figure 8) and has unremarkable infrared colors (see Figures 9(a) and (b)). The placement of ChI J194310+2318_5 in the aforementioned figures, combined with its stellar classification, makes this ChIcAGO source compatible with an ASC identification.

4.5. Confirmed and Tentative Identifications of the AGPS Sources

Table 12 reproduces the original list of the 163 AGPS sources from Sugizaki et al. (2001), now including the corresponding ChIcAGO sources with >20 X-ray counts in the second column. The confirmed or tentative identifications of these ChIcAGO sources are listed in the third column, where the abbreviations are given in the table notes. Those AGPS sources and corresponding ChIcAGO sources with confirmed identifications either were obtained from the literature, and are therefore called "archival AGPS" sources, or were obtained through the ChIcAGO survey's *Chandra* observations (i.e., this paper and Anderson et al. 2011, 2012). The tentative identifications were made through the multiwavelength follow-up and population statistics conducted on the ChIcAGO sources in Section 4.2. The fourth column gives the most common name for the AGPS and/or ChIcAGO source, while the fifth column lists the references from which the X-ray and infrared properties of a given source were obtained for use in the statistical plots (Figures 7, 8, and 9).

The tentative identifications of the ChIcAGO sources are based on the statistical plots in Section 4.2. For example, if a ChIcAGO source falls within Region i of Figure 8, then its type in Table 12 has been listed as being either an ASC or PMS star (ASC/PMS). If the ChIcAGO source falls within Region ii of Figure 8 and also within one or both of the WR color spaces in Figures 9(a) and (b), then its type has been classified as a WR star. Those ChIcAGO sources that fall within Region ii of Figure 8 and near AX J144547–5931 in Figures 9(a) and (b) (see Section 4.2.2) have been classified as massive O-type stars (MS-O). All Region ii stars that fall within the general stellar loci of Figures 9(a) and (b) could be either massive stars (MS) or ASC and so are listed as MS/ASC. (A PMS star interpretation is also possible for these Region ii sources.)

Those Region ii ChIcAGO sources listed as WR, MS, or MS-O still need to be properly investigated for evidence of X-ray emission emanating from colliding winds in a CWB. Such an identification requires further X-ray spectroscopic follow-up to identify plasma temperatures between 1 and 10 keV (Usov 1992). There are also seven AGPS sources that are listed as H II regions. Those AGPS sources identified as "H II" are actually made up of many X-ray point sources that were detected in our ChIcAGO *Chandra* observations (see Section 4.1) and are therefore young and massive stars in the H II region listed. If there is an identified X-ray star that is a significant contributor to the X-ray emission, the stellar type is listed before the H II abbreviation in the third column, along with its ChIcAGO source name in the second column. The suffixes of the other ChIcAGO sources coincident with the H II region are listed in parentheses. All other AGPS and ChIcAGO sources for which there is no identification information are classified as unknown (U). If no sources were detected in a ChIcAGO *Chandra* observation, then the AGPS source falls in the no detection (ND) category. A detailed description of some of the AGPS sources identified through the ChIcAGO survey and of the archival AGPS sources (i.e., those sources identified in the literature and therefore not observed with *Chandra* as part of the ChIcAGO survey) can be found in Section 4.3 and Appendix A, respectively.

The final column in Table 12 contains a flag for the first and second columns that indicates whether an AGPS and/or ChIcAGO source has a confirmed identification (I) obtained through work in the ChIcAGO survey or a tentative identification (T) using the population statistics in Section 4.2. Those AGPS sources for which no ChIcAGO sources were detected within 3′ of the *ASCA* position or only faint (<20 X-ray counts) ChIcAGO sources were detected (F) are also indicated. (This flag excludes those AGPS sources that have been identified as H II regions.) The unidentified population of ChIcAGO sources that fall in Region iv of Figure 8 (R) is also included. There is also a flag for the third column that indicates whether the type identification for a ChIcAGO source is unconfirmed (N) because it is based on its tentative statistical identification in Section 4.2.

5. CONCLUSIONS

The main aim of the ChIcAGO survey is to identify the Galactic plane X-ray source populations that make up the $F_x \sim 10^{-13}$ to 10^{-11} erg cm^{-2} s^{-1} flux range. To achieve this we

have used new observations from the *Chandra* X-ray telescope, along with extensive multiwavelength follow-up, to identify sources from the *ASCA* Galactic Plane Survey (Sugizaki et al. 2001). We have reported observations of the *ASCA* positions of 93 unidentified AGPS sources with *Chandra*, from which a total of 253 X-ray point sources, termed "ChIcAGO sources," have been detected.

Through visual inspection of Galactic plane radio surveys, we have found five ChIcAGO sources within SNRs that have no cataloged optical or infrared counterparts. These sources could potentially be compact objects associated with their surrounding SNRs. Further radio analysis has also demonstrated that the ChIcAGO sources detected in the *Chandra* observations of the AGPS sources AX J144519–5949, AX J151005–5824, AX J154905–5420, AX J162208–5005, AX J194310+2318, AX J194332+2323, and AX J195006+2628 are all coincident with H II regions. Table 11 demonstrates that the range of luminosities, which are calculated using kinematic distances to the H II regions, is consistent with the luminosities we expect from flaring PMS stars, massive stars, and CWBs. We therefore identify the 54 separate ChIcAGO sources seen in these *Chandra* observations as young and massive stars within H II regions.

Of the 93 *Chandra*-observed AGPS fields, 62 have 1 or more sources with >20 X-ray counts, resulting in the detailed study of 74 ChIcAGO sources in this paper. The multiwavelength follow-up of these ChIcAGO sources demonstrates the need for *Chandra*'s subarcsecond localization capabilities to correctly identify likely infrared and optical counterparts. The main focus of this paper has been on those unidentified ChIcAGO sources with >20 X-ray counts and with near-infrared or infrared counterparts. This has allowed us to perform population statistics to identify some of the likely objects that make up the $F_x \sim 10^{-13}$ to 10^{-11} erg cm^{-2} s^{-1} Galactic plane X-ray source populations.

We have developed a new statistical diagnostic for identifying likely populations of X-ray emitting sources using *K*-band fluxes and upper limits (see Figure 8). The unidentified ChIcAGO sources in Region i of Figure 8 have soft X-ray emission and low X-ray to infrared flux ratios, making them consistent with many of the archival and identified ChIcAGO stars. Their X-ray to infrared flux ratios are also similar to the COUP stars (see Figure 7), which are predominantly PMS stars. The majority of the Region i sources also fall within the general stellar locus that is expected in Figures 9(a) and (b) (Hadfield et al. 2007). They are therefore likely to be ASCs, which is consistent with the main soft X-ray populations expected in the Galactic plane (Hong et al. 2005), or PMS stars.

Many of the ChIcAGO sources in Region ii of Figure 8 have infrared colors similar to known WR stars, as demonstrated in Figure 9, which indicates the presence of excess infrared emission resulting from strong, dense stellar winds. These sources are therefore likely to be massive stars generating X-rays through instability-driven wind shocks or even colliding winds in CWBs (for example, see Anderson et al. 2011).

Only two unidentified ChIcAGO sources are located within Region iii of Figure 8, along with the archival high-mass and symbiotic X-ray binaries (and AGNs). As such X-ray binaries (XRBs) are rare, only a few unidentified ChIcAGO sources are expected to fall within this group. This result therefore demonstrates that Figure 8 may be a very useful diagnostic for identifying XRBs.

Region vi contains four identified magnetars and a candidate LMXB. Even though there are likely two different source populations in Region vi, Figure 8 demonstrates that hard X-ray sources ($E_{50} > 1.3$ keV), with an X-ray to infrared flux ratio $F_x/F_{Ks} > 10^2$, are very rare and interesting Galactic X-ray sources.

The population of ChIcAGO sources in Region iv of Figure 8 remains unidentified. On the basis of their position relative to the identified AGN in Figure 7 and their high N_H values compared to the Galactic column density, we suggest that ChIcAGO sources ChI J181116–1828_2, ChI J181213–1842_7, ChI J190749+0803_1, and ChI J194152+2251_2 could be background AGNs. The remaining eight unidentified Region iv ChIcAGO sources have N_H values far lower than the Galactic column densities, indicating that they could be located in our own Galaxy. Optical and infrared spectroscopic follow-up is required to identify the true nature of this population.

With further source identifications, a full log N–log S model of the hard (2–10 keV) Galactic plane X-ray populations between $F_x \sim 10^{-13}$ and 10^{-11} erg cm^{-2} s^{-1} will be able to be constructed. This log N–log S model will be more complete than those constructed from previous X-ray surveys in the same flux range, as it will be representative of 40 deg^2 of the Galactic plane. It will also show individual contributions from different Galactic X-ray source populations including nonaccretion-powered sources such as CWBs, SNRs, PWNe, and magnetars, which have not been a focus of previous work. Using the log N–log S distribution and distance estimates, it will then be possible to construct luminosity functions and three-dimensional spatial distributions of each class of X-ray source in the Galactic plane.

G.E.A. acknowledges the support of an Australian Postgraduate Award. B.M.G. acknowledges the support of an Australian Laureate Fellowship through ARC grant FL100100114. P.O.S. acknowledges partial support from NASA contract NAS8-03060. D.T.H.S. acknowledges a STFC Advanced Fellowship. J.J.D. was supported by NASA contract NAS8-39073 to the Chandra X-ray Center (CXC). Support for this work was also provided by NASA through *Chandra* award number GO9-0155X issued by the CXC, which is operated by the Smithsonian Astrophysical Observatory for and on behalf of NASA. The access to major research facilities program is supported by the Commonwealth of Australia under the *International Science Linkages program*. This research makes use of data obtained with the *Chandra X-ray Observatory* and software provided by the CXC in the application packages CIAO. The ATCA is part of the Australia Telescope, funded by the Commonwealth of Australia for operation as a National Facility managed by CSIRO. The MOST is operated with the support of the Australian Research Council and the Science Foundation for Physics within the University of Sydney. Observing time on the 6.5 m Baade Magellan Telescope, located at Las Campanas Observatory, was allocated through the Harvard-Smithsonian Center for Astrophysics and the Massachusetts Institute of Technology. 2MASS is a joint project of the University of Massachusetts and the IPAC/Caltech, funded by NASA and the NFS. GLIMPSE survey data are part of the Spitzer Legacy Program. The *Spitzer Space Telescope* is operated by JPL/Caltech under a contract with NASA. This research has made use of NASA's Astrophysics Data System.

Facilities: ASCA, ATCA, CXO (ACIS,HRC), CTIO:2MASS, FLWO:2MASS, Magellan:Baade (IMACS, MagIC, PANIC), Molonglo Observatory, Spitzer, VLA, XMM (EPIC)

APPENDIX A

SOURCE DESCRIPTIONS OF THE ARCHIVAL AGPS SOURCES

As mentioned in Section 1, approximately one-third of the AGPS sources were identified by Sugizaki et al. (2001) or were classified by other research groups prior to the ChIcAGO survey. It is these identified AGPS sources, referred to as "archival sources" in Section 4.2.1, that have been used to narrow down the possible unidentified ChIcAGO source populations. The archival AGPS sources are listed in Table 12 and are briefly described below.

AX J143416–6024. RS CVn-type variable star, HD 127535, with spectral type K1IIIe (Sugizaki et al. 2001).

AX J155052–5418. X-ray and radio emitting magnetar 1E 1547.0-5408, associated with the possible radio SNR G327.24-0.13 (Gelfand & Gaensler 2007).

AX J155644–5325. KOIIIe-type star, TYC 8697–1438-1 (Torres et al. 2006).

AX J161929–4945. SFXT, a subclass of HMXBs that displays fast X-ray outbursts (Sguera et al. 2006; Tomsick et al. 2006).

AX J162155–4939. K3III-type star, HD 147070 (Sugizaki et al. 2001); this identification needs to be confirmed by follow-up X-ray observations.

AX J163159–4752. Accretion-driven 1300 s X-ray pulsar in a supergiant HMXB (Rodriguez et al. 2006; Walter et al. 2006). This system is one of the highly absorbed HMXBs identified by *Integral* (Negueruela & Schurch 2007).

AX J163351–4807. The magnetic Of?p star HD 148937 (Nazé et al. 2012).

AX J163555–4719. The X-ray emission associated with SNR G337.2+0.1 and its PWN (Combi et al. 2006). This system is also associated with the *Fermi*-LAT source 1FGL J1635.7–4715 (Abdo et al. 2010).

AX J163904–4642. Originally identified as a 912 s pulsating, heavily absorbed HMXB (Bodaghee et al. 2006; Thompson et al. 2006), this source has now been reclassified as a SyXB (Nespoli et al. 2010).

AX J164042–4632. X-ray PWN associated with the radio SNR G338.3–0.0 and the very high energy γ-ray source HESS J1640–465 (Funk et al. 2007; Lemiere et al. 2009). This system is also associated with the *Fermi*-LAT source 1FGL J1640.8–4634 (Abdo et al. 2010; Slane et al. 2010).

AX J165437–4333. The F7V-type star HD 152335 (Sugizaki et al. 2001).

AX J165904–4242. Herbig Be star V921 Sco, where the X-ray emission may arise from magnetic activity (Hamaguchi et al. 2005). (Sugizaki et al. 2001 incorrectly assigned this star as the counterpart to AX J165901–4208.)

AX J170006–4157. Magnetized CV, likely of the IP class, with 715 s X-ray pulsations (Torii et al. 1999; Kaur et al. 2010).

AX J170047–4139. A 38 s pulsating HMXB with an Ofpe/WNL-type mass donor (Chakrabarty et al. 2002; Mason et al. 2009).

AX J170349–4142. SNR G344.7–0.1 and its possible CCO (Combi et al. 2010). There is a possible γ-ray counterpart, HESS J1702–420 (Giacani et al. 2011).

AX J171804–3726. SNR G349.7+0.2 and its possible CCO (Slane et al. 2002; Lazendic et al. 2005). This remnant is also associated with the *Fermi*-LAT source 1FGL J1717.9–3729 (Castro & Slane 2010).

AX J172105–3726. SNR G350.1–0.3 and its CCO (Gaensler et al. 2008; Lovchinsky et al. 2011).

AX J172743–3506. SNR G352.7–0.1 (Giacani et al. 2009).

AX J173441–3234. CWB HD 159176 (07V+07V) in the young open cluster NGC 6383. The short period of this binary implies that the winds likely collide well before reaching their terminal velocities, limiting the hardness of the resulting thermal X-ray emission (De Becker et al. 2004).

AX J173518–3237. SNR G355.6–0.0 (Yamauchi et al. 2008).

AX J180225–2300. X-ray emission associated with the OB-type and pre-main-sequence stars in the Trifid Nebula. The main X-ray contributor is the HD 164492 multiple system of OB stars (Rho et al. 2004).

AX J180838–2024. Magnetar SGR 1806–20 (Kouveliotou et al. 1998).

AX J180902–1948. SNR G10.5–0.0. Other than this *ASCA* detection (Sugizaki et al. 2001), no other X-ray papers exist on this source. The radio SNR was discovered by Brogan et al. (2006).

AX J180948–1918. PSR J1809–1917 and its PWN, which are likely associated with HESS J1809–193 (Kargaltsev & Pavlov 2007; Aharonian et al. 2007).

AX J180951–1943. The X-ray and radio emitting magnetar XTE J1810–197 (Ibrahim et al. 2004; Halpern et al. 2005).

AX J181211–1835. SNR G12.0–0.1 (Yamauchi et al. 2008).

AX J182104–1420 SNR G16.7+0.1 and its central PWN (Helfand et al. 2003a).

AX J183039–1002. A Compton-thick active galactic nucleus (Bassani et al. 2009). A K_s-band magnitude of 14.3 ± 0.2 was obtained for this source with PANIC on 2007 July 29 (see Section 4.3.15).

AX J183221–0840. Magnetized CV, likely of the IP class, with 1549.1 s X-ray period pulsations (Sugizaki et al. 2000; Kaur et al. 2010).

AX J183528–0737. The 112 s pulse period X-ray binary, Scutum X-1. This system is likely to be a SyXB (Kaplan et al. 2007).

AX J183800–0655. The 70.5 ms pulsar, PSR J1838–0655, and its PWN. This system is possibly associated with HESS J1837–069 (Gotthelf & Halpern 2008; Kargaltsev et al. 2012).

AX J183931–0544. The LBV candidate G26.47+0.02. This source is possibly in a CWB (Paron et al. 2012). It is assumed that 2MASS J18393224–0544204 is the correct NIR counterpart for the purpose of the statistical analysis in Section 4.2.

AX J184121–0455. The magnetar 1E 1841–045 and its associated SNR G27.4+0.0 (Kes 73; Gotthelf & Vasisht 1997; Morii et al. 2003).

AX J184355–0351. X-ray emission associated with the nonthermal SNR G28.6–0.1/AX J1843.8–0352 and the thermal source CXO J184357–035441 (which may or may

Table 13
Chandra Point Sources with >20 X-Ray Counts Detected between 3′ and 5′ from the AGPS Position

AGPS Source[a]	wavdetect Position		Position[b]	Offset[c]	Net Counts[d]	Predicted Counts[e]	Total Counts[f]	2MASS Name
AX	R.A. (J2000)	Decl. (J2000)	Error (″)	from *ASCA* (′)	0.3-8 (keV)		<3′	2MASS J
J150436–5824	15:04:13.54	−58:25:07.4	0.84	3.0	47.7 ± 8.0	139	154	
J154557–5443	15:46:09.08	−54:39:12.9	0.89	4.2	48.0 ± 8.1	147	96	15460913–5439128
	15:45:54.60	−54:38:49.6	0.94	4.3	38.9 ± 7.4			
J154905–5420	15:49:12.40	−54:16:30.2	0.94	4.1	31.8 ± 6.8	178	84	15491237–5416301
	15:49:14.67	−54:24:54.6	1.03	4.6	20.2 ± 5.7			15491463–5424549
J155035–5408	15:50:19.25	−54:11:27.3	0.89	3.6	35.5 ± 7.1	152	242	15501925–5411271
	15:50:05.97	−54:07:23.1	1.07	4.5	22.8 ± 6.0			
J170444–4109	17:04:26.88	−41:07:34.9	0.95	3.9	26.7 ± 6.3	95	170	17042687–4107351
J172642–3504	17:26:27.79	−35:07:27.2	0.88	4.5	72.1 ± 9.6	206	120	17262781–3507281
J181213–1842	18:12:29.26	−18:45:21.6	1.02	4.7	21.9 ± 5.8	92	172	18122923–1845222
J181915–1601	18:19:29.65	−16:04:33.3	0.95	4.6	30.0 ± 6.5	201	132	
J184738–0156	18:47:52.81	−01:59:57.9	0.89	4.8	96.5 ± 10.9	150	120	18475281–0159575
J184741–0219	18:47:32.53	−02:22:23.8	0.93	4.0	34.2 ± 7.0	211	53	
J194332+2323	19:43:29.97	+23:20:52.3	0.88	3.1	28.4 ± 6.5	143	64	19432997+2320524

Notes.
[a] The AGPS source for which one or two X-ray point sources with >20 counts were detected in the corresponding ChIcAGO *Chandra* observation between 3′ and 5′.
[b] The total 95% position error circle (in arcseconds) of the *Chandra* point source taking into account the `wavdetect` position error and the absolute astrometric accuracy of *Chandra*.
[c] The offset, in arcminutes, between the AGPS position published in Sugizaki et al. (2001) and the `wavdetect` position of the *Chandra* point source.
[d] The net number of counts in the 0.3–8.0 energy range. The source counts were calculated using a source region with a radius equal to 95% of the PSF at 1.5 keV. The total counts have been background subtracted and the error corresponds to the upper 1σ confidence limit calculated using Gehrels (1986) statistics.
[e] The number of X-ray counts that *Chandra* PIMMS predicts should be detected in the ChIcAGO *Chandra* observation based on the power law spectral fits measured by Sugizaki et al. (2001).
[f] The total number of X-ray counts (rounded to the nearest count) from all the sources detected in the ChIcAGO *Chandra* observations within 3′ of the AGPS position.

not be part of SNR G28.6–0.1; Bamba et al. 2001; Ueno et al. 2003).

AX J184629–0258. X-ray emission from the SNR G29.7–0.3 (Kes 75), its central pulsar PSR J1846–0258, and associated PWN (Helfand et al. 2003b).

AX J184848–0129. X-ray sources in the Galactic globular cluster GLIMPSE–C01 (Pooley et al. 2007) and the nearby diffuse source CXOU J184846.3–013040 (either a PWN or the globular cluster's bow shock; Mirabal 2010). These sources may also be associated with the *Fermi*-LAT source 0FGL J1848.6–0138 (Luque-Escamilla et al. 2009).

AX J184930–0055. X-ray emission associated with the thermal composite SNR G31.9+0.0 (3C 391; Chen & Slane 2001; Chen et al. 2004). This SNR is likely associated with 1FGL J1849.0–0055 (Castro & Slane 2010).

AX J185015–0025. The X-ray synchrotron-dominated SNR G32.4+0.1 (Yamaguchi et al. 2004).

AX J185240+0038. X-ray emission associated with the SNR G33.6+0.1 (Kes 79) and the 105 ms pulsar PSR J1852+0040 (there is no detectable PWN; Gotthelf & Halpern 2005). This pulsar has been described as an "antimagnetar" (Halpern & Gotthelf 2010).

AX J185551+0129. X-ray emission from SNR G34.7–0.4 (also known as W44 and 3C392) and the PWN associated with its central pulsar, PSR B1853+0.1 (Petre et al. 2002). This system may be associated with the *Fermi*-LAT source 0FGL J1855.9+0126/1FGL 1856.1+0122 (Abdo et al. 2009, 2010).

AX J190734+0709. SNR G41.1–0.3 (3C 397; Safi-Harb et al. 2005).

AX J191105+0906. SNR G43.3–0.2 (W49B; Hwang et al. 2000).

AX J194649+2512. X-ray emission likely associated with the Hα emission line star VES 52 (Kohoutek & Wehmeyer 1997; Sugizaki et al. 2001, this identification still needs to be properly confirmed by follow-up X-ray observations).

APPENDIX B

CHANDRA-DETECTED X-RAY POINT SOURCES BEYOND THE 3′ SEARCH REGION

Table 13 lists the 14 *Chandra*-detected X-ray point sources with >20 X-ray counts that lie within 3′–5′ of the *ASCA* position of 11 AGPS sources and therefore outside the ChIcAGO MAP default search radius. Table 13 includes the name of the AGPS sources for which the above applies, the position of the X-ray source, the offset from the original *ASCA* position, the net number of counts, and the most likely 2MASS counterpart.

A thorough analysis of these 14 X-ray point sources is beyond the scope of this paper; however, we have done a preliminary investigation of their possible contribution to the fluxes originally measured in the AGPS (Sugizaki et al. 2001). Using a technique similar to that described in Section 2.1, we entered the power-law spectral fit of the AGPS source measured by Sugizaki et al. (2001) into *Chandra* PIMMS in order to estimate the number of source counts expected to be detected in the corresponding ChIcAGO *Chandra* observation. (Once again the photon index and absorption were set to $\Gamma = 2$ and $N_{\rm H} = 10^{22}\,{\rm cm}^{-2}$ if no power-law fit was provided.) These count predictions are listed in Table 13. The total number of counts detected from all the X-ray sources within 3′ of

the AGPS position are also included alongside these values. In the case of AX J154557–5420, AX J154905–5420, AX J172642–3504, AX J181915–1601, AX J184741–0129, and AX J194332+2323, the total number of X-ray counts detected within 3′ of the AGPS position contributes ⩽65% of the predicted number of counts. It is therefore possible that the eight X-ray point sources detected between 3′ and 5′ from these AGPS sources could have contributed to the X-ray flux originally detected with *ASCA*. Such a result would not be unexpected for AX J154905–5420 and AX J194332+2323 as their corresponding *Chandra*-resolved point sources are stars in H II regions, which were not individually resolved with *ASCA*. This analysis demonstrates that few X-ray sources beyond 3′ of the *ASCA* position contributed to the overall flux of a given AGPS source. The 3′ search radius used in ChIcAGO MAP is therefore reasonable for detecting the majority of AGPS associated point sources detected with *Chandra*. (Note that Table 13 does not include the magnetar PSR J1622–4950 that was detected in the *Chandra* observation of AX J162246–4946, with 4′ for its *ASCA* position, as it was well investigated in Anderson et al. 2012).

REFERENCES

Abdo, A. A., Ackermann, M., Ajello, M., et al. 2009, ApJS, 183, 46
Abdo, A. A., Ackermann, M., Ajello, M., et al. 2010, ApJS, 188, 405
Aharonian, F., Akhperjanian, A. G., Bazer-Bachi, A. R., et al. 2007, A&A, 467, 1075
Anderson, G. E., Gaensler, B. M., Kaplan, D. L., et al. 2011, ApJ, 727, 105
Anderson, G. E., Gaensler, B. M., Slane, P. O., et al. 2012, ApJ, 751, 53
Bamba, A., Ueno, M., Koyama, K., & Yamauchi, S. 2001, PASJ, 53, L21
Bassani, L., Landi, R., Campana, R., et al. 2009, MNRAS, 395, L1
Benjamin, R. A., Churchwell, E., Babler, B. L., et al. 2003, PASP, 115, 953
Bernardini, F., Israel, G. L., Stella, L., et al. 2011, A&A, 529, A19
Bertin, E., & Arnouts, S. 1996, A&AS, 117, 393
Bird, A. J., Bazzano, A., Bassani, L., et al. 2010, ApJS, 186, 1
Bird, A. J., Malizia, A., Bazzano, A., et al. 2007, ApJS, 170, 175
Bocchino, F., Parmar, A. N., Mereghetti, S., et al. 2001, A&A, 367, 629
Bock, D. C.-J., Large, M. I., & Sadler, E. M. 1999, AJ, 117, 1578
Bodaghee, A., Walter, R., Zurita Heras, J. A., et al. 2006, A&A, 447, 1027
Brogan, C. L., Gelfand, J. D., Gaensler, B. M., Kassim, N. E., & Lazio, T. J. W. 2006, ApJL, 639, L25
Broos, P. S., Feigelson, E. D., Townsley, L. K., et al. 2007, ApJS, 169, 353
Buccheri, R., Bennett, K., Bignami, G. F., et al. 1983, A&A, 128, 245
Busfield, A. L., Purcell, C. R., Hoare, M. G., et al. 2006, MNRAS, 366, 1096
Cackett, E. M., Wijnands, R., & Remillard, R. 2006, MNRAS, 369, 1965
Cash, W. 1979, ApJ, 228, 939
Castro, D., & Slane, P. 2010, ApJ, 717, 372
Caswell, J. L., Clark, D. H., Crawford, D. F., & Green, A. J. 1975, AuJPA, 37, 1
Caswell, J. L., & Haynes, R. F. 1987, A&A, 171, 261
Chakrabarty, D., Wang, Z., Juett, A. M., Lee, J. C., & Roche, P. 2002, ApJ, 573, 789
Chen, Y., & Slane, P. O. 2001, ApJ, 563, 202
Chen, Y., Su, Y., Slane, P. O., & Wang, Q. D. 2004, ApJ, 616, 885
Churchwell, E., Povich, M. S., Allen, D., et al. 2006, ApJ, 649, 759
Churchwell, E., Watson, D. F., Povich, M. S., et al. 2007, ApJ, 670, 428
Combi, J. A., Albacete Colombo, J. F., López-Santiago, J., et al. 2010, A&A, 522, A50
Combi, J. A., Albacete Colombo, J. F., Romero, G. E., & Benaglia, P. 2006, ApJL, 653, L41
Condon, J. J., Cotton, W. D., Greisen, E. W., et al. 1998, AJ, 115, 1693
Crowther, P. A., Smith, L. J., Hillier, D. J., & Schmutz, W. 1995, A&A, 293, 427
Davis, J. E. 2001, ApJ, 562, 575
De Becker, M., Rauw, G., Pittard, J. M., et al. 2004, A&A, 416, 221
Degenaar, N., Starling, R. L. C., Evans, P. A., et al. 2012, A&A, 540, A22
Dickey, J. M., & Lockman, F. J. 1990, ARA&A, 28, 215
Dorman, B., & Arnaud, K. A. 2001, in ASP Conf. Ser. 238, Astronomical Data Analysis Software and Systems X, ed. F. R. Harnden, F. A. Primini, Jr., & H. E. Payne (San Francisco, CA: ASP), 415
Draper, P. W., Berry, D. S., Jenness, T., & Economou, F. 2009, in ASP Conf. Ser. 411, Astronomical Data Analysis Software and Systems XVIII, ed. D. A. Bohlender, D. Durand, & P. Dowler (San Francisco, CA: ASP), 575
Dressler, A., Hare, T., Bigelow, B. C., & Osip, D. J. 2006, Proc. SPIE, 6269, 13
Drew, J. E., Greimel, R., Irwin, M. J., et al. 2005, MNRAS, 362, 753
Durant, M., & van Kerkwijk, M. H. 2005, ApJ, 627, 376
Ebeling, H., & Wiedenmann, G. 1993, PhRvE, 47, 704
Ebisawa, K., Tsujimoto, M., Paizis, A., et al. 2005, ApJ, 635, 214
Evans, I. N., Primini, F. A., Glotfelty, K. J., et al. 2010, ApJS, 189, 37
Favata, F., Flaccomio, E., Reale, F., et al. 2005, ApJS, 160, 469
Fich, M., & Blitz, L. 1984, ApJ, 279, 125
Freeman, P. E., Kashyap, V., Rosner, R., & Lamb, D. Q. 2002, ApJS, 138, 185
Funk, S., Hinton, J. A., Pühlhofer, G., et al. 2007, ApJ, 662, 517
Gaensler, B. M., & Hunstead, R. W. 2000, PASA, 17, 72
Gaensler, B. M., Tanna, A., Slane, P. O., et al. 2008, ApJL, 680, L37
Garmire, G. P., Bautz, M. W., Ford, P. G., Nousek, J. A., & Ricker, G. R., Jr. 2003, Proc. SPIE, 4851, 28
Gehrels, N. 1986, ApJ, 303, 336
Gehrels, N., Chincarini, G., Giommi, P., et al. 2004, ApJ, 611, 1005
Gelfand, J. D., & Gaensler, B. M. 2007, ApJ, 667, 1111
Getman, K. V., Flaccomio, E., Broos, P. S., et al. 2005, ApJS, 160, 319
Giacani, E., Smith, M. J. S., Dubner, G., & Loiseau, N. 2011, A&A, 531, A138
Giacani, E., Smith, M. J. S., Dubner, G., et al. 2009, A&A, 507, 841
Gotthelf, E. V., & Halpern, J. P. 2005, ApJ, 632, 1075
Gotthelf, E. V., & Halpern, J. P. 2007, Ap&SS, 308, 79
Gotthelf, E. V., & Halpern, J. P. 2008, ApJ, 681, 515
Gotthelf, E. V., & Vasisht, G. 1997, ApJL, 486, L133
Green, A. J., Cram, L. E., Large, M. I., & Ye, T. 1999, ApJS, 122, 207
Green, D. A. 2009, BASI, 37, 45
Grindlay, J. E., Hong, J., Zhao, P., et al. 2005, ApJ, 635, 920
Haberl, F., Eger, P., & Pietsch, W. 2008, A&A, 489, 327
Hadfield, L. J., van Dyk, S. D., Morris, P. W., et al. 2007, MNRAS, 376, 248
Halpern, J. P., & Gotthelf, E. V. 2010, ApJ, 710, 941
Halpern, J. P., Gotthelf, E. V., Becker, R. H., Helfand, D. J., & White, R. L. 2005, ApJL, 632, L29
Hamaguchi, K., Yamauchi, S., & Koyama, K. 2005, ApJ, 618, 360
Hands, A. D. P., Warwick, R. S., Watson, M. G., & Helfand, D. J. 2004, MNRAS, 351, 31
Haverkorn, M., Gaensler, B. M., McClure-Griffiths, N. M., Dickey, J. M., & Green, A. J. 2006, ApJS, 167, 230
Helfand, D. J., Agüeros, M. A., & Gotthelf, E. V. 2003a, ApJ, 592, 941
Helfand, D. J., Becker, R. H., White, R. L., Fallon, A., & Tuttle, S. 2006, AJ, 131, 2525
Helfand, D. J., Collins, B. F., & Gotthelf, E. V. 2003b, ApJ, 582, 783
Helfand, D. J., Velusamy, T., Becker, R. H., & Lockman, F. J. 1989, ApJ, 341, 151
Hong, J. 2012, MNRAS, 427, 1633
Hong, J., Schlegel, E. M., & Grindlay, J. E. 2004, ApJ, 614, 508
Hong, J., van den Berg, M., Schlegel, E. M., et al. 2005, ApJ, 635, 907
Hong, J. S., van den Berg, M., Laycock, S., Grindlay, J. E., & Zhao, P. 2009, ApJ, 699, 1053
Hwang, U., Petre, R., & Hughes, J. P. 2000, ApJ, 532, 970
Ibrahim, A. I., Markwardt, C. B., Swank, J. H., et al. 2004, ApJL, 609, L21
Israel, G., Covino, S., Mignani, R., et al. 2005, A&A, 438, L1
Israel, G. L., Rea, N., Mangano, V., et al. 2004, ApJL, 603, L97
Israel, G. L., Rea, N., Rol, E., et al. 2009, ATel, 1909
Jannuzi, B. T., Dey, A., Brown, M. J. I., et al. 2004, BAAS, 36, 1478
Kaastra, J. S. 1992, An X-ray Spectral Code for Optically Thin Plasmas Updated Version 2.0 (Leidon: SRON)
Kalberla, P. M. W., Burton, W. B., Hartmann, D., et al. 2005, A&A, 440, 775
Kaplan, D. L., Frail, D. A., Gaensler, B. M., et al. 2004, ApJS, 153, 269
Kaplan, D. L., Levine, A. M., Chakrabarty, D., et al. 2007, ApJ, 661, 437
Kargaltsev, O., & Pavlov, G. G. 2007, ApJ, 670, 655
Kargaltsev, O., Schmitt, B. M., Pavlov, G. G., & Misanovic, Z. 2012, ApJ, 745, 99
Kashyap, V. L., van Dyk, D. A., Connors, A., et al. 2010, ApJ, 719, 900
Kaur, R., Wijnands, R., Paul, B., Patruno, A., & Degenaar, N. 2010, MNRAS, 402, 2388
Kenter, A., Murray, S. S., Forman, W. R., et al. 2005, ApJS, 161, 9
Kohoutek, L., & Wehmeyer, R. 1997, AAHam, 11, 1
Kouveliotou, C., Dieters, S., Strohmayer, T., et al. 1998, Natur, 393, 235
Krivonos, R., Revnivtsev, M., Lutovinov, A., et al. 2007, A&A, 475, 775
Kuchar, T. A., & Bania, T. M. 1994, ApJ, 436, 117
Kuchar, T. A., & Clark, F. O. 1997, ApJ, 488, 224
Lazendic, J. S., Slane, P. O., Hughes, J. P., Chen, Y., & Dame, T. M. 2005, ApJ, 618, 733
Lemiere, A., Slane, P., Gaensler, B. M., & Murray, S. 2009, ApJ, 706, 1269

Levin, L., Bailes, M., Bates, S., et al. 2010, ApJL, 721, L33
Liedahl, D. A., Osterheld, A. L., & Goldstein, W. H. 1995, ApJL, 438, L115
Liu, Q. Z., van Paradijs, J., & van den Heuvel, E. P. J. 2006, A&A, 455, 1165
Lovchinsky, I., Slane, P., Gaensler, B. M., et al. 2011, ApJ, 731, 70
Lucy, L. B. 1982, ApJ, 255, 286
Lucy, L. B., & White, R. L. 1980, ApJ, 241, 300
Luque-Escamilla, P. L., Martí, J., Muñoz-Arjonilla, A. J., et al. 2009, A&A, 508, 1095
Maercker, M., & Burton, M. G. 2005, A&A, 438, 663
Maercker, M., Burton, M. G., & Wright, C. M. 2006, A&A, 450, 253
Mainieri, V., Bergeron, J., Hasinger, G., et al. 2002, A&A, 393, 425
Manchester, R. N., Hobbs, G. B., Teoh, A., & Hobbs, M. 2005, AJ, 129, 1993
Markwardt, C. B., Baumgartner, W. H., Skinner, G. K., & Corbet, R. H. D. 2010, ATel, 2564
Martini, P., Persson, S. E., Murphy, D. C., et al. 2004, Proc. SPIE, 5492, 1653
Masetti, N., Landi, R., Pretorius, M. L., et al. 2007, A&A, 470, 331
Mason, A. B., Clark, J. S., Norton, A. J., Negueruela, I., & Roche, P. 2009, A&A, 505, 281
Mateos, S., Warwick, R. S., Carrera, F. J., et al. 2008, A&A, 492, 51
Mauerhan, J. C., Muno, M. P., Morris, M. R., Stolovy, S. R., & Cotera, A. 2010, ApJ, 710, 706
Mauerhan, J. C., Van Dyk, S. D., & Morris, P. W. 2011, AJ, 142, 40
McClintock, J. E., & Remillard, R. A. 2006, in Compact Stellar X-ray Sources, ed. W. H. G. Lewin & M. van der Klis (Cambridge: Cambridge Univ. Press), 157
McClure-Griffiths, N. M., Green, A. J., Dickey, J. M., et al. 2001, ApJ, 551, 394
McLean, B. J., Greene, G. R., Lattanzi, M. G., & Pirenne, B. 2000, in ASP Conf. Ser. 216, Astronomical Data Analysis Software and Systems IX, ed. N. Manset, C. Veillet, & D. Crabtree (San Francisco, CA: ASP), 145
Mereghetti, S., Esposito, P., Tiengo, A., et al. 2012, A&A, 546, A30
Mereghetti, S., Tiengo, A., Esposito, P., et al. 2005, ApJ, 628, 938
Mewe, R., Gronenschild, E. H. B. M., & van den Oord, G. H. J. 1985, A&AS, 62, 197
Mewe, R., Lemen, J. R., & van den Oord, G. H. J. 1986, A&AS, 65, 511
Mirabal, N. 2010, MNRAS, 402, 1391
Monet, D. G., Levine, S. E., Canzian, B., et al. 2003, AJ, 125, 984
Morii, M., Sato, R., Kataoka, J., & Kawai, N. 2003, PASJ, 55, L45
Motch, C., Guillout, P., Haberl, F., et al. 1997, A&A, 318, 111
Motch, C., Guillout, P., Haberl, F., et al. 1998, A&AS, 132, 341
Motch, C., Warwick, R., Cropper, M. S., et al. 2010, A&A, 523, A92
Muno, M. P., Baganoff, F. K., Bautz, M. W., et al. 2003, ApJ, 599, 465
Murphy, T., Mauch, T., Green, A., et al. 2007, MNRAS, 382, 382
Murray, S. S., Chappeu, J. H., Kenter, A. T., et al. 2000, Proc. SPIE, 4140, 144
Nazé, Y., Rauw, G., & Manfroid, J. 2008, A&A, 483, 171
Nazé, Y., Zhekov, S. A., & Walborn, N. R. 2012, ApJ, 746, 142
Negueruela, I., & Schurch, M. P. E. 2007, A&A, 461, 631
Nespoli, E., Fabregat, J., & Mennickent, R. E. 2010, A&A, 516, A94
Ohashi, T., Ebisawa, K., Fukazawa, Y., et al. 1996, PASJ, 48, 157
Osip, D. J., Floyd, D., & Covarrubias, R. 2008, Proc. SPIE, 7014, 70140A
Oskinova, L. M. 2005, MNRAS, 361, 679
Paron, S., Combi, J. A., Petriella, A., & Giacani, E. 2012, A&A, 543, A23
Pavan, L., Bozzo, E., Ferrigno, C., et al. 2011, A&A, 526, A122
Peretto, N., & Fuller, G. A. 2009, A&A, 505, 405
Petre, R., Kuntz, K. D., & Shelton, R. L. 2002, ApJ, 579, 404
Pooley, D., Rappaport, S., Levine, A., Pfahl, E., & Schwab, J. 2007, arXiv:0708.3365
Ramos-Larios, G., Phillips, J. P., & Pérez-Grana, J. A. 2010, MNRAS, 405, 245
Reig, P. 2011, Ap&SS, 332, 1
Rho, J., Ramírez, S. V., Corcoran, M. F., Hamaguchi, K., & Lefloch, B. 2004, ApJ, 607, 904
Rodriguez, J., Bodaghee, A., Kaaret, P., et al. 2006, MNRAS, 366, 274
Russeil, D. 2003, A&A, 397, 133
Safi-Harb, S., Dubner, G., Petre, R., Holt, S. S., & Durouchoux, P. 2005, ApJ, 618, 321
Sana, H., Rauw, G., Nazé, Y., Gosset, E., & Vreux, J. 2006, MNRAS, 372, 661
Sguera, V., Bazzano, A., Bird, A. J., et al. 2006, ApJ, 646, 452
Shaver, P. A., & Goss, W. M. 1970, AuJPA, 14, 133
Simpson, J. P., & Cotera, A. S. 2004, BAAS, 36, 734
Skrutskie, M. F., Cutri, R. M., Stiening, R., et al. 2006, AJ, 131, 1163
Slane, P., Castro, D., Funk, S., et al. 2010, ApJ, 720, 266
Slane, P., Chen, Y., Lazendic, J. S., & Hughes, J. P. 2002, ApJ, 580, 904
Smith, D. A., Guillemot, L., Camilo, F., et al. 2008, A&A, 492, 923
Stetson, P. B. 2000, PASP, 112, 925
Stil, J. M., Taylor, A. R., Dickey, J. M., et al. 2006, AJ, 132, 1158
Sugizaki, M., Kinugasa, K., Matsuzaki, K., et al. 2000, ApJL, 534, L181
Sugizaki, M., Mitsuda, K., Kaneda, H., et al. 2001, ApJS, 134, 77
Thompson, T. W. J., Tomsick, J. A., Rothschild, R. E., in't Zand, J. J. M., & Walter, R. 2006, ApJ, 649, 373
Tody, D. 1986, Proc. SPIE, 627, 733
Tody, D. 1993, in ASP Conf. Ser. 52, Astronomical Data Analysis Software and Systems II, ed. R. J. Hanisch, R. J. V. Brissenden, & J. Barnes (San Francisco, CA: ASP), 173
Tomsick, J. A., Chaty, S., Rodriguez, J., et al. 2006, ApJ, 647, 1309
Torii, K., Sugizaki, M., Kohmura, T., Endo, T., & Nagase, F. 1999, ApJL, 523, L65
Torres, C. A. O., Quast, G. R., da Silva, L., et al. 2006, A&A, 460, 695
Ueno, M., Bamba, A., Koyama, K., & Ebisawa, K. 2003, ApJ, 588, 338
Usov, V. V. 1992, ApJ, 389, 635
van den Berg, M., Penner, K., Hong, J., et al. 2012, ApJ, 748, 31
Voges, W., Aschenbach, B., Boller, T., et al. 1999, A&A, 349, 389
Vogt, N., & Bateson, F. M. 1982, A&AS, 48, 383
Walborn, N. R. 1973, AJ, 78, 1067
Walter, R., Zurita Heras, J., Bassani, L., et al. 2006, A&A, 453, 133
Watson, M. G., Schrder, A. C., Fyfe, D., et al. 2009, A&A, 493, 339
Weisskopf, M. C., Aldcroft, T. L., Bautz, M., et al. 2003, ExA, 16, 1
Weisskopf, M. C., Wu, K., Trimble, V., et al. 2007, ApJ, 657, 1026
Whiteoak, J. B. Z., & Green, A. J. 1996, A&AS, 118, 329
Wolk, S. J., Harnden, F. R., Jr., Flaccomio, E., et al. 2005, ApJS, 160, 423
Yamaguchi, H., Ueno, M., Koyama, K., Bamba, A., & Yamauchi, S. 2004, PASJ, 56, 1059
Yamauchi, S., Bamba, A., & Koyama, K. 2011, PASJ, 63, 957
Yamauchi, S., Ueno, M., Koyama, K., & Bamba, A. 2008, PASJ, 60, 1143
Zhao, P., Grindlay, J. E., Hong, J. S., et al. 2005, ApJS, 161, 429
Zolotukhin, I. Y., & Chilingarian, I. V. 2011, A&A, 526, A84